The Role of Complex Type N-Glycans in Neuronal Development

BY
Cody Hatchett
DECEMBER 2024
DIRECTOR: Dr. Ruth Schwalbe , Ph.D.
DEPARTMENT OF Biochemistry and Molecular Biology

Oligosaccharides are attached to up to 70% of human proteins. N-linked glycosylation is one of the predominant forms of co- and post-translational modifications in vertebrates. Discrepancies in glycan processing result in congenital disorders of glycosylation (CDGs), a group of rare genetic disorders characterized by impaired glycan synthesis or processing, leading to a wide range of clinical manifestations. CDGs are divided into two classes: type 1 and type 2. Regarding N-glycosylation, CDG type 1 disorders result from improper glycan synthesis or transfer of the precursor oligosaccharide, while CDG type 2 disorders result from disrupted processing of the precursor oligosaccharide linked to protein. Many identified CDG disorders are lethal within the first year of life, and those that survive often have neurological complications. Those who survive are impacted by epilepsy, locomotor skill deficiency, and slowed or stunted growth. N-linked oligosaccharides are processed by many enzymes, such as N-acetylglucosaminyltransferases (GnTs) and transporters. The three common types of N-glycans are oligomannose, hybrid, and complex. The first GnT to act is GnT-I, which is responsible for the processing of oligomannose to hybrid N-glycans via addition of a N-acetylglucosamine (GlcNaC) residue to the conserved core of N-glycans. The importance of glycan processing by GnT-I has been implicated in several studies using knockdown organismal and cell models. Global GnT-I knockout in mice was found to be lethal at the embryonic age of 8.5-10.5 days. This timeframe coincides with neurogenesis and the neural tube formation from the neural plate, which involves cell migration and proliferation. GnT-

I was inactivated in developing neural tissue of mice, which perturbed neuron development. Further, these mice suffered from a shortened life span and reduced body size. These findings highlight the critical role of GnT-I in neurogenesis, growth, and longevity.

This study used zebrafish as an organismal model since embryonic and larval development stages are well-characterized, and the number of individual fish studied can be relatively large. Zebrafish, unlike mice, possess two gene copies of GnT-I referred to as *mgat1a* and *mgat1b,* resulting from multiple whole genome duplications. Inactivation of one of the two *mgat1* genes, *mgat1b*, reduced the level of glycan processing from oligomannose to hybrid and complex N-glycans. Glycomics profiling supported this knockout with an increase in the Glc_2Man_5 structure acted upon by GnT-I. The GnT-Ib knockout fish had reduced complex N-glycans. Survivability was greatly reduced in the mutant fish line which began to drop around 10hpf. Developmental milestones were delayed when *mgat1b* was knocked out such as the presence of a heartbeat and swim bladder inflation. Sensory motor function was reduced in mutant line fish as indicated by reduced motor activity and slow touch or vibrational startle response as well as motor coordination and stamina. Muscle structure development of mgat1b knockout fish was delayed until up to 72 hpf via birefringence microscopy. Spinal cord caudal primary (CaP) primary motor neurons transiently expressing electric green fluorescent protein (EGFP) were examined using fluorescent microscopy with the mutant line having reduced collateral branching. These results indicate the importance of complex N-glycosylation on zebrafish development and motor function.

The Role of Complex Type N-Glycans in Neuronal Development

A Dissertation

Presented to the Faculty of the Department of Biochemistry and Molecular Biology

East Carolina University

In Partial Fulfillment of the Requirements for the Degree

Doctor of Philosophy in Biomedical Sciences with a Concentration in Biochemistry and Molecular Biology

By
Cody J. Hatchett, M.S.

December 2024

Director of Dissertation: Dr. Ruth Schwalbe, Ph.D.
Dissertation Committee Members:
Dr. Kyle Mansfield, Ph.D.
Dr. Morgan Milton, Ph.D.
Dr. Karen Mruk, Ph.D.

ACKNOWLEDGEMENTS

I wish to express my deepest thanks to my research advisory committee chair, Dr. Ruth Schwalbe, for her time, support, and guidance throughout the entire thesis study. Aside from my advisor, I would like to thank our laboratory technician, Kristen Hall, for her time, effort, and assistance. I would also like to think Adam Bruch for his support and the undergrads from the SchwaIbe lab, Abel Messer, Erin Lang, and Caitlin Spurlock, for their assistance in dissections and other experiments, as well as my friends and family for their unwavering support.

I would also like to thank my thesis committee members, Dr. Schwalbe, Dr. Mansfield, Dr. Milton, and Dr. Mruk, for their time, comments, and advice.

- Funding for this research was provided by the National Institute of Health Grant R15GM129679 (R.A.S.) and DK52990 NIH (R.A.S.) as well as the Wooten Family Initiative for Brain Health Research grant (R.A.S.)

TABLE OF CONTENTS

LIST OF TABLES

LIST OF FIGURES

LIST OF SYMBOLS OR ABBREVIATIONS

Δ- Change

BiP- Binding Immunoglobular Protein

CaP – Caudal Primary

$CaCl_2 \bullet 2H_2O$- Calcium chloride dihydrate

CB- Coomassie Blue

CDG- Congenital Disorders of Glycosylation

CDS- Coding Sequence

CO_2- Carbon Dioxide

CRISPR- Clustered Regularly Interspaced Palindromic Repeats

CRT- Calreticulin

DDS- Data-Dependent Scan

DIC- Differential Interference Contrast

DMEM - Dulbecco's Modified Eagle Medium

DNA- Deoxyribonucleic Acid

Dol-P – Dolichol Phosphate

dpc- Days Post Coitus

dpf – Days Post Fertilization

DTT- Dithiothreitol

ECU- East Carolina University

ER- Endoplasmic Reticulum

ESI-MS- Electrospray Ionization Mass Spectroscopy

EPHA- Phaseolus Vulgaris Erythroagglutinin

EVL- Enveloping Layer

F-actin- Filamentous Actin

FBS- Fetal Bovine Serum

G-actin- Globular Actin

GFP- Green Fluorescent Protein

GlcNAc- N-acetylglucosamine

GNL- Galanthus Nivalis Lectin

GnT- N-acetylglucosaminyltransferases

GnT-I- N-acetylglucosaminyltransferases I

GnT-II- N-acetylglucosaminyltransferases II

gRNA- Guide Ribonucleic Acid

hpf- Hours Post Fertilization

HSP- Heat Shock Protein

IACUC- Institutional Animal Care & Use Committee

KATP- ATP-Sensitive Potassium Channel

KCl- Potassium Chloride

KIF- Kinesin Superfamily Proteins

Kv- Voltage Gated Potassium Channel

LC-ESI-MS- Liquid Chromatography Electrospray Mass Spectroscopy

MALDI-TOF MS -MALDI Coupled To Time-Of-Flight Mass Spectrometry

Man- Mannose

Gal- Galactose

MBT- Mid-Blastoderm Transition

$MgSO_4 \cdot 7H_2O$- Magnesium Sulfate Heptahydrate

MiP- Middle Primary

MSD- Mean Square Difference

MS-222- Tricaine Methanesulfonate

NaCl – Sodium Chloride

NaOH- Sodium Hydroxide

NB- Neuroblastoma

NF-L- Neurofilament-Light Chain

NMJ- Neuromuscular Junction

PBS- Phosphate Buffered Saline

PCR- Polymerase Chain Reaction

PVDF- Polyvinylidene fluoride

RE- Restriction Enzyme

RNA- Ribonucleic Acid

RoP- Rostral Primary

RT-PCR- Reverse Transcription Polymerase Chain Reaction

SARL - Sinnhuber Aquatic Research Laboratory

SDS- Sodium Dodecyl Sulfate (SDS)

TIRF- Total Internal Reflection Fluorescence Microscope

VaP- Variable Primary

YSL- Yolk Syncytial Layer

CHAPTER I: INTRODUCTION

N-Glycosylation

N-glycosylation is a common co- and post-translational modification of proteins (Stanley 2022). The co-translational phase of N-glycosylation is the addition of a precursor oligosaccharide to a protein using an N-glycosidic covalent bond to the Asn residue of the consensus sequence (-Asn-Xxx-Thr-) where Xxx is known as any amino acid other than Pro (Figure 1.1). The N-linked oligosaccharides known as N-glycans, are classified into three common types: oligomannose, hybrid, and complex (Figure 1.1). All N-glycans have a conserved core consisting of two N-acetylglucosamine (GlcNAc) residues and three mannose residues, known as $GlcNAc_2Man_3$ (Figure 1.1(inset)) (Chen, Tan et al. 2020). Oligomannose N-glycans have only mannose residues attached to the conserved pentasaccharide (Figure 1.1, Left panels). Hybrid N-glycans have a GlcNAc residue attached to the Manα1,3 arm of $GlcNAc_2Man_5$ (Figure 1.1, Middle panel). Complex N-glycans have GlcNAc residues attached to the Manα1,3 arm and Manα1,6 arm of $GlcNAc_2Man_3$(Figure 1.1, Right panel). These GlcNaC residues serve as branch points as other enzymes add monosaccharides, one at a time, to form antennae, which give rise to the various hybrid and complex types of N-glycans.

N-glycosylation begins in the endoplasmic reticulum membrane, where the glycan is synthesized on the dolichol-phosphate lipid carrier known as dolichol-phosphate (Dol-P) (Cantagrel and Lefeber 2011). The GlcNAc-1-phosphotransferase (*DPAGT1*) adds another phosphate and a GlcNAc residue to the Dol-P lipid (Dong, Wang et al. 2018). ALG7 adds a second GlcNAc residue to the oligosaccharide (Ramirez and Locher 2023). ALG1, ALG2, and ALG11 then build upon the glycan precursor via the addition of five mannose residues, producing $GlcNAc_2Man_5$ (Ramirez and Locher 2023). This precursor structure is then transferred from the cytoplasmic side to the luminal side of the ER via RFT1 (Hirata, Sakata et al. 2024).

The precursor sugar, $GlcNAc_2Man_5Glc_3$, is complete after the addition of four more mannose residues and three glucose residues, resulting in $GlcNAc_2Man_9Glc_3$ (Figure 1.3).

The remaining steps of N-glycosylation processing follow the secretory pathway (Figure 1.2)(Ahmed, Amin et al 2018). Both secreted and transmembrane proteins follow this pathway, which involves the ER, Golgi apparatus, transport vesicles, and plasma membrane. Only the extracellular regions of the transmembrane protein will enter the lumen, while the entire secreted protein enters the ER. As such, only extracellular N-glycosylation sites will be N-glycosylated.

The precursor oligosaccharide $GlcNAc_2Man_9Glc_3$ is transferred to an asparagine residue via an oligosaccharyltransferase, OST, in the lumen of the ER (Breitling and Aebi 2013). After the oligosaccharide is attached, the glucose residues are removed by α-glucosidases, along with one of the terminal mannose residues on Man α1,6 arm of the conserved core via α-mannosidase, in a stepwise fashion. The aforementioned steps are involved in protein quality control. The correctly folded glycoprotein then exits the ER and enters the *cis* Golgi.

Mannosidases remove additional mannose residues in preparation for the conversion from an oligomannose type to hybrid type N-glycan, which is carried out via N-acetylglucosaminyltransferases encoded by *MGAT* genes. N-acetylglucosaminyltransferase I (GnT-I) encoded by *MGAT1* in the *cis* Golgi. GnT-I transfers a GlcNAc residue from UDP-GlcNAc to the α1-3 Man residue of the conserved pentasaccharide to generate hybrid type N-glycans (Strasser, Stadlmann et al. 2005). GnT-I is a membrane-bound N-acetylglucosaminyltransferase that has three domains known as an N-terminal cytoplasmic region, a transmembrane domain, and a C-terminus luminal domain (Burke, Pettitt et al. 1994). The catalytic domain is in the C-terminal domain. However, all three domains are necessary for proper protein function. The transmembrane domain and cytoplasmic tail are crucial for properly

localizing the protein to the cis golgi apparatus. The N-terminal cytoplasmic tail is believed to also assist in transmembrane-assisted dimerization (Burke, Pettitt et al. 1994).

Next, the nascent N-glycosylated protein moves to the medial Golgi, where mannosidase II removes the Man α1,6 terminal residue that was attached to the conserved core in preparation for N-acetylglucosaminyltransferase-II (GnT-II) encoded by *MGAT2* which adds a GlcNAc residue generating a complex type N-glycan (Shah, Kuntz et al. 2008); (Yoo, Ko et al. 2015). GnT-IV and GnT-V via the expression of *MGAT4* and *MGAT5* can further process the N-glycan to generate tri-and tetra-antennary N-glycans in a non-sequential manner. (Figure 1.4) (Link-Lenczowski, Bubka et al. 2018, Nagae, Yamaguchi et al. 2020). *MGAT3* which encodes GnT-III can act on hybrid or complex types of N-glycans by adding a GlcNaC residue via a β1,4 linkage to the center mannose of the conserved core structure, resulting in bisecting N-glycans. When a bisecting GlcNaC is added, glycan processing is terminated (Chen, Tan et al. 2020).

The GlcNAc residues added to the conserved core via the GnTs are referred to as branch points and are required for the extension of an antenna (Stanley 2022). Extension of branch points involves the addition of one residue at a time, such as galactose, GlcNAc, and sialic acid (Figure 1.4) (Stanley 2022). The conserved core structure can be modified via the addition of a fucose residue to the GlcNAc residue nearest the protein, referred to as core fucosylation, or fucose can be added to the antennae (Figure 1.4) (Stanley 2022). After processing, the glycoprotein is secreted to the extracellular regions or released into the plasma membrane.

Congenital disorders of glycosylation (CDG) are the result of improper N-glycosylation (Chang, He et al. 2018). There are two types of CDG known as type I and type II. Type I disorders result from improper precursor oligosaccharide formation or glycan transfer to the protein. Type II CDGs result from incorrect processing of N-glycans attached to the protein.

Most CDGs are lethal within the first year of life (Chang, He et al. 2018). The effects of CDG-related disorders are organism-wide, though neurological tissues such as the brain are heavily impacted with symptoms including cognitive impairment and seizures, as well as loss of motor skills (Ezgu, 2016).

Previous studies have involved a global knockout of *Mgat1*, which encodes GnT-I and converts oligomannose to hybrid N-glycans. In mice, the *Mgat1* knockout was lethal at 9.5 embryonic days, which was attributed to the improper closure of the neural tube, evidenced by decreased cephalic area size, larger tail area, and reduced somite count (Ioffe and Stanley 1994). *mgat1* drosophila mutants resulted in altered neuromuscular junctions (NMJ), disrupted signaling of proteins, and loss of synaptic recruitment of membrane scaffolding proteins necessary for neuromuscular junction formation (Parkinson, Dear et al. 2013). These studies indicate the importance of complex N-glycans, along with hybrid N-glycans, in organismal development, including neuronal structure and function.

Neuron Axon formation

Axon development is critical to neuron function, as it allows the transmission of action potentials to other neurons and the innervation of tissues. Growth cones are a crucial factor in axon formation and extension. Growth cones are expansions from developing neurons used to investigate their environment and determine the optimal direction for axon expansion by expanding and collapsing in various directions. Growth cones consist of lamellipodia, a web-like expansion at the tip of the growth cone, and filopodia, small tentacle protrusions that reach and retract to sense the environment (Dent, Gupton et al. 2011). A network of microtubules and actin filaments control the movement of these growth cone structures. Growth cones contain three zones known as the peripheral (P-domain), central (C-domain), and transition domains (T-zone)

(Vallee, Seale et al. 2009). The P-domain includes a large quantity of F-actin, providing the growth cone with its source of movement. The C-domain is comprised of microtubules and other vesicles. The T-zone is the thin area where the P-domain and C-domain meet. Axon extension takes place in 3 phases: protrusion, engorgement, and consolidation. During protrusion, filopodia and lamellipodia form via the polymerization of F-actin in the P-domain. Engorgement starts with the advancement of microtubules into the P-domain from the C-domain. Consolidation then occurs due to the collapse of the previous C-domain, resulting in the extension of the axon.

Kv3

Potassium channels are extensively distributed throughout the central nervous system (CNS). Their widespread presence underscores their crucial role in enabling rapid firing rates exceeding (>100 Hz), which is essential for neuronal development and the regulation of neuronal excitability (Gunthorpe 2022). There are five basic types of potassium channels: calcium-activated, inwardly rectifying, tandem pore domain, ATP-sensitive channels (KATP), and voltage-gated channels (Kv) (Rajkovic, Djokic et al. 2020). This research focused on the voltage-gated potassium channels, particularly Kv3 channels, which are encoded by KCNC genes, *KCNC1* (Kv3.1), *KCNC2* (Kv3.2), *KC*NC3 (Kv3.3), and *KCNC4* (Kv3.4). These genes have splice variants due to alternative splicing. KCNC1, for example, can result in two splice variants, Kv3.1a and Kv3.1b (Liu and Kaczmarek 1998). The Kv3.1b and Kv3.1a alpha subunits contain six transmembrane units with two N-glycosylation sites running from amino acid residues 220 to 222 (NKT) and from 229 to 231 (Snowden, Leborgne-Castel et al.) in the S1- S2 extracellular loop (Figure 1.5) (Schwalbe, Corey et al. 2008); (Hall, Weidner et al. 2015); (Vicente, Kim et al. 2018). Complex N-glycans occupy these N-glycosylation sites (Schwalbe, Corey et al. 2008); (Cartwright and Schwalbe 2009). The difference between these splice

variants is the shorter cytoplasmic tail of Kv3.1a (Liu and Kaczmarek 1998); (Song and Kaczmarek 2006). The first four transmembrane units act to sense changes in voltage, and the final two units act as a pore. These alpha subunits form homomeric and heteromeric multimer channels with other Kv subunits in the same subfamily, such as Kv3.1, Kv3.2, Kv3.3, Kv3.4 (Rudy and McBain 2001).

Kv3 channels are responsible for the rapid repolarization of neurons during an action potential (Gazulla and Berciano 2024). Before an action potential, the resting membrane potential of a cell is about -70 mV. To initiate an action potential, a massive depolarization of the membrane, denoting the opening of sodium channels, results in a membrane potential of around 35 mV. These depolarizations to generate an action potential are all-or-nothing style activations, meaning the cell membrane potential must surpass -55 mV to initiate an action potential, or one will not occur. At around 35 mV, K^+ channels open to repolarize the membrane and begin to close around -60 mV. There is usually a slight overshoot of the resting potential of -70 mV due to some channels closing slower. However, the membrane potential is slowly restored to -70 mV. Kv3 channels have a deactivation rate much faster than other Kv channels. This rapid activation/deactivation allows fast-firing neurons to fire in rapid trains of action potentials (Kaczmarek and Zhang 2017).

N-glycosylation has a profound effect on protein distribution throughout the cell (Hall, Weidner et al. 2017); (Hall, Shajahan et al. 2023). Proper localization of K^+ channels is critical to their function as it impacts morphological and electrophysiological properties of the cell (Trimmer 2015, Hall, Weidner et al. 2017). In adult mouse primary neurons heterologously expressing unglycosylated Kv3.1b (N220Q/N229Q), results revealed a higher concentration of

Kv3.1b expression around the cell soma compared to the fully glycosylated Kv3.1b (Wt) which favored the outgrowths of the cell (Hall, Weidner et al. 2017). Our lab also found reduced levels of Wt Kv3.1b in neurites of neuronal-derived cells when the complex N-glycans were substituted with oligomannose or hybrid types of N-glycans (Hall, Weidner et al. 2017); (Issa, Hall et al. 2021). Thus, Kv3.1b associated with oligomannose or hybrid types of N-glycans were expressed more intensely in the soma of neuronal-derived cells, indicating that it is not just the occupancy of the N-glycan sites on Kv3.1 necessary for proper protein distribution throughout the cell but also the type of glycan present in those sites. The disruption of Kv3.1b distribution from defects in N-glycosylation likely impacts neuronal morphology, such as branching and length (Issa, Hall et al. 2021); (Hall, Shajahan 2023); (Hatchett 2021); (Hatchett, Hall et al. 2024). This could be explained by the fact that Kv3 channels are thought to regulate outgrowth formation via the regulation of membrane excitability and, in return, alter the Ca^{2+} ion concentration at optimal levels for growth cone formation (Huang, Lien et al. 2017). Alterations of the N-glycosylation state of Kv3.1b result in not only morphological changes but have also been shown to alter the electrical physiological properties of the cells expressing the channels.

B35 neuroblastoma cell lines expressing various glycoforms of Kv3.1b showed that altered N-glycosylation by the ablation of the consensus sequence resulted in slower channel activation and deactivation rates (Hall, Cartwright et al. 2011). Using the NB_1(-*Mgat2*) cell line, our lab has previously shown that when N-glycosylation processing is reduced, channels showed an increase in rise times, which is the time it takes for the current to go from minimum to maximum levels, which indicates slower channel opening (Hall, Weidner et al. 2017). When the processing was further reduced to only oligomannose N-glycans, the rise times were again

increased from that of the NB_1 cell line, which shows reduced channel opening (Issa, Hall et al. 2021).

Zebrafish Development

Zebrafish development begins at fertilization, evident by the darkening of the yolk membrane, followed by heavy periods of cytoplasmic migration, creating the animal and vegetal poles (Kimmel, Ballard et al. 1995). The first of the cleavage stages occurs about 40 minutes post-fertilization (O'Farrell, Stumpff et al. 2004). This cleavage generates the first cells, or blastomere, with further rounds of cell divisions in approximately 15-minute intervals. These cleavages are classified into stages by the number of cells present from the 2-64 cell stage (Kimmel, Ballard et al. 1995). The cleavage period is followed by the blastula period, which lasts from the 128-cell stage to gastrulation or the 8^{th} to 14^{th} cleavage set (Li, White et al. 2011).

The blastula period is characterized by heavy periods of cell migration, such as mid-blastula transition (MBT) and epiboly. MBT is when embryo development switches from increasing cell number to generating the organismal body plan (Kimelman, Kirschner et al. 1987). Epiboly occurs during gastrulation in anamniotes and involves the thinning and spreading of cells into sheets of tissue called the enveloping layer (EVL), yolk syncytial layer (YSL), and yolk (Zalik, Lewandowski et al. 1999); (Bruce and Heisenberg 2020). The formation of these three layers begins in MBT under maternal genes (Solnica-Krezel 2020). However, initiating epiboly requires the zygote to have begun transcription independently, as MBT is known to involve the clearance of maternal RNAs (Giraldez, Mishima et al. 2006); (Williams and Solnica-Krezel 2020). The driving force of epiboly is thought to be driven by the remodeling of the microtubules in the YSL and F-actin (Strahle and Jesuthasan 1993).

After epiboly proceeds to around 50% and involution begins, the embryo enters the gastrulation phase of development, which occurs around five and a half hours post-fertilization (hpf) (Tucker, Mintzer et al. 2008). At nine hpf, the embryo reaches 90% epiboly, and the brain anlagen is formed by the thickening of the dorsal epiblast (Kimmel, Ballard et al. 1995). Epiboly continues till 10 hpf, during which the blastoderm completely engulfs the yolk, and the tail bud becomes evident (Bruce and Heisenberg 2020). Following gastrulation, the embryo enters the segmentation phase. During segmentation, somites are formed at a constant rate of two somites per hour after 18 hpf (Hanneman and Westerfield 1989). The constant somite production provides another avenue for development tracking. Segmentation is followed by the pharyngula phase, which begins around 24 hpf and lasts until hatching. During this period, the fish takes a more adult body plan. The pigmented cells, such as melanophoresbegin to develop, and essential organs, such as the heart, start regular function (Echeazarra, Hortigon-Vinagre et al. 2020). Following hatching, zebrafish are considered larvae (Kimmel, Ballard et al. 1995); (Arduini and Henion 2004).

Zebrafish enter the larval phase upon hatching from their chorion at ~3 days post fertilization (dpf) and remain in the larval stage for approximately six weeks (Singleman and Holtzman 2014). The main developmental feature of larval fish include swim bladder inflation (Yue, Peterson et al. 2015), musculature, gut (Wallace and Pack 2003), liver function (Chu and Sadler 2009), and respiration method alterations (Rombough 2007). Zebrafish then enter the juvenile stage at around 45 dpf; during this time, zebrafish undergo morphological changes from their larval appearance to a more adult-style body plan and develop scales (Alfonso, Peyrafort et al. 2020); (Singleman and Holtzman 2014). Zebrafish become sexually mature at around 3 months and are considered adults (Singleman and Holtzman 2014).

N-Glycosylation in zebrafish

The glycome of zebrafish (*Danio rerio*) is quite diverse, and all three N-glycan types are present as early as 6 h postfertilization (hpf), with an abundance of oligomannose type N-glycans (Hanzawa, Suzuki et al. 2017). Although complex type N-glycans are found in smaller amounts, a sharp increase is noted in the segmentation to pharyngula period (10–48 hpf) of embryonic development (Hanzawa, Suzuki et al. 2017). In adult zebrafish, although the proportion of complex- to oligomannose-type N-glycans varies among specific organs, most of the brain regions revealed a higher population of complex N-glycans relative to oligomannose N-glycans (Yamakawa, Vanbeselaere et al. 2018) (Hall, Hatchett et al. 2023)(Hatchett, Hall et al. 2024). Further, complex N-glycans found in adult brains had the highest percentage of core fucose and the highest overall sialyation pattern relative to other organs (Yamakawa, Vanbeselaere et al. 2018). Zebrafish spinal cord structures were very diverse with over 17 different complex structures identified (Hatchett, Hall et al. 2024).These complex structures were primarily biantennary and most contained fucosylation and sialyation (Hatchett, Hall et al. 2024). Hybrid type N-glycans were the least diverse group identified in Wt AB spinal cord with only three structures, all of which contained sialic acid residues (Hatchett, Hall et al. 2024). This study also looked at the effects of increased oligomannose type N-glycans on zebrafish development via knockdown of GnT-I. GnT-I is the enzyme necessary for converting oligomannose to hybrid type N-glycans. It should be noted that, unlike mice and humans, zebrafish have two genes (*mgat1a/b*) that encode GnT-Ia/b (Sprague, Doerry et al. 2001). As such, zebrafish are an ideal model to study the effects of increased oligomannose N-glycans with less lethal outcomes due to knockdown of each GnT-I gene independently. The *mgat1* genes exhibit similar expression patterns throughout the zebrafish (Sur, Wang et al. 2023). However, recent data from *mgat1b*

knockout fish indicate an increase in Glc_2Man_5, which is the substrate for GnT-I. This spike in Glc_2Man_5 was also accompanied by a reduction in complex N-glycans, indicating that *mgat1a* expression does not fully overlap with the expression of *mgat1b* (Hatchett, Hall et al. 2024); ; (Hall, Hatchett et al. 2023); (Sur, Wang et al. 2023). The reduction in complex N-glycans resulted in reduced embryonic viability during gastrulation as well as delayed organ development such heart, swim bladder, and sensory motor impairments (Hall, Hatchett et al. 2023); (Hatchett, Hall et al. 2024). Skeletal muscle organization development of mgat1b knockout fish was delayed for 72 hpf (Hall, Hatchett et al. 2023).

Spinal Cord Primary Motor Neuron Development

The first motor neurons in the spinal cord are called primary motor neurons, and the somas appear between 9-11 hpf (Ahmed, Amin et al. 2018). There are three of these neurons that survive to adulthood. They are named based on their location when viewing the fish from the rostral end to the caudal end; these are the Rostral primary (Aamodt, Waligorska et al. 2021), Middle Primary (MiP), and Caudal Primary (CaP) motor neurons (Figure 1.6). The CaP axon is the first to descend from the spinal cord in the vertical myoseptum, where it passes across the horizontal myoseptum and hooks around the ventral musculature, innervating fast twitch ventral trunk axial musculature. The migration of the CaP axon from the spinal cord usually occurs between 18-20 hpf (Myers, Eisen et al. 1986); (Zelenchuk and Bruses 2011). Although MiP and RoP axons utilize the same route down the vertical myoseptum, RoP extends rostrally and ventrally along the horizontal myoseptum and innervates the middle axial muscle, while MiP has a collateral branch that travels dorsally and caudally, and innervates the dorsal axial muscles (Eisen, Myers et al. 1986); (Myers, Eisen et al. 1986).

N-glycosylation has been implicated in axon development of zebrafish. When the N220 N-glycosylation site was ablated in Kv3.1b via changing the Asn to Gln and expressed in neurons of Wt AB zebrafish, CaP primary motor neurons had reduced axon length, area, and branching relative to those in Wt AB (Issa, Hall et al. 2021). When CaP motor neuron axon formation was studied in the GnT-Ib knockout AB strain zebrafish, CaP neurons had a reduction in collateral branching when compared with that of Wt AB (Hatchett, Hall et al. 2024). The study attempted to image the other primary motor neurons but RoP's relatively flat branching along the horizontal myoseptum which makes branching indiscernible. MiP is a possible imaging target though the effect might not be as pronounced due to heavy overlaying of secondary motor neurons making branching less discernable. Thus, our results indicate a vital role of complex and hybrid types of N-glycans on CaP neuron development.

The three zebrafish motor neurons exhibit different electrical membrane properties from each other. CaP for instance in 48 hpf embryos had a higher rate of rise and decay than that of MiP during spontaneous action potentials (Moreno and Ribera 2009). CaP neurons also exhibited a higher inward current density meaning that the ions flow more rapidly into CaP than MiP which is likely due to Na and K^+ ion channel activity and possibly Kv3 channels (Moreno and Ribera 2009). The difference in ion flow rate becomes more evident during repetitive action potential recordings, which reveal that CaP repolarizes much more rapidly than MiP. This difference in repolarization indicates a higher concentration of voltage gated ion channels in CaP, such as Kv3 channels that can more rapidly repolarize the membrane (Moreno and Ribera 2009).

CRISPR/Cas9

Responsible for recognizing and destroying viral DNA from bacteriophages, CRISPR/Cas9 originated from the immune system of bacteria (Jinek, Chylinski et al. 2012). Clustered regularly interspaced palindromic repeats (CRISPR) sequences are obtained from previously encountered bacteriophages, allowing the bacteria to recognize the contagion quickly. Upon detection of viral DNA, transcription occurs in the bacteria, converting the viral DNA held in its CRISPR sequences into what is known as CRISPR RNA (crRNA). CrRNA is combined with Trans-activating CRISPR RNA (tracrRNA) that codes endonuclease activity to form the CRISPR/Cas9 complex (Jinek, Chylinski et al. 2012). The CRISPR/Cas9 protein complex uses the guide RNA to search viral DNA to its complementary viral DNA. Cas9 will generate a double-stranded break of three nucleotides upstream of a promotor adjacent motif (PAM) sequence.

The PAM sequence recognized by the endonuclease Cas9 is the sequence -XGG-, where X is any nucleotide (Hirano, Gootenberg et al. 2016). The double-stranded break from Cas9 activity prevents viral DNA replication (Jinek, Chylinski et al. 2012). CRISPR/Cas9 gene modification uses a constructed gRNA to target the desired gene. Cas9 endonuclease will then induce a double-stranded break at the targeted location that the cell or organism will attempt to repair using one of the two double-strand break repair mechanisms, such as nonhomologous end joining or homologous recombination. Nonhomologous end joining will result in an insertion, deletion, or combination of an insertion and a deletion, referred to as an indel, and under certain circumstances, will result in a frameshift mutation and prevent proper gene function. CRISPR/Cas9 was used to generate the N-glycosylation mutant cell lines and *mgat1b* mutant

zebrafish model by introducing a frameshift mutation resulting from indels, reducing gene product function. (Figure 1.7).

Project Summary

N-glycosylation is one of the most common types of co- and post-translational modifications. Disruptions of N-glycosylation contribute to many diseases, such as CDG, Alzheimer's, Parkinson's, and other neurodegenerative diseases. This research will look at the role of complex N-glycans in zebrafish development. Previous animal models were embryonically lethal and allowed for limited study throughout development. However, zebrafish have two copies of the *mgat1* gene known as *mgat1a* and *mgat1b*. They also have easily identifiable primary motor neurons for neurodevelopmental studies and are transparent for long periods of development. It was hypothesized that limiting the level of complex type N-glycans will result in dysfunctions in neurogenesis, growth, and development, leading to reduced sensory and motor functions. The central hypothesis was addressed with the following aims. Aim 1: To determine the N-glycan structures in adult zebrafish brain, and spinal cord. Both tissue types were expected to exhibit all three common structure types. However, the *mgat1b*$^{-/-}$ fish will have a more significant percentage of the $GlcNAc_2Man_5$ structure, the substrate for GnTI. Aim 2: To investigate the requirement of complex type N-glycans in embryonic and larval development using Wt AB and *mgat1b* mutant zebrafish. Based on our labs' previous cellular studies, it was expected that *mgat1b*$^{-/-}$ would have reduced survivability or delayed development in periods heavy in cell migration and differentiation.

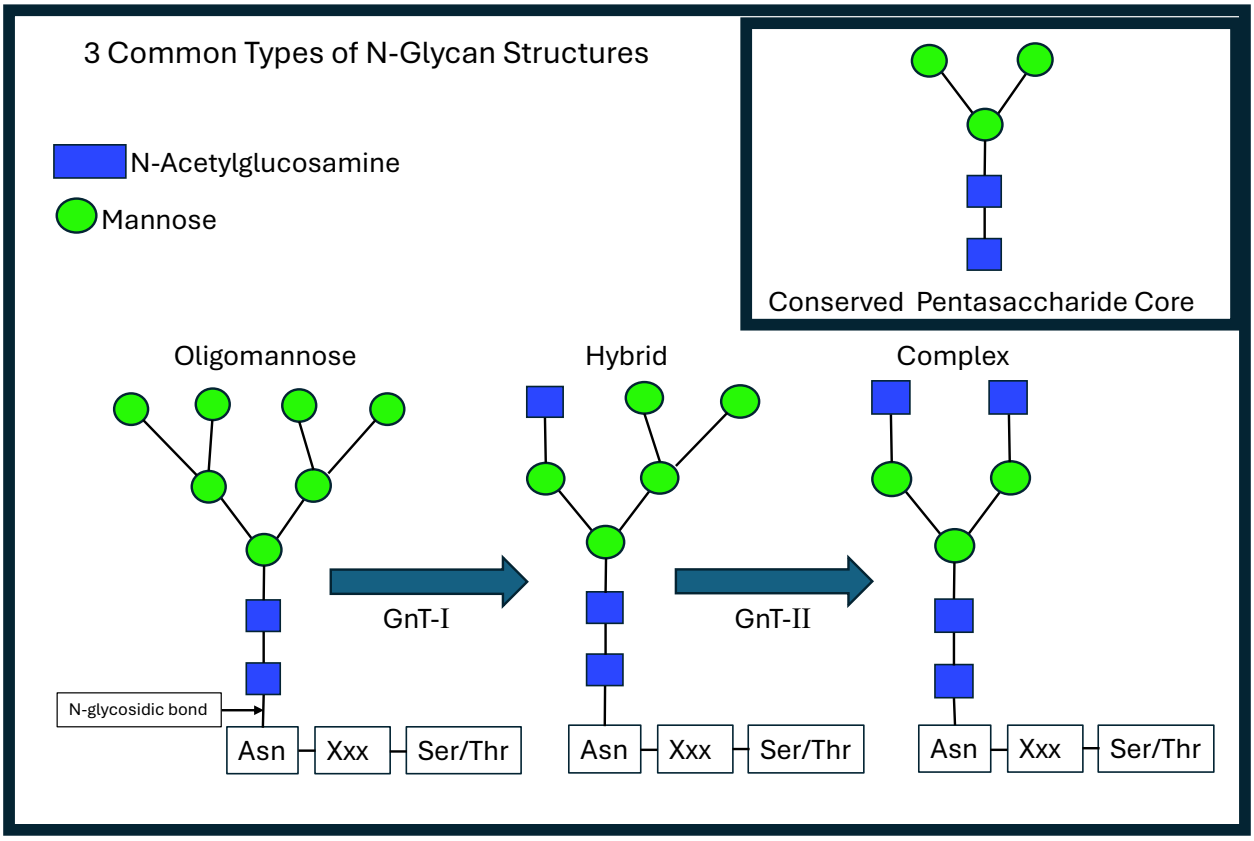
3 Common Types of N-Glycan Structures
N-Acetylglucosamine
Mannose
Conserved Pentasaccharide Core
Oligomannose
Hybrid
Complex
GnT-I
GnT-II
N-glycosidic bond
Asn
Xxx
Ser/Thr
Asn
Xxx
Ser/Thr
Asn
Xxx
Ser/Thr

Figure 1.1 Common Glycan Structures – All N-glycan structures contain a conserved core (inset) with two GlcNaC residues and three mannose residues. These structures are connected to a protein via an N-glycosidic bond to the nitrogen of the Asn residue's side chain in the consensus sequence -Asn-Xxx-Ser/Thr-. Oligomannose are the simplest form of N-glycans that terminate in only mannose residues. GnT-I acts by adding a GlcNaC residue generating a hybrid type N-glycan. Hybrid N-glycans have a GlcNAc residue that is usually further processed to form one branch while the other branch is absent and only mannose remains. Complex N-glycans are formed by GnT-II adding a GlcNAc residue on the right mannose residue from the core structure for further processing.

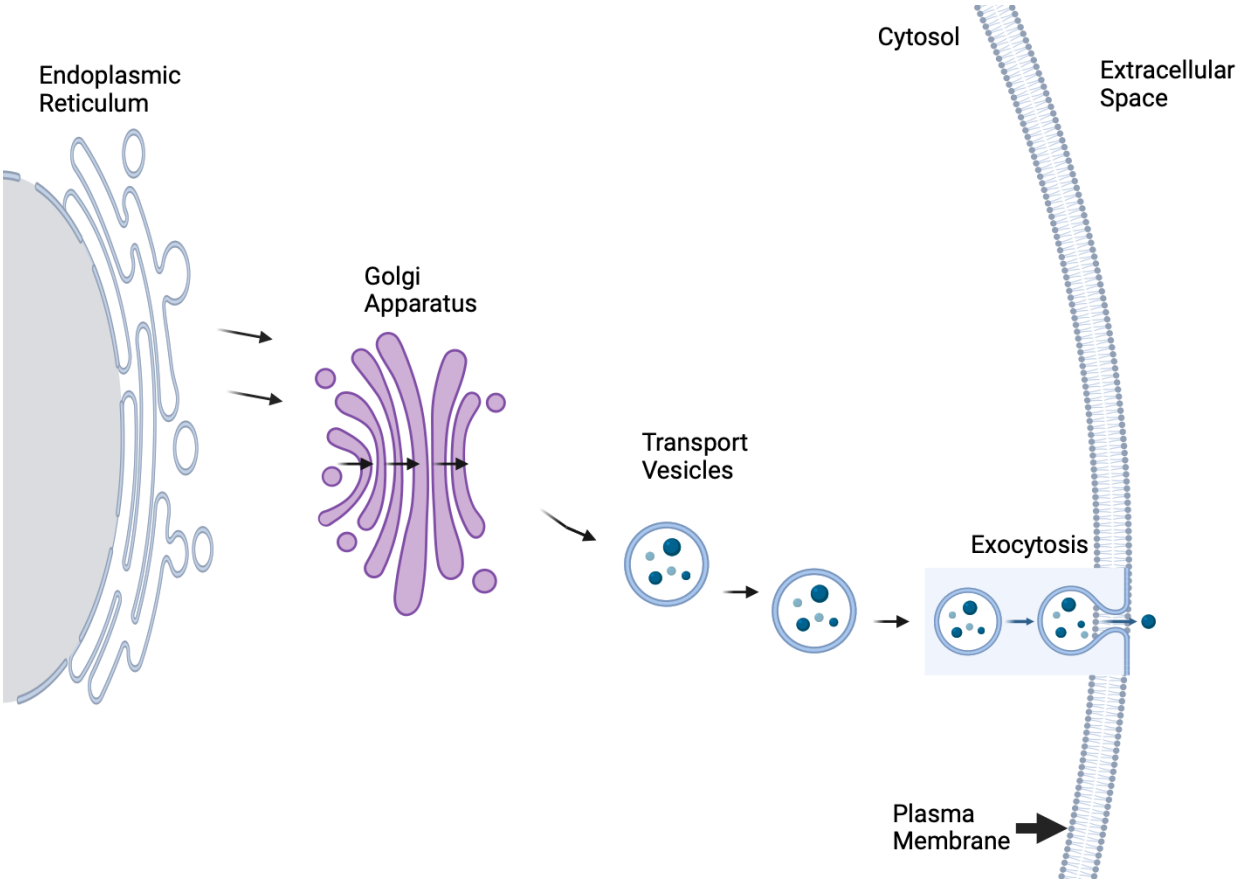
Endoplasmic
Reticulum
Golgi
Apparatus
Transport
Vesicles
Cytosol
Extracellular
Space
Exocytosis
Plasma
Membrane

Figure 1.2 Depiction of the Secretory Pathway for Protein Synthesis and Transport
The secretory pathway involves the ER, Golgi apparatus, transport vesicles, and the plasma membrane. Protein synthesis occurs on ribosomes on the ER. Once the nascent protein is localized to the ER folding and N-glycosylation occurs. N-glycosylated proteins then enter the Golgi apparatus where their glycans are processed further and the proteins are packaged into transport vesicles. Endocytosis occurs to transport proteins to the cell surface or extracellular space. Created in BioRender. Hatchett, C. (2024)
BioRender.com/o22d490

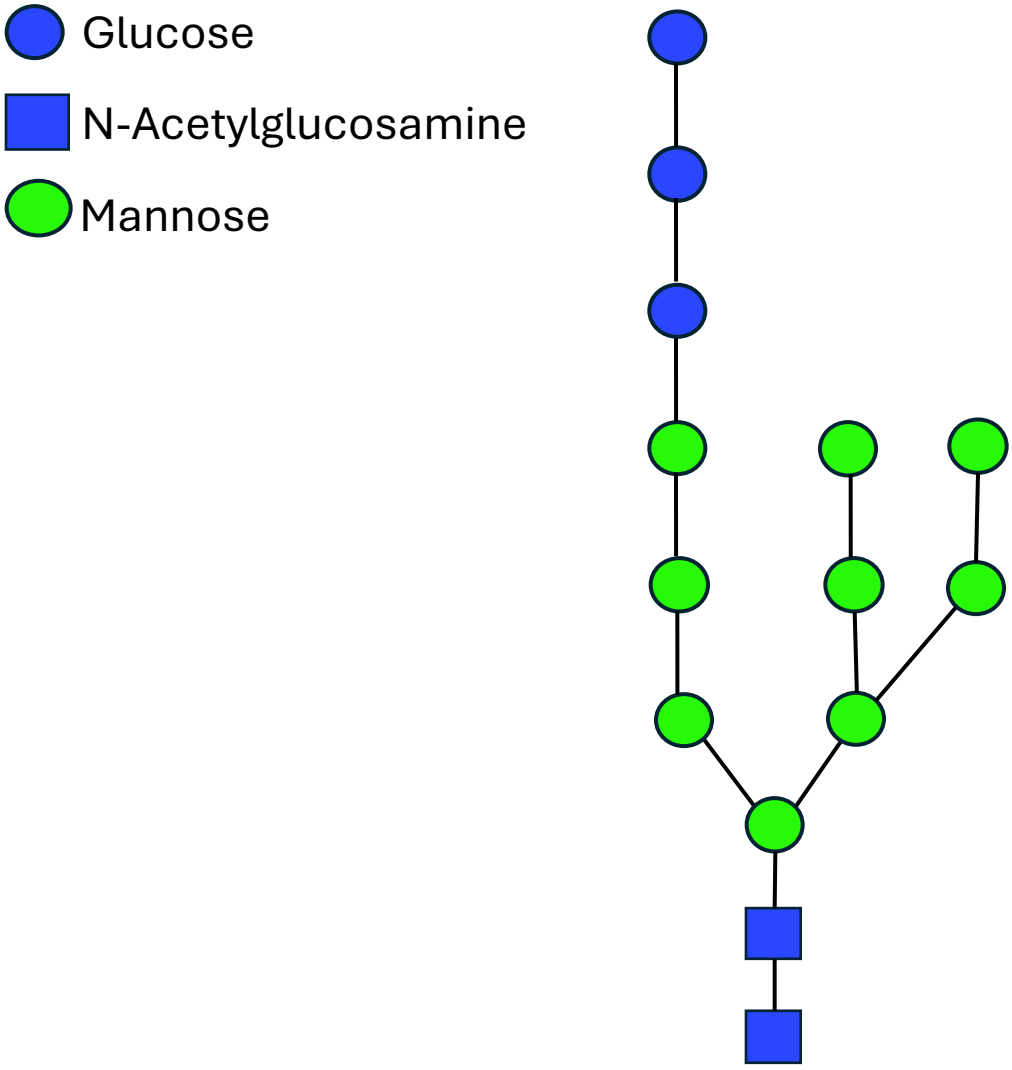

Precursor N-glycan

Figure 1.3 Precursor Glycan Structure – The glycan precursor structure is $GlcNAc_2Man_9Glc_3$. The Glc residues are added in the ER lumen by AL6, ALG8, and ALG10. Glucose residues are removed before the N-glycosylated protein continues through the secretory pathway. If the Glu is remaining the protein will continue to be acted upon by the calnexin and calreticulin cycle chaperone systems or undergo degradation.

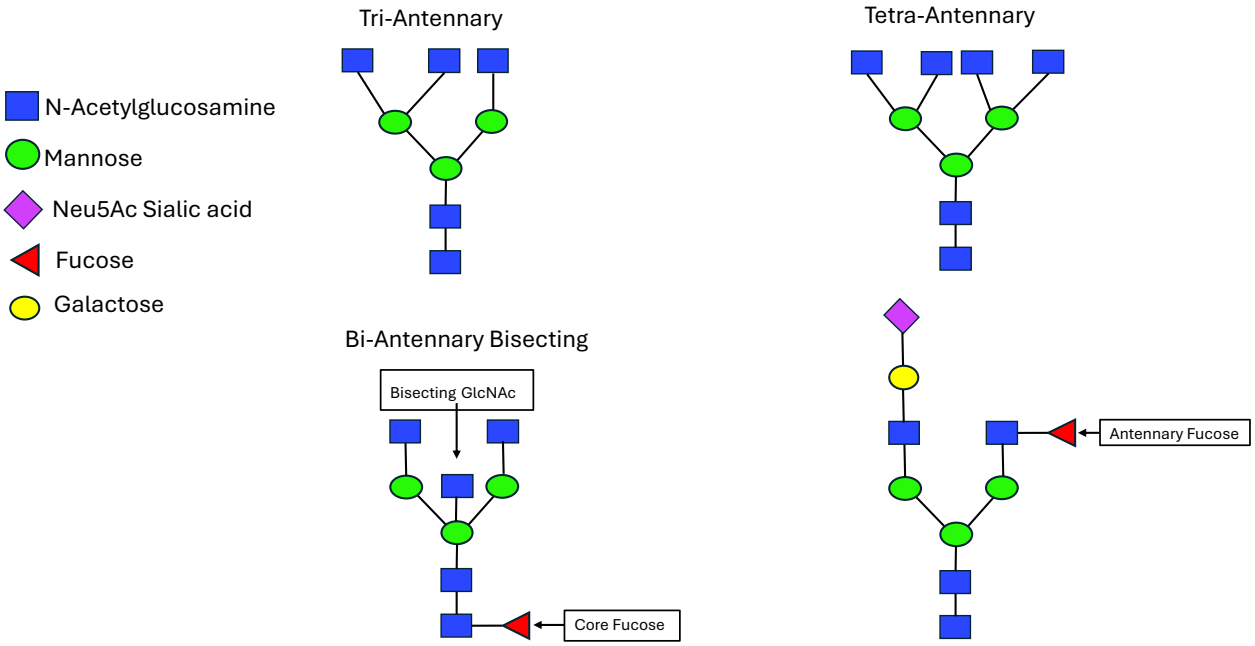
N-Acetylglucosamine
Mannose
Neu5Ac Sialic acid
Fucose
Galactose
Tri-Antennary
Tetra-Antennary
Bi-Antennary Bisecting
Bisecting GlcNAc
Core Fucose
Antennary Fucose

Figure 1.4 Common N-Glycan Structures – Complex N-glycans can be processed into bi-antennary, tri-antennary and tetra-antennary structures. The addition of a bisecting GlcNaC residue to the core pentasaccharide such as that of the bi-antennary complex N-glycan (Bottom left) is known as a bisecting N-glycan. The conserved pentasaccharide can be edited further via the addition of fucose to the core by α—fructosyltransferases (FUT8 (Bottom left) or to a GlcNAc of the antennae (Bottom right). Glycan antennae can also be adorned with galactose, sialic acids, and other monosaccharides (Bottom Right).

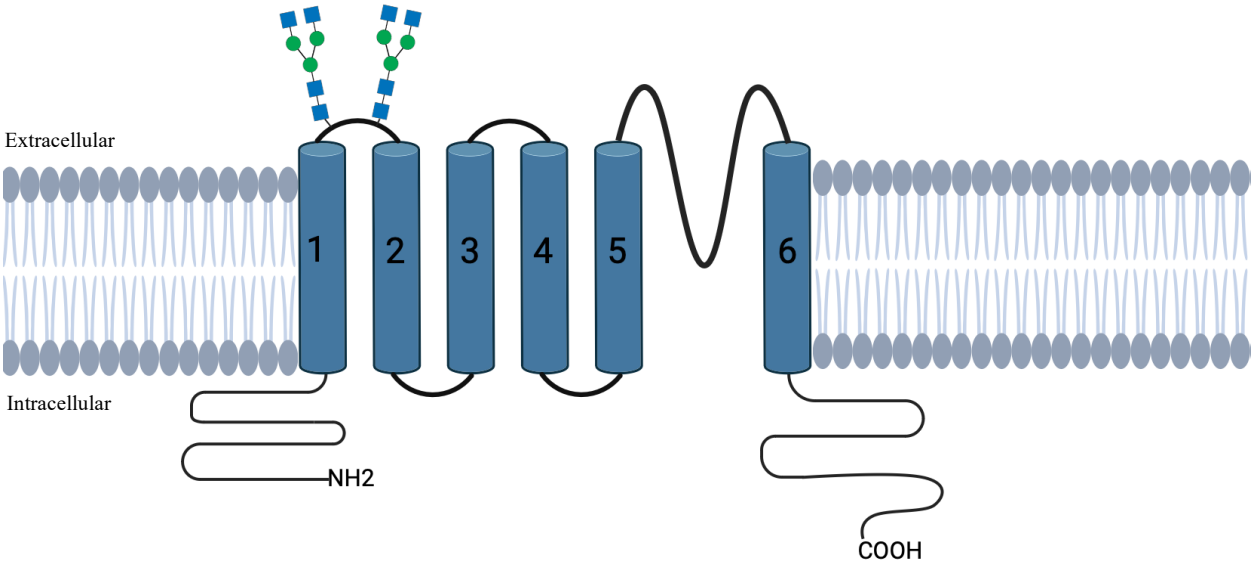
Extracellular
Intracellular
1
2
3
4
5
6
NH2
COOH

Figure 1.5: Depiction of a Kv3.1b α-Subunit - The alpha subunit is made up of six transmembrane segments connected by intra- and extra-cellular loops. There are two N-glycosylation sites present on the S1-S2 extracellular loop that are occupied by complex N-glycans. Created in BioRender.com

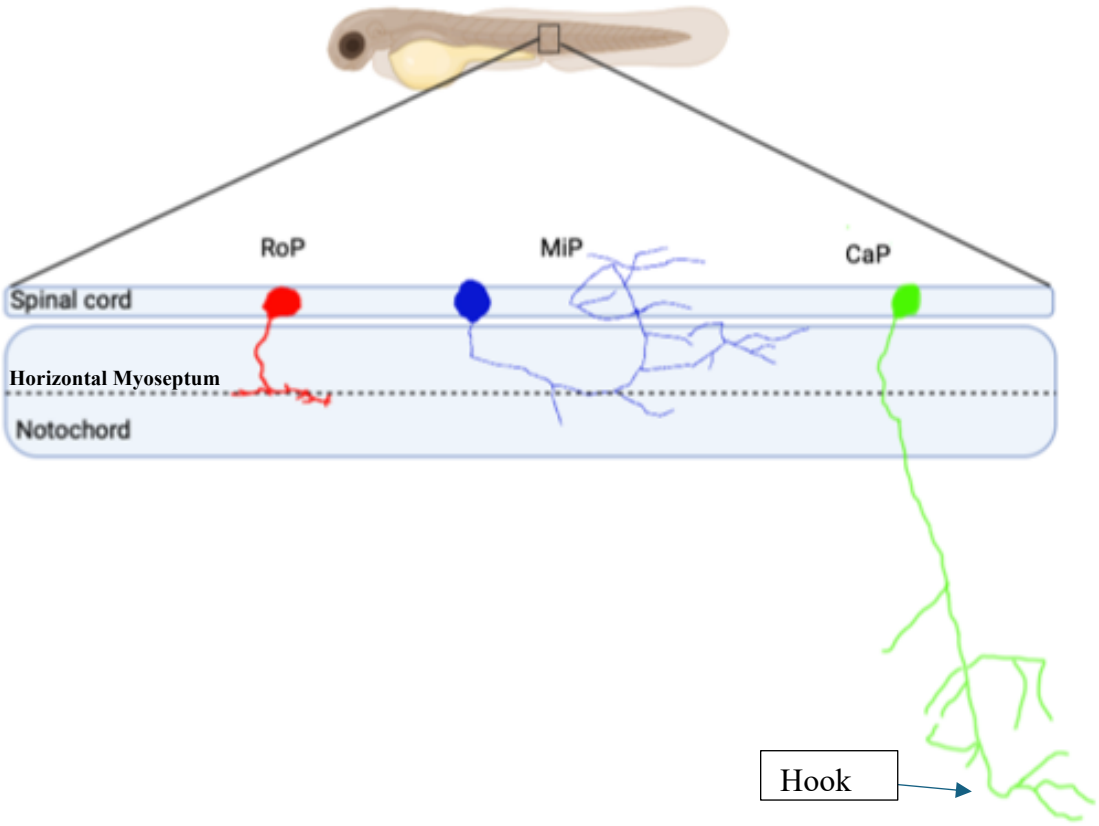
RoP
MiP
CaP
Spinal cord
Horizontal Myoseptum
Notochord
Hook

Figure 1.6 – Zebrafish Spinal Cord Primary Motor Neurons – Three of the primary motor neurons found in the spinal cord of zebrafish. These neurons are differentiated by the positions of their somas and axon trajectories. RoP is the most rostral primary neuron with an axon that extends down to the horizontal myoseptum. MiP follows the path of RoP before turning back upwards to innervate the more dorsal muscle, and the down growth will slowly recede with age. CaP axon travels down across the horizontal myoseptum and is the only primary neuron to do so before forming a hook around the ventral musculature.

Cell Line Sequences

RatNB_1: ctt gtg ctt tgg ggt gct atc atc ttt gtg ggc tgg aat gcc

RatNB_1(-*Mgat1*): ctt gtg ctt tgg ggt gct atc atc ttt gtg ggg ctg gaa tgc

RatNB_1(-*Mgat1*): ctt gtg ctt tgg ggt gct atc atc ttt gtg _gc tgg aat gcc

---

NB_1: ggtggacttcgtgttgccgg

RatNB_1(-*Mgat3*): ggtggacttcgtgttgccccgg

RatNB_1(-*Mgat3*): ggtggacttcgtgtttgg—cgg

RatNB_1(-*Mgat3*): ggtggacttcgtgtt----cgg

NB_1: atg agg ttc cgc atc tac aaa cgg aag gtg cta atc ctg acg

NB_1(-Mgat2): atg agg ttc cgc atc tac aaa ccg gaa ggt gct gat cct gac

Figure 1.7 Cell Line Sequences – The coding sequence of rat *Mgat1* from 25 to 66 was compared to that isolated from a newly created NB_1(-*Mgat1*) cell line. Two frameshift mutations were identified, including an inserted g nucleotide and a deletion of a guanine nucleotide as indicated in bold red font and dash line, respectively taken from (Hall, Burch et al. 2021) (Top). The coding sequence of rat *Mgat3* from 284 to 304 was compared to that of a newly created NB_1(-*Mgat3*) cell line (Middle) taken from (Hall, Shajahan et al. 2023). NB_1 (-*Mgat2*) has the Mgat2 gene silenced, resulting from insertion of cytosine after the 22nd nucleotide. This inserted nucleotide is denoted in bold red font and the red font reveals the different codons in the sequence taken from (Hall, Weidner et al. 2017)(Bottom).

CHAPTER II: Kv3-Expressing Cells Present More Elaborate N-Glycans with Changes in Cytoskeletal Proteins, Neurite Structure and Cell Migration

This chapter is modified from M Kristen Hall et al, Kv3-Expressing Cells Present More Elaborate N-Glycans with Changes in Cytoskeletal Proteins, Neurite Structure and Cell Migration. COJ Biomed Sci Res. 2(3). COJBSR. 000540. 2023.

Summary:

The cues contained by N-glycans relay the quality, cellular destination, and interactions of proteins, thereby, impacting cellular physiology. Voltage-gated K^+ (Kv3) channels have two conserved N-glycosylation sites which are vital for Kv3 channel activity, and primary motor neuron development. Our previous studies showed that the parental (NB_1) and N-glycan mutant (NB_1(-*Mgat1*), NB_1(-*Mgat2*), and NB_1*(-Mgat3*)) Neuroblastoma (NB) cell lines have compromised N-acetylglucosaminyltransferase activities: GnT-I, GnT-II, or GnT-III. Herein, we stably expressed Kv3.1b in the parental and engineered N-glycan mutant Neuroblastoma (NB) cell lines to examine how changes in N-glycans alter the cytoskeleton, and subsequently cellular properties. MALDI-TOF MS verified that the parental and mutant cell lines had different N-glycan profiles. When Kv3.1b was expressed in NB cells with an intact Mgat1, the N-glycan population had more complex N-glycans with increased branching. Further NB cells with an intact Mgat2 had higher and lower levels of hybrid and oligomannose N-glycans, respectively. N-Glycan populations changed cytoskeletal protein abundancies and cell morphology. Moreover, all Kv3.1b-expressing cells, except NB_1(-*Mgat2*), had changed levels of F-actin, neurofilament and vimentin, along with modified neurite formation. In all cases, migratory rates were enhanced when cells expressed WtKv3.1b. Glycan populations and glycans attached to Kv3.1b altered spatial arrangement in membranes and both ER folding and transport proteins were not increased

by expression of unglycosylated Kv3.1b. Kv3.1b expression in NB cells alters N-glycan populations and mediates adjustments in cytoskeletal proteins, and thereby cell morphology and cell migration, supporting roles in neuronal development and maintenance.

Introduction:

Defects in the N-glycosylation pathway result in conditions known as Congenital Disorders of Glycosylation (CDG)(Chang, He et al. 2018). Although CDGs affect different organ systems, the neurological impact is detrimental and is noted in most types (Verheijen, Tahata et al. 2020). Glycosylation is a post translational modification necessary for protein development, function, and stability. As such, glycosylation is paramount in the development of an organism. The glycosylation process occurs via the addition of monosaccharides to proteins (Verheijen, Tahata et al. 2020). N-glycosylation is characterized by the addition of an oligosaccharide to a protein at an asparagine residue via an N-glycosidic bond. The three major types of N-glycans are classified as oligomannose, hybrid, and complex (Stanley 2022). N-glycans are composed of a conserved pentasaccharide region, and processing occurs via the actions of N-Acetylglucosaminyltransferases (GnTs), which are enzymes encoded by *MGAT* genes. GnTs add a GlcNAc residue to the conserved pentasaccharide yielding the various types of N-glycans. GnT-I activity promotes the transition from oligomannose to hybrid type N-glycans, while GnT-II converts hybrid glycans to complex type N-glycans. GnT-III adds a bisecting GlcNAc residue and results in termination of glycan processing (Stanley 2022). For this reason, evaluation of how modifications in N-glycan content of cells, including processing of N-glycosylated proteins (e.g., voltage-gated ion channels), is a critical area of research for therapeutic development of CDG and neurodegenerative diseases. Voltage-gated Kv3 channels are a family of potassium

ion channels that are associated with high-frequency firing neurons because of their unique depolarized activation range and rapid activation/deactivation rates (Grissmer, Ghanshani et al. 1992, Kanemasa, Gan et al. 1995, Kaczmarek and Zhang 2017). In addition to the traditional conducting role of ion channels, Kv3 also regulates cell signaling, cell adhesion, and cytoskeleton networks through its non-conducting roles (Kaczmarek 2006). The conducting and non-conducting functions of Kv3 are essential for proper neurodevelopment as alterations in the activity or expression of Kv3 has been linked to various neurodevelopmental disorders (Waters, Minassian et al. 2006, Zhang, Varela et al. 2021) and cancer (Ousingsawat, Spitzner et al. 2007). N-glycosylation has been shown to influence both conducting and non-conducting roles of Kv3 channels. Removal of one or both conserved N-glycosylation sites of the α-subunit of Kv3.1, along with replacement of complex N-glycans of Kv3.1 with oligomannose or hybrid, was shown to reduce cell migration, encourage localization of Kv3 in the cell body rather than the neurites, hinder the opening and closing kinetics of Kv3 channels, and reduce neurite length in rat neuroblastoma cells (Hall, Cartwright et al. 2011, Hall, Weidner et al. 2017, Issa, Hall et al. 2021). Furthermore, Kv3 channels with only one of the two conserved N-glycosylation sites occupied resulted in shortened axons and reduced synapse formation of motor neurons in zebrafish.

Protein folding and quality control within the Endoplasmic Reticulum (ER) are regulated by molecular chaperones. These ER chaperones are crucial to the regulation/maintenance of ER stress response, intracellular signaling, proper protein folding and Ca^{2+} storage (Halperin, Jung et al. 2014). Proper N-glycosylation of proteins is regulated by two different families of chaperones: Heat Shock Proteins (HSP), which interact with unglycosylated and glycosylated proteins; and lectins that interact with incompletely folded glycosylated proteins (Pobre, Poet et

al. 2019). Grp94 and Bip belong to the HSP family of ER chaperones, and they are responsible for directing misfolded N-glycosylated proteins for degradation or correction (Dorner, Bole et al. 1987, Marzec, Eletto et al. 2012). Likewise, Calreticulin belongs to the lectin family and is a calcium binding protein that assists in proper protein folding (Fucikova, Spisek et al. 2021). Calreticulin acts within the calnexin/ calreticulin cycle which dictates the shuttling of glycosylated proteins from the ER to the Golgi apparatus (Schroder and Kaufman 2005). ER function also involves ER transport proteins. The kinesin superfamily proteins (KIFs) are involved in bidirectional mobility from the ER, and neuronal cells have an advanced transport system . For instance, KIF5 (kinesin-1) is the most abundant microtubule motor protein and is vital for axonal transport (Hirokawa and Noda 2008). Cytoskeletal proteins, such as actin filaments, intermediate filaments and microtubules, help to form the shape of the cell, assist in movement, and play fundamental roles in neuronal development (Fletcher and Mullins 2010). The function and role of actin is highly dependent upon its ability to self-polymerize into actin filaments (F-actin) or depolymerize into Globular Actin (G-actin) (Konietzny, Bar et al. 2017). Vimentin, an intermediate filament, has been linked to neurons undergoing differentiation and neurite extension, and is thought to be associated with neuronal damage in Alzheimer's patients . Neurofilament, like vimentin, is involved in neuronal development, but is associated with more differentiated/mature neurons (Nixon and Shea 1992, Yabe, Chan et al. 2003, Yuan, Rao et al. 2017). In fact, Yabe et al. (Yabe, Chan et al. 2003) describes a transition from vimentin to neurofilament as part of neuronal development. Here we examine Neurofilament-Light chain(NF-L), which has been implicated as a biomarker in the progression of Parkinson's disease (Mollenhauer, Dakna et al. 2020, Aamodt, Waligorska et al. 2021), and other neurodegenerative diseases. Our goal of this paper was to determine whether Kv3.1b expression in NB cell lines

with different N-glycan populations, could influence the N-glycosylation pathway, and consequently, cell structure and function in cultured Neuroblastoma (NB) cells, a neuronal-derived cell model. Previously, ESI-MS studies showed that our engineered N-glycan mutant cell lines NB_1(- *Mgat*1), NB_1(-*Mgat*2) and NB_1(-*Mgat*3) have compromised N-acetylglucosaminyltransferase (GnT-I), (GnT-II), or (GnT-III) activities, relative to the parental cell line (Hall, Shajahan et al. 2023). Here MALDI-TOF MS was employed to compare N-glycan populations in non-transfected NB cell lines, and NB cell lines stably transfected with wild type (Wt) Kv3.1b. Western blotting was utilized to examine N-glycosylation of Kv3.1b in NB cell lines transfected with Kv3.1b. This technique was also employed to compare expression levels of ER chaperone (Grp94 and calreticulin) and ER transport (KIF5B) proteins, along with proteins of the cytoskeletal network (F-actin, vimentin, and neurofilament-L), in parental and glycosylation mutant NB cell lines without and with expression of Wt Kv3.1b. Changes in cytoskeleton protein levels supported modifications in neurite structure and cell mobility. Taken together, we postulate that changes in the N-glycosylation pathway and Kv3.1b levels mediate adaptions to neurite structure and cell migration through cytoskeletal and ER proteins which are needed for neuronal development and maintenance.

Materials and methods

Cell lines, cell culture and cell transfection

NB_1 is a clonal cell line derived from Rat B35 Neuroblastoma (NB) (American Type Culture collection, Manassas, VA, USA) and was the parental cell line utilized to engineer the glycosylation mutant cell lines (NB_1(-*Mgat*1) and NB_1(-*Mgat*2), and NB_1(- *Mgat*3) via CRISPR/Cas9 technology (Hall, Shajahan et al. 2023). The different N-glycan populations in the

various cell lines were identified via ESI-MS supporting at least partial knock-down of the mutant cell lines [30]. The construction of the NB_1, NB_1(-*Mgat*1) and NB_1(-*Mgat*2) cell lines stably expressing Wt (wild type) or N220/229Q Kv3.1b were previously described [12], and NB_1(-*Mgat*3)_Wt Kv3.1b and NB_1(-*Mgat*3)_N220/229Q Kv3.1b cell lines were completed in a similar manner. In all cases, an EGFP tag is fused to the C-terminus of Kv3.1b. All cells were maintained in DMEM containing 10% FBS, 50U/mL penicillin, and 50µg/mL streptomycin at 37˚in a 5% CO_2 atmosphere.

Total membrane protein fractions and whole cell lysates of NB cells

Harvesting of total membranes was performed via ultracentrifugation as described previously (Hall, Weidner et al. 2017). Whole cell lysates were collected in RIPA buffer (PBS, 1% Triton X-100, 0.5% sodium deoxycholate, 0.1% SDS) containing protease inhibitor cocktail set III (EMD Biosciences San Diego, CA, USA) (Hall, Cartwright et al. 2011). Samples were reduced/denatured for western blotting by addition of SDS-PAGE sample buffer. Samples were stored at -20˚C until needed.

F-actin and G-actin Isolation

Cells were resuspended in LAS3 buffer (50mM Pipes, 50mM NaCl, 5mM $MgCl_2$, 5mM EGTA, 5% Glycerol, 0.1% Nonidet P40, 0.1% Triton X100, 0.1% Tween 20, 0.1% 2-mercaptoethanol, 0.001% Antifoam C, 1mM ATP, 1mM Tris pH7.5, and protease inhibitor cocktail set III (EMD Biosciences San Diego, CA, USA) by scraping and gentle pipetting, and then incubated at 37˚for 10 min. An aliquot of resuspended cell solution was transferred to a clean Eppendorf tube and spun at 2,000rpm for 5 minutes. The remaining cell solution was stored at -20˚for future use.

The supernatant was transferred to an ultracentrifuge tube and then spun at 100,000x g for 1h at 37˚using a Beckman Coulter Optima^{TM} MAX-XP ultracentrifuge (Beckman Coulter, Brea, CA). The supernatant, containing G-actin, was transferred to an Eppendorf tube while the pellet, containing the F-actin, was resuspended in 100µL depolymerization buffer (5mM Tris HCl, 8M urea). Samples were stored in reducing buffer containing 2% 2-mercaptoethanol at -20˚for future use.

Western blotting

Total membranes from Kv3.1b transfected cells were separated on 10% SDS gels at 20mA and transferred to PVDF membranes (Millipore, Billercia, MA, USA) at 0.25 A, as previously described (Chen, Tan et al. 2020). Subsequently, transferred membranes were incubated with anti-Kv3.1b (NeuroMab, Davis, CA, USA) antibody and visualized with NBT/BCIP. Multiplex fluorescent western blotting was used for quantification of the protein of interest. In short, whole cell lysate samples from Kv3.1b transfected and non-transfected cells were electrophoresed on Any kD^{TM} or 10% SDS gels (Biorad, Hercules, CA). Separated proteins were transferred to PVDF membranes and were incubated in EveryBlot Blocking Buffer, primary, and secondary antibodies, and then imaged using a ChemiDoc MP imaging system which allowed visualization of two proteins simultaneously using fluorescent antibodies. Primary antibodies include: BiP, vimentin, calreticulin, Grp94, neurofilament-L (NF- L) and KIF5B from (Cell Signaling Technology, Danvers, MA) and rhodamine conjugated β-actin (Biorad, Hercules, CA). Secondary antibodies (Biorad, Hercules, CA) include anti-mouse IgG starBright Blue 700, anti-rabbit IgG starBright Blue 700, anti-mouse IgG starBright Blue 520, anti-rabbit IgG starBright Blue 520. Image Lab software (Biorad, Hercules, CA) was used for data acquisition and

quantification of the immuno-band of interest. The protein of interest and β-actin were simultaneously analyzed in a single sample on the same blot which allowed for correction of sample load and the transfer of proteins from gel to membrane. The ratio of immuno-band intensities for the protein of interest and β-actin were determined in a single sample. The means of ratio values for a given protein from at least 3 separate loads were determined, and thus plotted relative to β-actin.

N-Glycomics method

Glycan profiling was performed like previously described (Shajahan et al., 2020) Total membrane protein fractions extracted from NB cells were diluted with 100µl of 50mM ammonium bicarbonate buffer. Subsequently, 25µL of 25mM Dithiothreitol (DTT) was added and incubated at 50 °C for 30min. The samples were desalted by centrifugation via Amicon centrifuge filters (MilliporeSigma, Cat. No. UFC501096). Desalted samples were then ultrasonicated to dissolve the proteins. 5µL of PNGaseF (New England Biolabs, Cat. No. P0709L) was added to desalted ultrasonicated samples followed by incubation at 37 °C for 48h to release the N-glycans. Addition of water quenched the reaction and permethylated N-glycans were extracted with dichloromethane. The dichloromethane layer was rinsed four times with water and dried via evaporation by nitrogen gas. Permethylated N-glycans were redissolved in 20µL of methanol. 1µL of a mixture of 1µL of the permethylated N-glycans and 1µL of DHB (dihydrobenzoic acid) matrix (10mg/mL in 1:1 methanol-water was spotted on a MALDI plate and analyzed by MALDI-TOF-MS (ABSciex MALDI- TOF/TOF 5800 mass spectrometer). GlycoworkBench software was used to identify the N-glycan structures based on precursor

masses (sodium adduct) obtained by MALDI-TOF-MS and common mammalian biosynthetic pathway (Hall, Shajahan et al. 2023).

Wound Healing assay

Cell migration assays were performed as previously described (Hall, Weidner et al. 2013). In brief, non-transfected and Kv3.1b transfected NB cells were plated on 60 mm cell bind dishes (Corning, Corning, NY, USA) and allowed to grow to confluency. Culture medium was then aspirated, and cell monolayer was disrupted using a beveled 200µl pipette tip (Fisher Scientific, Suwanee, GA, USA). Cellular debris was removed from the plate by washing dish two times with DMEM. DMEM was added to plate and images were obtained at 0- and 19-hour time points (4x objective) using an Olympus IX73 Microscope (Olympus, Shinjuku City, Tokyo, Japan). Wound size was measured using Adobe Photoshop (Adobe Inc., San Jose, California, USA). Initial wound size (0 hour) and final wound size (19 hour) was determined, and percent wound closure was calculated using the following equation: $\frac{initial\ wound\ size - final\ wound\ size}{inital} * 100$. The mobility due the N-glycan was calculated using the following equation: $\frac{glycosylated\ Kv3.1b\ cell\ mobility - unglycosylated\ Kv3.1b\ mobility}{unglycosylated\ Kv3.1b\ mobility}$.

TIRF Microscopy

Microscopy images were captured and analyzed as previously described (Hall, Weidner et al. 2015). In brief, Kv3.1b-EGFP transfected cells were seeded at low density on 35 mm poly-L-lysine glass bottom dishes followed by 18hrs incubation. Images were acquired using an Olympus IX-71 microscope (Olympus, Center Valley, PA, USA) with an Apo 60x 1.45 objective with all laser controls mediated by Cell^TIRF 1.1 with Metamorph software. Cell excitation was mediated via a

488nm Argon laser with 1000 ms exposure time. The percent of protein localized to the neurites was calculated using ImageJ software. The percent of Kv3.1b in the neurites was determined by dividing area of fluorescent intensity of the neurites by area of fluorescent intensity of the entire cell.

Confocal Microscopy

Kv3.1b-EGFP transfected cells were plated on 35 mm poly-L-lysine glass bottom dishes. Imaging was carried out after 18 hours post incubation using a Carl Zeiss LSM 700 Microscope using either Plan-Apochromat 40x/1.40 oil immersion DIC M27 objective. Optical sectioning was performed at 1µm increments to generate image stacks. Excitation of the tagged Kv3.1b protein was performed using a 488nm solid state laser with a frame size of 2048 x 2048 pixels, 8-bit image depth and a scanning speed of 6. Image stacks were compressed and the percent of Kv3.1b in the neurites was calculated using ImageJ software. Measurements were obtained for both the entire cell and the neurites individually. The percent of Kv3.1b in the neurites was determined by dividing area of fluorescent intensity of the neurites by area of fluorescent intensity of the entire cell. In all cases, bright field images were obtained to verify neurite and soma areas.

Data Analysis

Adobe Photoshop was utilized for Western blot pictures. Western blots were quantified using Bio-Rad Image Lab 6.1. Graphics and statistics were obtained using Origin 9.55. Data are presented as the mean S.E. where *n* signifies the number of observations. Statistical comparison between two groups was completed using Student's t-test. One-way ANOVA with Bonferroni adjustments was implemented when comparing more than two groups, unless otherwise denoted.

Results

Expression of glycosylated and unglycosylated Kv3.1b NB cells

Herein we investigated whether expression of Wt Kv3.1b in rat parental (NB_1) and N-glycosylation mutant NB_1 cell lines could alter N-glycan populations and cellular properties. The mutant cell lines (NB_1(-*Mgat1*), NB_1(-*Mgat2*) and NB_1(-*Mgat3*)) have different N-glycan profiles due to compromised activity of a N-acetylglucosaminyltransferase (GnT-I, -II, or -III) (Hall et la., 2023). GnT-I catalyzes the conversions of oligomannose to hybrid while GnT-II converts hybrid to complex (Stanley, Taniguchi et al. 2015). GnT-III (encoded by *Mgat3*) catalyzes the addition of bisecting GlcNAc residues to hybrid and complex N-glycans to create N-glycans with bisecting GlcNAc residues (Chen, Tan et al. 2020). Moreover, the presence of a bisecting GlcNac residue terminates processing of N-glycans. Western blotting of total membrane proteins from the N-glycosylation mutant and parental cell lines expressing Wt Kv3.1b protein showed that the glycosylated Kv3.1b protein (green arrowhead) expressed in NB_1(-*Mgat3*) had a slower electrophoretic mobility compared to Kv3.1b (yellow arrowhead) in NB_1 (Figure 1). This is expected, if the activity of GnT-III was reduced, since the addition of a bisecting GlcNAc prevents processing of the N-glycan. In both cases, the faint lower band denotes oligomannose-containing Kv3.1b glycoprotein (pink arrowhead) (Hall, Cartwright et al. 2011). When the unglycosylated (N220/229Q) Kv3.1b protein was expressed in NB_1(-*Mgat3*) cells, N220/229Q Kv3.1 (green line) migrated much faster, as expected (Hall, Cartwright et al. 2011). The N-glycan types attached to glycosylated Kv3.1b in NB_1, NB_1(-*Mgat2*), and NB_1(-*Mgat1*) are complex (Cartwright and Schwalbe 2009), hybrid (blue arrowhead) (Hall, Weidner et al. 2017), and oligomannose (Issa, Hall et al. 2021), respectively. Taken together, the results suggest that N-glycans attached to Kv3.1b in NB_1(-*Mgat3*) cells are of complex type but different from those

attached to Kv3.1b in NB_1 cells. For instance, the increased mobility of glycosylated Kv3.1b may have complex N-glycans which are more branched and/or greater extension of the antenna.

Expression of Wt Kv3.1b in neuronal-derived cells enhanced processing of N-glycans

To identify specific glycan structures, isolated permethylated N-glycans of the parental and N-glycosylation mutant cell lines without and with Wt Kv3.1b were analyzed by MALDI-TOF MS (Cho, Veillon et al.). The permethylated N-glycans were produced and purified by labeling N-glycosylated protein from total membranes of various NB cells grown under standard 2D cell culture conditions. Mass spectra of N-glycan structures from NB_1 (Figure 2.2A), NB_1_Wt Kv3.1b (Figure 2.2B), NB_1(-*Mgat3*) (Figure 2.2C), NB_1(-*Mgat3*)_Wt Kv3.1b (Figure 2.2D), NB_1(-*Mgat2*) (Figure 2.3A), NB_1(-*Mgat2*)_Wt Kv3.1b (Figure 2.3B) and NB_1(-*Mgat1*) (Figure 2.3C) cell lines. NB_1, NB_1(-*Mgat2*) and NB_1(-*Mgat3*) cell lines contained detectable levels of oligomannose, hybrid, and complex types of N-glycans while only oligomannose N-glycans were detected in the NB_1(-*Mgat1*) cell line. Since the NB_1(-*Mgat1*) cell line had only oligomannose type N-glycans, N-glycan profiling was not conducted for NB_1(-*Mgat1*)_Kv3.1b. Two more spectra for NB_1 cells (Figure 2.S1), and the relative abundancies of each of the glycan structures from all spectra are shown in the supplementary section (Figure 2.S2 & 2.S3). Of interest, the N-glycan profiles appeared to have raised levels of complex and hybrid types of N-glycans in NB_1, NB_1(-*Mgat3*), and NB_1(-*Mgat2*) expressing Kv3.1b. The red exclamation mark signifies N-glycans that were solely observed in the nontransfected cell lines while the green exclamation marks denote N-glycans which increased when Kv3.1b was expressed in the cell lines.

The pie graphs show the levels of complex (blue), hybrid (Pivac, Knezevic et al.) and oligomannose (Panousopoulou, Hobbs et al.) types of N-glycans in each of the NB cell lines (Figure 2.4A). When NB cells were stably transfected with glycosylated Kv3.1b, both NB_1_Wt

Kv3.1b and NB_1(-Mgat3)_Wt Kv3.1b cell lines increased levels of complex and hybrid types while the oligomannose type decreased. The NB_1(-Mgat2)_Wt Kv3.1b cell line also increased the level of complex type N-glycan which was accompanied with a decrease in hybrid type N-glycans. Fucosylation of all types of N-glycans were increased in Kv3.1b-expressing NB_1 and NB_1(-*Mgat3*) cells (Figure 2.5B). Further the level of fucosylated complex and oligomannose types of N-glycans were higher in NB_1(-*Mgat2*) cells expressing Wt Kv3.1b. The branching of the complex type of N-glycans were increased in Kv3.1b-expressing cell (Figure 2.5C). Although the levels of both bi- and tri-antennary complex N-glycans were higher in all three cell lines expressing Wt Kv3.1b, there was a much larger increase in the levels of tri-antennary complex N-glycans. Moreover, the level was highest in the NB_1(-*Mgat*3)_Wt Kv3.1b cell line. Thus, these results indicate that Kv3.1b-expressing cells increase the level of complex type N-glycans, along with increased branching.

Types of N-glycan and Kv3.1b expression influence neurite structure

The morphology of the NB_1 cells consisted of a soma, one to several projections (neurites) from the cell body and projections from the tips of neurites (neurite tip projections) (Figure 5A). Arrows point to the various neurite tip projections. Neurite tips enclosed with circles were increased by 3-fold magnification to clearly show filopodia (pink), lamellipodia (yellow) and a mix of filopodia/lamellipodia (Pivac, Knezevic et al.). The number of neurites per cell were relatively similar in the parental and N-glycosylation mutant NB_1 cell lines (Figure 5B). However, differences could be detected when the cells were stably transfected with glycosylated Kv3.1b. Both NB_1(-*Mgat1*)_Wt Kv3.1b and NB_1(-*Mgat3*)_Wt Kv3.1b cell lines were more likely to express more than two neurites per cell than either NB_1_Wt Kv3.1b or NB_1(-*Mgat2*)_Wt

Kv3.1b cell lines. Types of N-glycans altered the length of neurites in NB cells. Neurite length of both NB_1(-*Mgat1*) and NB_1(-*Mgat2*) cell lines were reduced to about 65% relative to those of NB_1 and NB_1(-*Mgat3*) cells (Figure 5C). When Wt Kv3.1b was expressed in both NB_1 and NB_1(-*Mgat3*) cells, there was a decrease in neurite length while expression in NB_1(-*Mgat1*) caused an increase in neurite length. The expression of Wt Kv3.1b in NB_1(-*Mgat2*) cells lacked an effect on neurite number and neurite length. Hence, NB cells expressing more processed N-glycans had longer neurites than those with less processed N-glycans. Further expression of Wt Kv3.1b in the various cell lines could impact neurite number and length.

NB cells were characterized by the percent of neurites that had structural projections from their tips, referred to as neurite tip projections (Figure 2.5D). In all cases, the non-transfected cell lines had similar levels of neurite tip projections. Expression of Wt Kv3.1b in NB_1(-*Mgat1*) had a significant increase in the number of neurite tip projections relative to its non-transfected cell line, as well as the other Kv3.1b expressing NB cell lines. To further elaborate, the neurite tip projections were categorized as having hair-like projections (filopodia), sheet-like projections (lamellipodia) and hair-like and sheet-like projections (filopodia/lamellipodia), respectively (Figure 5E, F, G). Nontransfected NB_1, NB_1(-*Mgat1*), and both NB_1(-*Mgat2*) and NB_1(-*Mgat3*) cell lines had the highest level of filopodia, lamellipodia, and filopodia/lamellipodia, respectively. Expression of Wt Kv3.1b in NB_1 cells greatly reduced and increased the levels of filopodia and lamellipodia, respectively. Kv3.1b expression in NB_1(-*Mgat1*) cells had decreases and increase in lamellipodia and filopodia/lamellipodia, respectively. The NB_1(-*Mgat3*)_Wt Kv3.1b cells had a decrease in the level of filopodia, like the parental cell line, but had an increase in the percent of filopodia/lamellipodia. The types of neurite tip projections were unchanged in

NB_1(-*Mgat2*) when they were transfected with Wt Kv3.1b. Overall, all four nontransfected cell lines had different levels of filopodia, lamellipodia, and filopodia/lamellipodia at the tips of their neurites. The percent of neurite tip projections only increased in NB_1(-*Mgat1*) cells in response to expression of Wt Kv3.1b; however, the type of structures at the tips of the neurites were different for NB_1_Wt Kv3.1b, NB_1(-*Mgat1*)_Wt Kv3.1b and NB_1(-*Mgat3*)_Wt Kv3.1b cell lines compared to their nontransfected cell lines. Of note, the morphology of NB_1(-*Mgat2*) cells were unchanged by the expression of Wt Kv3.1b. These results demonstrate that N-glycan populations and Kv3.1b expression can modify NB cell morphology.

Expression of glycosylated Kv3.1b enhances NB migratory rates

Cell migratory rates between parental and N-glycosylation mutant cell lines had less than 10% differences (Hall, Weidner et al. 2018, Hall, Whitman et al. 2020, Hall, Burch et al. 2021). Here each of the nontransfected cell lines was compared to their respective cell line expressing Wt Kv3.1b. Cell wounds were produced in NB_1, NB_1 (-*Mgat1*), NB_1 (-*Mgat2*) and NB_1 (-*Mgat3*) cells expressing Wt Kv3.1b and then allowed to recover for 19h (Figure 6A, upper panels). The nontransfected cell lines were conducted in parallel (Figure 2.6A, lower panels). The percent of wound closures were determined to quantify the cell mobility of each cell line (Figure 6B). In all cases, expression of Wt Kv3.1b increased cell migratory rates relative to their respective nontransfected cell line. Moreover, expression of Wt Kv3.1b in NB_1 and NB_1(-*Mgat1*) cells had larger changes in cell mobility compared to the other two cell lines (NB_1, 0.27 ± 0.02, n=22; NB_1(-*Mgat1*), 0.21 ± 0.05, n=13); NB_1(-*Mgat2*), 0.07 ± 0.02, n=39); and NB_1(-*Mgat3*), 0.11 ± 0.04, n=6). Thus, these results indicate that expression of glycosylated Kv3.1b enhances NB cell migratory rates.

Impact of N-glycans and Kv3.1b on actin polymerization/depolymerization and intermediate filaments in NB cells

Since cell morphology and migration were changed by N-glycan populations and Kv3.1b expression, it was determined whether these changes in the cells were accompanied by differences in the cytoskeleton. In all cases, the level of F-actin was lower than G-actin (Figure 2.7A). Quantification of F-actin to G-actin levels were lowest in NB_1(-*Mgat1*), along with NB_1, while highest in NB_1(-*Mgat2*) and NB_1(-*Mgat3*) (Figure 2.7B). The amount of F-actin dramatically increased when Wt Kv3.1b was expressed in NB_1 and NB_1(-*Mgat3*) cells. In terms of intermediate filaments, neurofilament-light chain (NF-L) immunobands were of high intensity in NB_1, NB_1(-*Mgat3*), NB_1(-*Mgat1*)_Wt Kv3.1b, and NB_1(-*Mgat3*)_Wt Kv3.1b cell lines (Figure 2.7C) while immunobands of vimentin (Vim) were of strong intensities in NB_1, NB_1(-*Mgat1*), NB_1(-*Mgat3*), and NB_1(-*Mgat1*)_Wt Kv3.1b, and those of intermediate intensities were in NB_1(-*Mgat2*), NB_1(-*Mgat2*)_Wt Kv3.1b, and NB_1(-*Mgat3*)_Wt Kv3.1b (Figure 2.7D). Quantification of the NF-L immunobands in the nontransfected cell lines showed highest expression in NB_1(-*Mgat3*) and NB_1 cell lines while the levels in NB_1(-*Mgat1*) and NB_1(-*Mgat2*) cell lines were much lower (Figure 2.7E). Expression of Wt Kv3.1b in NB_1 decreased NF-L levels while it increased levels in NB_1(-*Mgat1*) and NB_1(-*Mgat3*) cells. Vimentin abundance was lowest in NB_1(-*Mgat2*) cells, intermediate in NB_1 and NB_1(-*Mgat1*), and highest in NB_1(-*Mgat3*) cells (Figure 2.7F). Expression of Wt Kv3.1b in NB_1 and NB_1(-*Mgat3*) cells greatly reduced vimentin levels while vimentin levels were unchanged in NB_1(-*Mgat1*) and NB_1(-*Mgat2*) cells expressing Wt Kv3.1b. Taken together, the data indicated that the cytoskeletal structure was different in all four cell lines due changes in N-glycan structures.

Moreover, Kv3.1b expression in NB_1, NB_1(-*Mgat1*), and NB_1(-*Mgat3*) cells impacted expression of F-actin, neurofilament and vimentin while Kv3.1b expression in NB_1(-*Mgat2*) cells had no effect on the expression of the cytoskeletal proteins.

Relationship of N-glycans on spatial arrangement of glycosylated and unglycosylated Kv3.1 proteins in membranes of NB cells

It was shown that the distribution of glycosylated Kv3.1b to the neurites was higher than the unglycosylated Kv3.1b protein in NB_1 cells and primary cortical/hippocampal neurons using TIRF microscopy (Hall, Weidner et al. 2017) which measured the amount of Kv3.1b protein in or near the adhered plasma membrane. Micrographs using TIRF microscopy were captured for control cells (NB_1_Wt and NB_1_N220/229Q) and the NB_1(-Mgat3) cell lines stably expressing Wt Kv3.1b or N220/229Q Kv3.1b (Figure 2.8A). In all cases, glycosylated and unglycosylated Kv3.1b proteins were distributed between the soma and neurites. Quantification showed that more glycosylated Kv3.1b in NB_1(-*Mgat3*) went to the neurites than its unglycosylated counterpart, like the control (Figure 2.8B). However, the level of unglycosylated Kv3.1b in neurites of NB_1(-*Mgat3*) cells were greater than that of the control (NB_1 cell line). To extend our findings using a different technique, total Kv3.1b protein in cell membranes of neurites and cell body was measured by employment of confocal microscopy. Confocal micrographs of the parental and N-glycosylation mutant cell lines expressing either Wt or N220/229Q Kv3.1b support that more glycosylated Kv3.1b protein was trafficked to the neurites than the unglycosylated protein (Figure 2.8C). Further this finding is supported by quantification of Kv3.1 in neurites and soma in parental and N-glycosylation mutant cell lines expressing either Wt or N220/229Q Kv3.1b (Figure 2.8D). There was also a significantly higher amount of

N220/229Q Kv3.1b in neurites for NB_1(-*Mgat3*) compared to NB_1_ N220/229Q Kv3.1b cells. Both TIRF and confocal microscopy measurements indicated that more of the unglycosylated Kv3.1b protein expressed in NB_1(-*Mgat3)* cells was in neurites than soma relative to the parental cell line. These results support that the N-glycan attached to the Kv3.1b protein enhanced its distribution to neurites relative to the soma. Further this distribution was similar if determined for Kv3.1b in adhered membrane or both adhered and non-adhered membranes of cells.

Expression levels of ER folding and transport proteins in various NB cells expressing glycosylated and unglycosylated Kv3.1 proteins

Here the aim was to determine whether unglycosylated Kv3.1b proteins in NB cells with different N-glycosylation pathways had greater difficulties in folding and ER exit than glycosylated Kv3.1b protein by evaluating levels of ER chaperone and transport proteins. The three chaperone proteins evaluated were BiP, Grp94, and calreticulin (CRT). The two earlier chaperones bind to exposed protein regions of unfolded proteins while the later one binds to specific N-glycan structures of nascent glycoproteins. The ER-to-Golgi transport protein is KIF5B. Representative Western blots of BiP, CRT, GRP94 and KIF5B (Figure 2.9A), and mean intensities of a given immunoband relative β-actin were plotted to bar graphs (Figure 2.9B). In several cases, the loads were inconsistent between samples; however, using multiplex for western blotting corrects for this as the ratio of protein of interest to β-actin for a single sample are averaged and reported as relative to β-actin. As such, when evaluating immunoband intensities it is more accurate to compare immunoband of interest to that of the β-actin in each sample. The levels of BiP were not significantly different for parental and N-glycosylation mutant cell lines expressing Wt or N220/229Q Kv3.1b proteins. Expression levels of CRT were higher in NB_1(-*Mgat1*) cells

expressing of Wt Kv3.1b relative to those expressing N220/220Q Kv3.1b. When comparing the various cell lines expressing unglycosylated Kv3.1b a significant increase was detected in NB_1(-Mgat3) cells. Levels of GRP94 were higher in NB_1(-*Mgat1*) cells expressing of Wt Kv3.1b relative to those expressing N220/220Q Kv3.1b. Further NB_1(-Mgat3)_N220/229Q Kv3.1b had higher levels of GRP94 than the other three cell lines expressing unglycosylated Kv3.1b. The levels of KIF5B were similar between each of the respective cell lines expressing Wt or N220/229Q Kv3.1b proteins. However, both NB_1_WtKv3.1b and NB_1(-*Mgat2*)_WtKv3.1b cell lines expressed more KIF5B than NB_1(-*Mgat1*)_WtKv3.1b and NB_1(-*Mgat3*)_WtKv3.1b. Thus, these results indicate that expression of the unglycosylated Kv3.1b protein could fold to its mature form and exit the ER a similar ease as the glycosylated Kv3.1b protein since the levels of ER folding and trafficking proteins were not increased NB cell lines expressing unglycosylated Kv3.1b.

Discussion

Our current study showed that expression of Kv3.1 in NB cells with different perturbations in their N-glycosylation pathway resulted in changes in their N-glycan populations. The NB_1, NB_1(-*Mgat1*), NB_1(-*Mgat2*), and NB_1(-*Mgat3*) cell lines had N-glycan populations like those identified by employment of ESI- MS (Hall, Shajahan et al. 2023). When NB cells were stably transfected with glycosylated (Wt) Kv3.1b, the level of complex type N-glycans were increased in NB_1, NB_1(-*Mgat2*), and NB_1(-*Mgat3*) cell lines. Moreover, the percent of triantennary were raised from 2 to 6.7-fold in the various Kv3.1b-expressing cells. Increases in hybrid type N-glycans were also observed in cell lines with an intact Mgat2 (NB_1, and NB_1(-*Mgat3*)). In addition to N-glycans with more branchpoints, there was more fucosylated complex

and hybrid types of N-glycans in the various cell lines. These results, along with the slower electrophoretic mobility Kv3.1b expressed in NB_1(-Mgat3), support that the N-glycans of Kv3.1b are more elaborate. It should also be mentioned that decreased activity of GnT-II and -III in the various cell lines do not appear to reduce activity of glycosyltransferases (e.g., GnT-II, -III, and -IV, ST8Sia-II and -IV) that undergo N-glycosylation processing (Mikolajczyk, Kaczmarek et al. 2020) since Kv3.1b expression caused similar trends in N-glycans of the various NB cell lines. Further changes in cell migration were increased in Kv3.1b-expressing NB cells, suggesting that neither poly-α-2,8- sialyltransferases, ST8SiaII and ST8SiaIV, had reduced activity via neural cell adhesion molecule (NCAM) (Seifert, Glanz et al. 2012). Hence, the expression of Kv3.1b in NB cells promote the synthesis of more elaborate N-glycans via addition of antenna and fucose residues.

The changes in the cytoskeletal network could explain the different NB cell morphologies. It is well-established that lamellipodia structures are rich in actin while filopodia are composed of microtubules (Leterrier, Dubey et al. 2017). Here a significant increase in F-actin was observed when the percent of filopodia was decreased and the lamellipodia containing structures were increased in Kv3.1b- expressing NB_1 and NB_1(-*Mgat3*) cells. Regarding NB_1(-*Mgat1*) and NB_1(-*Mgat2*) cell lines, their levels of F-actin were unchanged as was ratio of filopodia to lamellipodia without and with Kv3.1b expression. The levels of neurofilament were greatly decreased and increased in NB_1_Wt Kv3.1b and NB_1(-*Mgat1*)_Wt Kv3.1b cells, respectively, compared to their nontransfected counterparts, which correlated with decreased and increased neurite length. These results agree with past structural studies that showed axons are composed of combined neurofilaments and microtubules (Hirokawa 1982, Schnapp and Reese 1982, Leterrier, Dubey et al. 2017). In all cases, we found that expression of Kv3.1b in the NB cell

lines enhanced cell migration. However, there was no correlation with the abundancies of the cytoskeletal proteins, such as vimentin, which has been shown to increase cell migration (Chen, Liu et al. 2023).

The different N-glycan populations were accompanied with modifications in neurite structure. We observed that neurites were longer in NB_1 and NB_1(-*Mgat3*) cell lines than NB_1(-*Mgat1*) and NB_1(-Mgat2) cell lines, and that neurite tip projections were different in all cell lines. These results support changes in N-glycosylation processing of proteins can alter cell morphology. Expression of glycosylated Kv3.1b in NB_1(-*Mgat1*) and NB_1(-*Mgat3*) cells increased neurite number, while neurite length was decreased and increased in both NB_1 and NB_1(-*Mgat3*) and NB_1(-*Mgat1*) cells, respectively, expressing Kv3.1b. The percent of neurite tips for NB_1(-*Mgat1*)_Wt Kv3.1b cells were raised while the other NB cell lines lacked this change. Further the type of structures formed at the tip of the projections were modified for NB_1_Wt Kv3.1b, NB_1(-*Mgat1*)_Wt Kv3.1b, and NB_1(-*Mgat3*)_Wt Kv3.1b relative to their nontransfected counterparts. NB_1(-*Mgat2*) cells expressing Wt Kv3.1b were virtually identical to nontransfected NB_1(-*Mgat2*). These changes in neurite structure were supported by different levels of cytoskeletal proteins, including F-actin, neurofilament and vimentin. In short, the cytoskeletal networks were different in the various NB cell lines and furthermore expression of glycosylated Kv3.1b in all NB cell lines, except NB_1(-*Mgat2*), had different cytoskeletal protein expression patterns. Taken together, these results support that change in N-glycan populations and glycosylated Kv3.1b expression alter the cytoskeletal network in the various NB cell lines, and consequently cell morphology. An anomaly was the expression of Kv3.1b in NB_1(-Mgat2) cells which lacked changes in neurite structure and cytoskeletal network. The reason for this could be due the attachment of hybrid N-glycans to glycosylated Kv3.1b (Chen,

Tan et al. 2020), and/or the high levels of hybrid N-glycans (>30%) in NB_1 cells with a mutated Mgat2 gene. Clearly, more future research is warranted to address the role hybrid N-glycans in making the NB cells resistant to changes in their cytoskeleton, as well as cell morphology, when Kv3.1b is expressed in the cell line.

The changes in the cytoskeletal network could explain the different NB cell morphologies. It is well-established that lamellipodia structures are rich in actin while filopodia are composed of microtubules (Leterrier, Dubey et al. 2017). Here a significant increase in F-actin was observed when the percent of filopodia was decreased and the lamellipodia containing structures were increased in Kv3.1b- expressing NB_1 and NB_1(-*Mgat3*) cells. Regarding NB_1(-*Mgat1*) and NB_1(-Mgat2) cell lines, their levels of F-actin were unchanged as was ratio of filopodia to lamellipodia without and with Kv3.1b expression. The levels of neurofilament were greatly decreased and increased in NB_1_Wt Kv3.1b and NB_1(-*Mgat1*)_Wt Kv3.1b cells, respectively, compared to their nontransfected counterparts, which correlated with decreased and increased neurite length. These results agree with past structural studies that showed axons are composed of combined neurofilaments and microtubules (Hirokawa 1982, Schnapp and Reese 1982, Leterrier, Dubey et al. 2017). In all cases, we found that expression of Kv3.1b in the NB cell lines enhanced cell migration. However, there was no correlation with the abundancies of the cytoskeletal proteins, such as vimentin, which has been shown to increase cell migration.

Our past studies established a mechanism of N-glycosylation processing of Kv3.1b in modulating its spatial arrangement and Kv3 channel activity in NB cells and primary neurons (Hall, Weidner et al. 2017), and furthermore we showed that fast-spiking motor neurons were maldeveloped in a multicellular organism, zebrafish, when Kv3.1b was not fully N-glycosylated

(Issa, Hall et al. 2021). A possible explanation for the hampered development could be due to ER function and/or its distribution between soma and neurites since a report showed that the N220Q Kv3.1b mutant protein was retained in the ER membrane of COS-7 cells (Vicente, Kim et al. 2018). This was addressed by expressing glycosylated and unglycosylated Kv3.1b in NB cells with different N-glycan populations. Our current results indicated that the glycosylated and unglycosylated Kv3.1b proteins were properly folding and being transported out of the ER, along with our past results that unglycosylated and partially glycosylated Kv3.1b proteins produced functional Kv3 channels in the plasma membrane (Hall, Cartwright et al. 2011). However, the level of Kv3.1b in neurites was considerably reduced for the unglycosylated Kv3.1b protein compared to the glycosylated Kv3.1b protein. In comparing the distribution of glycosylated Kv3.1b in the various cell lines, less Kv3.1b was detected in neurites of NB_1(-*Mgat1*) and NB_1(-*Mgat3*) cells relative to NB_1 and NB_1(-*Mgat2*) cells, and furthermore levels of KIF5B, an axonal transport protein (Hirokawa and Noda 2008), were lower in NB_1(-*Mgat1*) and NB_1(-*Mgat3*) cells. Future studies should unravel the link between KIF5B and N-glycan populations in axonal transport of Kv3.1b. Thus, this comprehensive study of expressing Kv3.1b in neuronal-derived cell lines with different N-glycan populations support that transport of the Kv3.1b to neurites likely contributes more greatly to underdeveloped fast- spiking motor neurons in zebrafish than ER folding and transport proteins.

Conclusion

In conclusion, we employed a systematic approach to demonstrate that disruptions in the N-glycosylation pathway influences cellular properties in neuronal-derived cell models. Moreover, expression of an N-glycosylated Kv3.1b protein yielded further changes in the N-glycan

population within each cell line, which is of great interest given the vital role of glycosylation on both the conducting (Hall, Cartwright et al. 2011, Hall, Weidner et al. 2017, Issa, Hall et al. 2021) and non-conducting (Kaczmarek 2006, Hall, Cartwright et al. 2011) functions of the Kv3 channel. Further, observations of neurite structure, including neurite tip projections, were associated with the levels of cytoskeletal proteins. Through the development of N-glycosylation mutant cell lines without and with ectopic expression of glycosylated Kv3.1b, along with the assignment of N-glycan populations of these cell lines, we demonstrate the close association of N-glycan content and cytoskeletal network in neuronal-derived cell structure/function. Consequently, the potential for targeted glyco-therapeutics for a variety of pathologies is enhanced from the results herein.

Contributions

For the work exhibited in this chapter I performed the confocal microscopy, and Wound healing assay. I contributed to the writing.

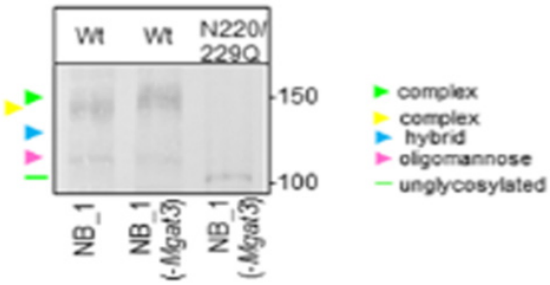
Wt
Wt
N220/
229Q
150
100
complex
complex
hybrid
oligomannose
unglycosylated
NB_1
NB_1
(-Mgat3)
NB_1
(-Mgat3)

Figure 2.1 N-Glycosylation processing of Wt. Kv3.1b is changed in NB_1(-*Mgat3*) cells relatice to the parental NB_1 cell line. Western blot of total membranes of NB_1 and NB_1(-*Mgat3*) stably expressing wild type (Wt) Kv3.1b or N220/229Q Kv3.1b. Molecular weight standards in kDa: 150,100. Arrowheads denote glycosylated Kv3.1b protein with complex (green and yellow arrowheads); oligomannose (pink), hybrid (blue) types of N-glycans. Green line denotes glycosylated Kv3.1 protein.

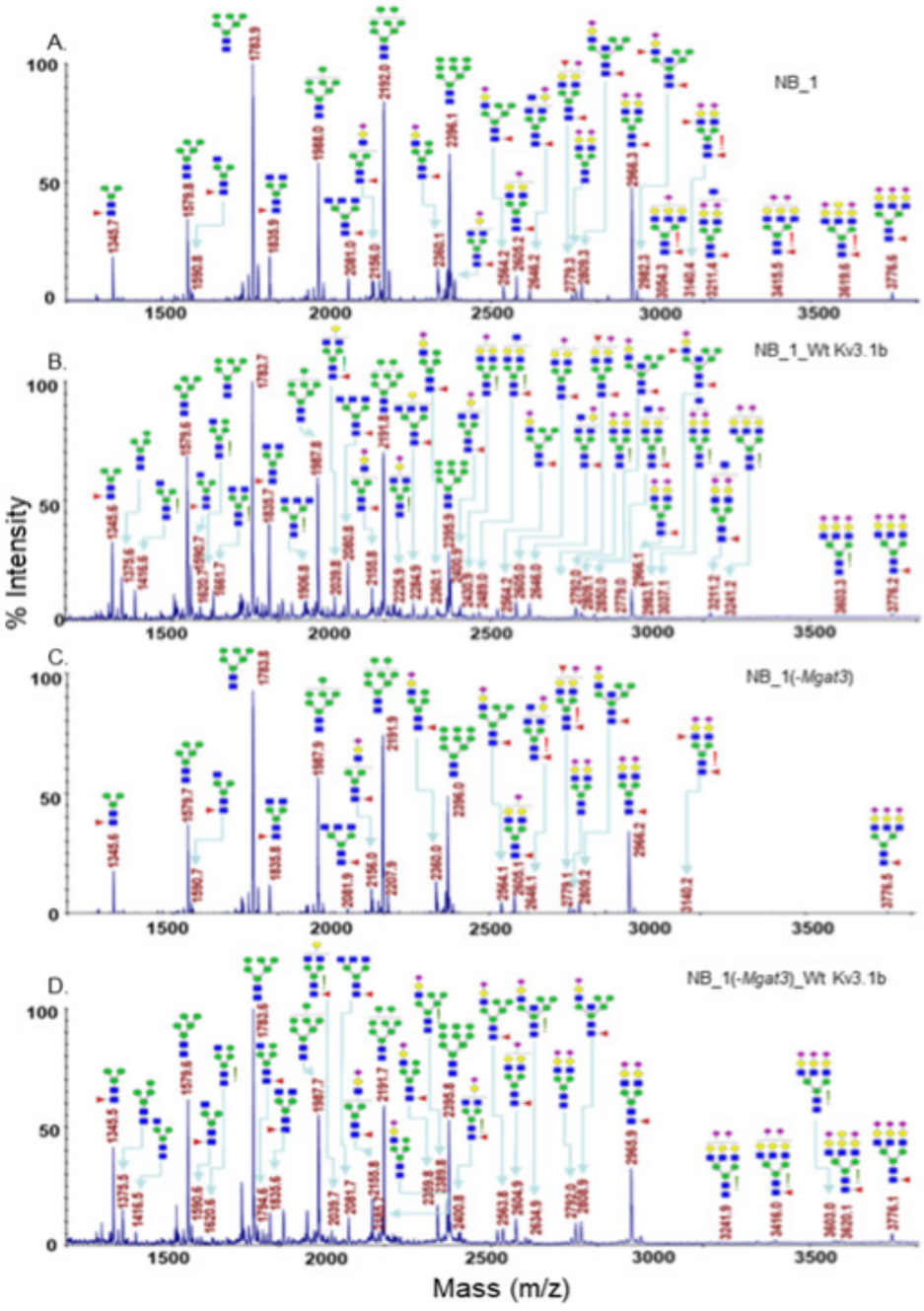
A.
NB_1
B.
NB_1_Wt Kv3.1b
C.
NB_1(-Mgat3)
D.
NB_1(-Mgat3)_Wt Kv3.1b
% Intensity
Mass (m/z)
0
50
100
1500
2000
2500
3000
3500

Figure 2.2 Comparison of MALDI-TOF MS profiles of the permethylated N-glycans derived from NB cell lines. NB cell lines without, NB_1(A) and NB_1(-*Mgat3*) (C), and with, NB_1_Wt Kv3.1b (B), and NB_1(-*Mgat3*) Wt Kv3.1b (D), glycosylated Kv3.1b expression. Data were obtained from dichloromethane extracted permethylated N0glycans with molecular ions present in sodiated form ([M+Na]+). Red exclamation points (A, C) signify N-glycans found only in NB cell lines not expressing Kv3.1b. Green exclamation points (B, D) denote increased N-glycans detected in NB cell lines expressing Kv3.1b.

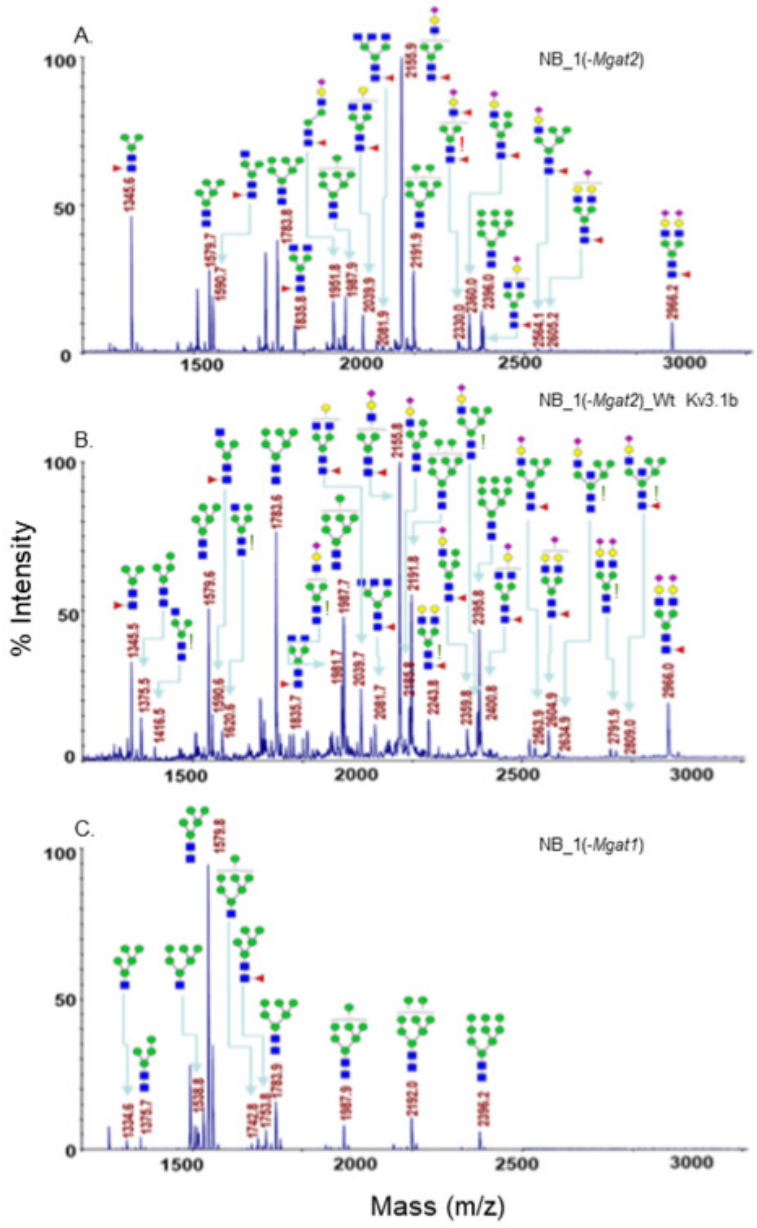
A.
NB_1(-Mgat2)
B.
NB_1(-Mgat2)_Wt Kv3.1b
C.
NB_1(-Mgat1)
% Intensity
Mass (m/z)
100
50
0
1500
2000
2500
3000

Figure 2.3 Glycan profiles of NB cell lines without an intact Mgat1 or Mgat2. MALDI- TOF MW profiles of permethylated N-glycans derived from NB_1(-*Mgat2*) (A), Nb_1(-*Mgat2*)_WtKv3.1b (B) and NB_1(-*Mgat1*) (C) cell lines. Data were obtained from dichloromethane extracted permethylated N-glycans and all molecular ions present in sodiated form ([M+Na]+). Red exclamation points (A) represent N-glycans detected only in the Nb cell lines not expressing Kv3.1b. Green exclamation points (B) signify increases in the NB cell lines expressing Kv3.1b.

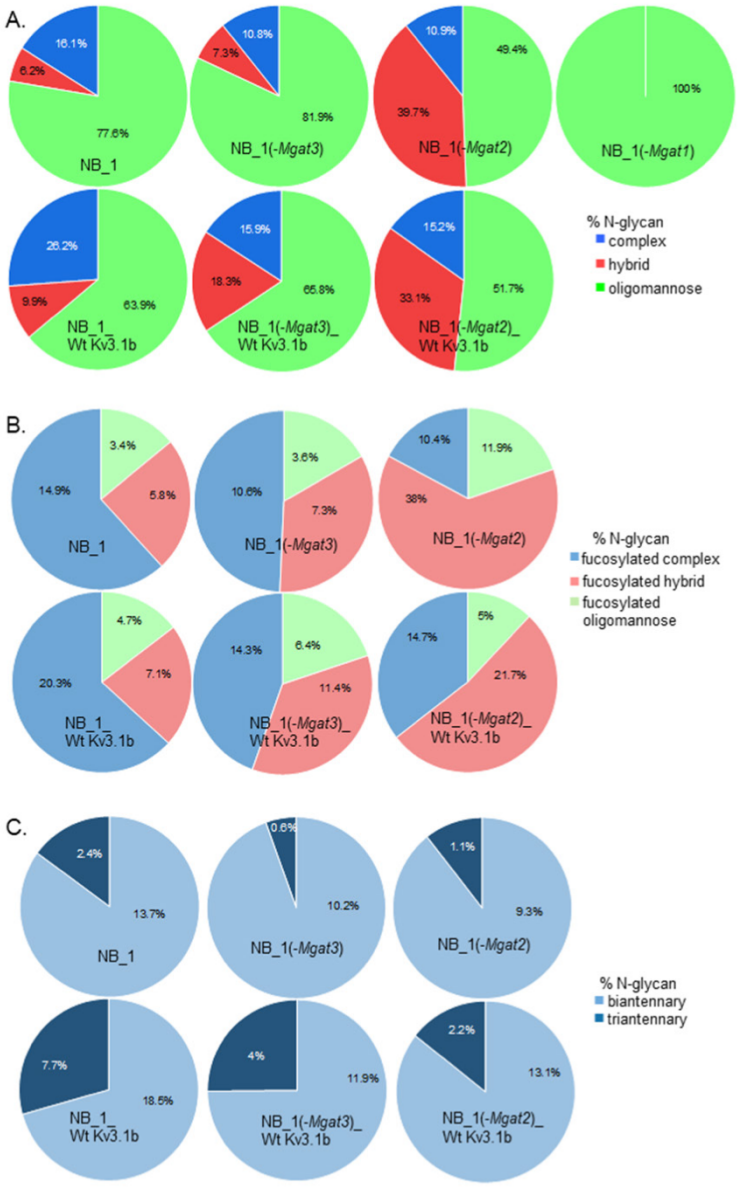
A.
16.1%
6.2%
77.6%
NB_1
10.8%
7.3%
81.9%
NB_1(-Mgat3)
10.9%
49.4%
39.7%
NB_1(-Mgat2)
100%
NB_1(-Mgat1)
26.2%
9.9%
63.9%
NB_1_ Wt Kv3.1b
15.9%
18.3%
65.8%
NB_1(-Mgat3)_ Wt Kv3.1b
15.2%
51.7%
33.1%
NB_1(-Mgat2)_ Wt Kv3.1b
% N-glycan
complex
hybrid
oligomannose
B.
3.4%
14.9%
5.8%
NB_1
3.6%
10.6%
7.3%
NB_1(-Mgat3)
10.4%
11.9%
38%
NB_1(-Mgat2)
4.7%
20.3%
7.1%
NB_1_ Wt Kv3.1b
14.3%
6.4%
11.4%
NB_1(-Mgat3)_ Wt Kv3.1b
14.7%
5%
21.7%
NB_1(-Mgat2)_ Wt Kv3.1b
% N-glycan
fucosylated complex
fucosylated hybrid
fucosylated oligomannose
C.
2.4%
13.7%
NB_1
0.6%
10.2%
NB_1(-Mgat3)
1.1%
9.3%
NB_1(-Mgat2)
7.7%
18.5%
NB_1_ Wt Kv3.1b
4%
11.9%
NB_1(-Mgat3)_ Wt Kv3.1b
2.2%
13.1%
NB_1(-Mgat2)_ Wt Kv3.1b
% N-glycan
biantennary
triantennary

Figure 2.4 Quantification of MALDI-TOF MS profiles of permethylated N-glycans. Quantification of N-glycan types expressed in NB_1,NB_1(-*Mgat3*), NB_1(-*Mgat2*), and NB_1(-*Mgat1*) cell lines (A, top row) and NB_1, NB_1(-*Mgat3*), and NB_1(-*Mgat2*) stably expressing Kv3.1b (A, bottom row). Fucosylated N-glycans by type in NB_1, NB_1(-*Mgat1*), NB_1(-*Mgat2*), and NB_1(-*Mgat3*) cell lines (B, top row) and NB_1, NB_1(-*Mgat3*), NB_1(-*Mgat2*) stably expressing Kv3.1b (B, bottom row). Percent biantennary (light blue) and tri-antennary (dark blue) N-glycans in NB_1(-*Mgat3*), NB_1(-*Mgat2*), NB_1 (*Mgat1*) cell lines (C, top row) and NB_1, and NB_1(-*Mgat3*), NB_1(-*Mgat2*) stably expressing Kv3.1b (C, bottom row).

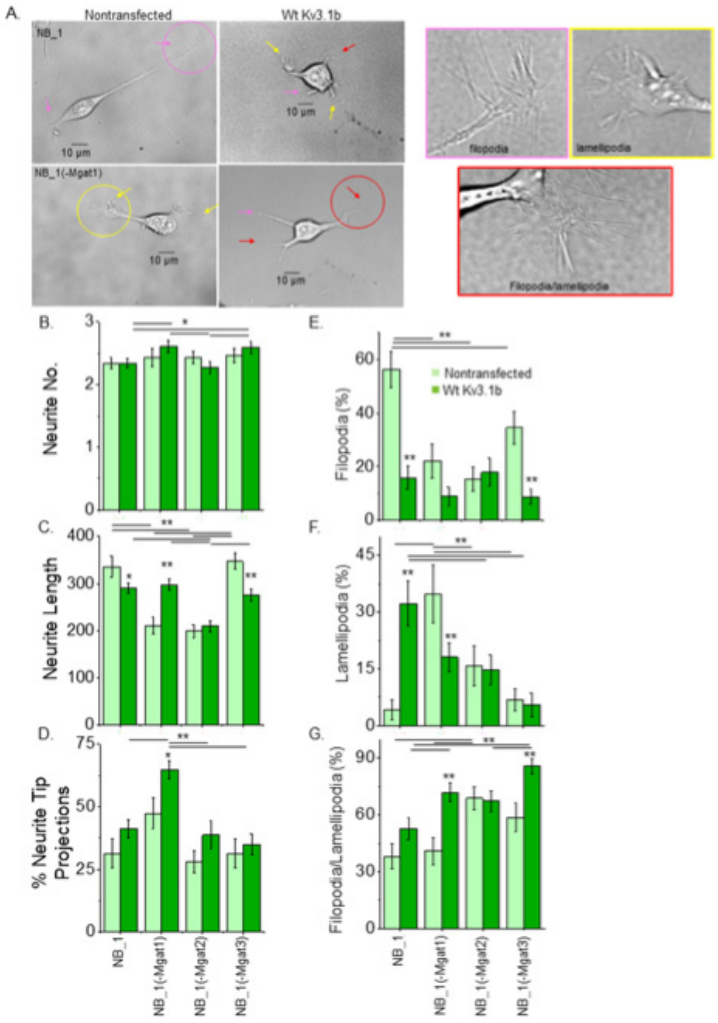
A.
Nontransfected
Wt Kv3.1b
NB_1
NB_1(-Mgat1)
10 μm
filopodia
lamellipodia
Filopodia/lamellipodia
B.
Neurite No.
C.
Neurite Length
D.
% Neurite Tip Projections
E.
Filopodia (%)
Nontransfected
Wt Kv3.1b
F.
Lamellipodia (%)
G.
Filopodia/Lamellipodia (%)
NB_1
NB_1(-Mgat1)
NB_1(-Mgat2)
NB_1(-Mgat3)

Figure 2.5 Impact of N-glycans and Kv3.1b on cell morphology. Images of NB_1 (upper row) and NB_1(-*Mgat1*) (lower row) non-transfected (left panel) or expressing glycosylated Kv3.1b (right panel) (A). Yellow, pink, and red arrows and circles correspond to legend indicating structure type. Images encased in yellow, pink and red boxes are magnified (3x) and correspond to encircled areas to highlight the various neurite structures analyzed. Quantification of neurite number (B; n≥20) length (C; n≥52), and % neurite tip protrusions (D; n≥52). Further analysis categorizing types of neurite tip protrusions as % filopodia (E; n≥23), % lamellipodia (F; n≥23), and % with both filopodia and lamellipodia (G; n≥23). Data are presented as mean ± SEM and were all compared by one-way ANOVA with Holm-Bonferroni mean comparison (*$p < 0.1$, **$p < 0.05$).

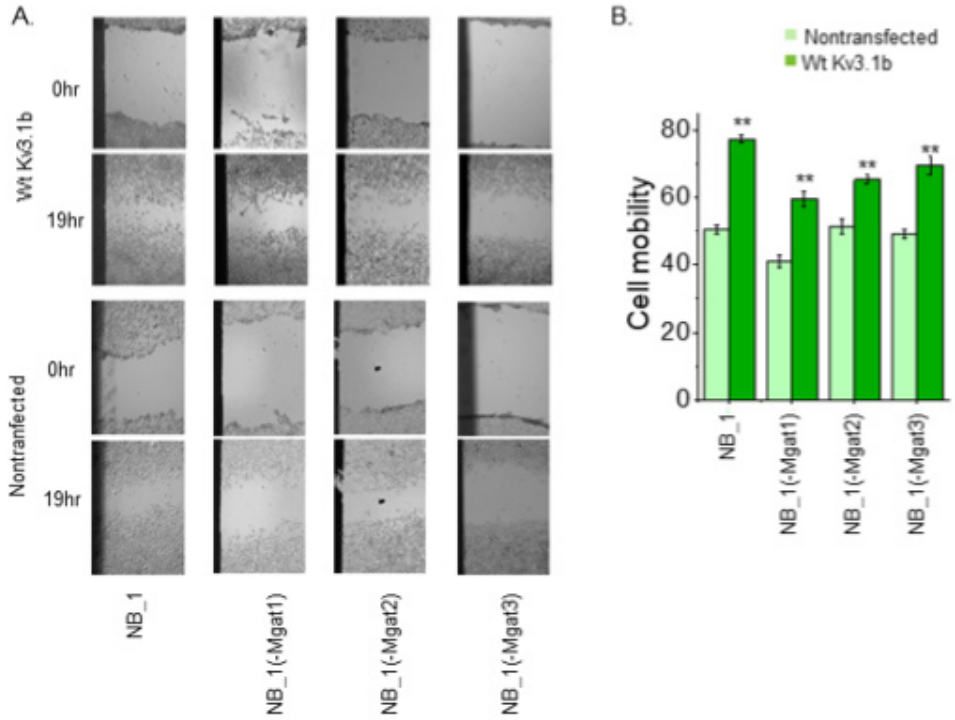
A.
Wt Kv3.1b
0hr
19hr
Nontranfected
0hr
19hr
NB_1
NB_1(-Mgat1)
NB_1(-Mgat2)
NB_1(-Mgat3)
B.
Nontransfected
Wt Kv3.1b
Cell mobility
80
60
40
20
0
**
**
**
**
NB_1
NB_1(-Mgat1)
NB_1(-Mgat2)
NB_1(-Mgat3)

Figure 2.6 N-glycan type associated with the Kv3.1b glycoprotein influences NB migratory rates. Representative images of cell wounds at 0 hours and 19 hours in non-transfected NB_1, NB_1 (-*Mgat1*), NB_1 (-*Mgat2*) and NB_1 (-*Mgat3*) (lower panels) or glycosylated Kv3.1b transfected (upper panels) (A). Bar graph illustrates cell mobility based on percent wound closure at 19h (B). Data are presented as mean ± SEM ($n \geq 6$) and Wt. Kv3.1 expressing NB cell line was compared to non-transfected NB cell line by student t-test (**$p < 0.001$).

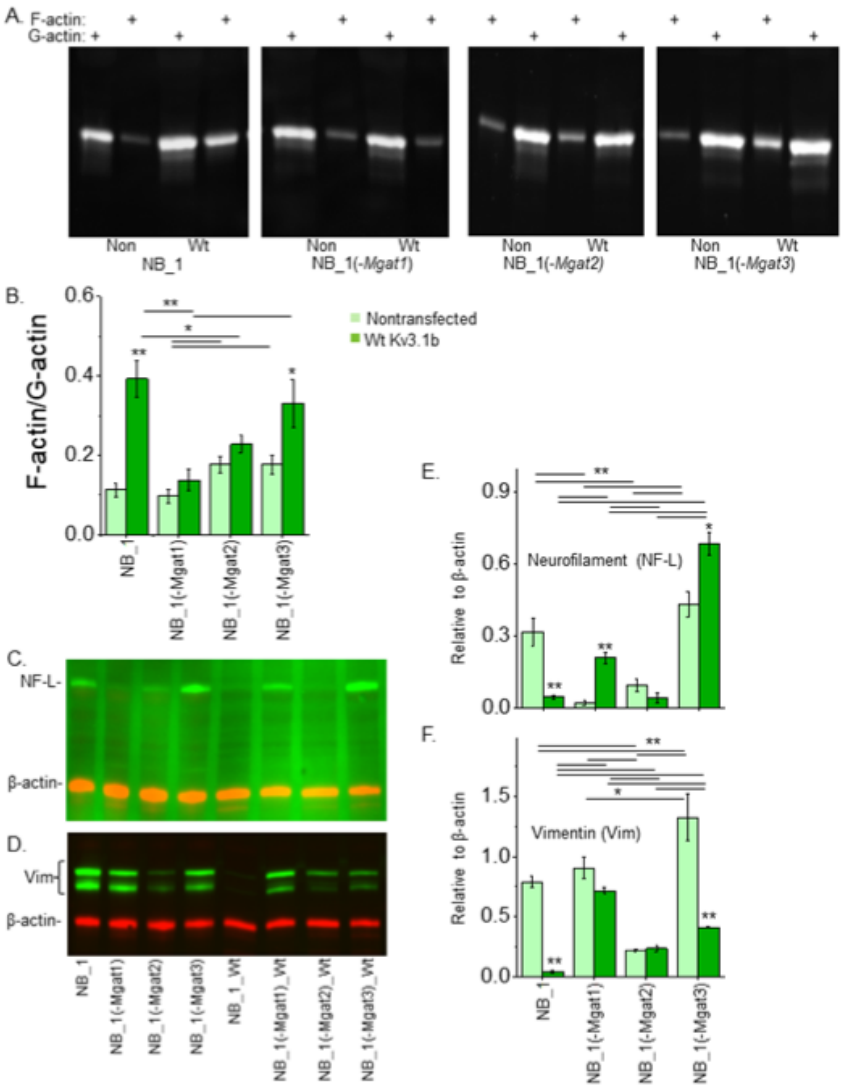
A.
F-actin:
G-actin:
Non
Wt
NB_1
NB_1(-Mgat1)
NB_1(-Mgat2)
NB_1(-Mgat3)
B.
F-actin/G-actin
Nontransfected
Wt Kv3.1b
C.
NF-L-
β-actin-
D.
Vim
β-actin-
E.
Relative to β-actin
Neurofilament (NF-L)
F.
Vimentin (Vim)

Figure 2.7 Influence of N-glycans and Kv3.1b on actin polymerization and intermediate in NB cells. Western blots (n≥3) of filamentous and globular actin (A) and quantification (B) in NB_1 (n=5,4), NB_1 (-*Mgat1*) (n=5, 4), NB_1 (-*Mgat2*) (n=4, 3), and NB_1 (-*Mgat3*) (n=4, 3) cells without Kv3.1 (light green) or expressing Kv3.1 WT (dark green). Western blots of Neurofilament-L (NFL; n=4) (C) and Vimentin (Vim; n=3) (D) multiplexed with β-actin: rhodamine in cell lines as indicated. Quantification of protein levels relative to β-actin (E, F) in NB_1, NB_1 (-*Mgat1*), NB_1 (-*Mgat2*), and NB_1 (-*Mgat3*) cells without Kv3.1 (light green) or expressing Kv3.1 WT (dark green). Data are presented as mean ± SEM. Wt Kv3.1 expressing NB cell line was compared to non-transfected NB_1 cell line by student t-test (*$p < 0.05$, **$p < 0.001$) and non-transfected and Wt Kv3.1b expressing NB_1 cell line were all compared by one-way ANOVA with Holm-Bonferroni mean comparison (*$p < 0.1$, **$p < 0.05$).

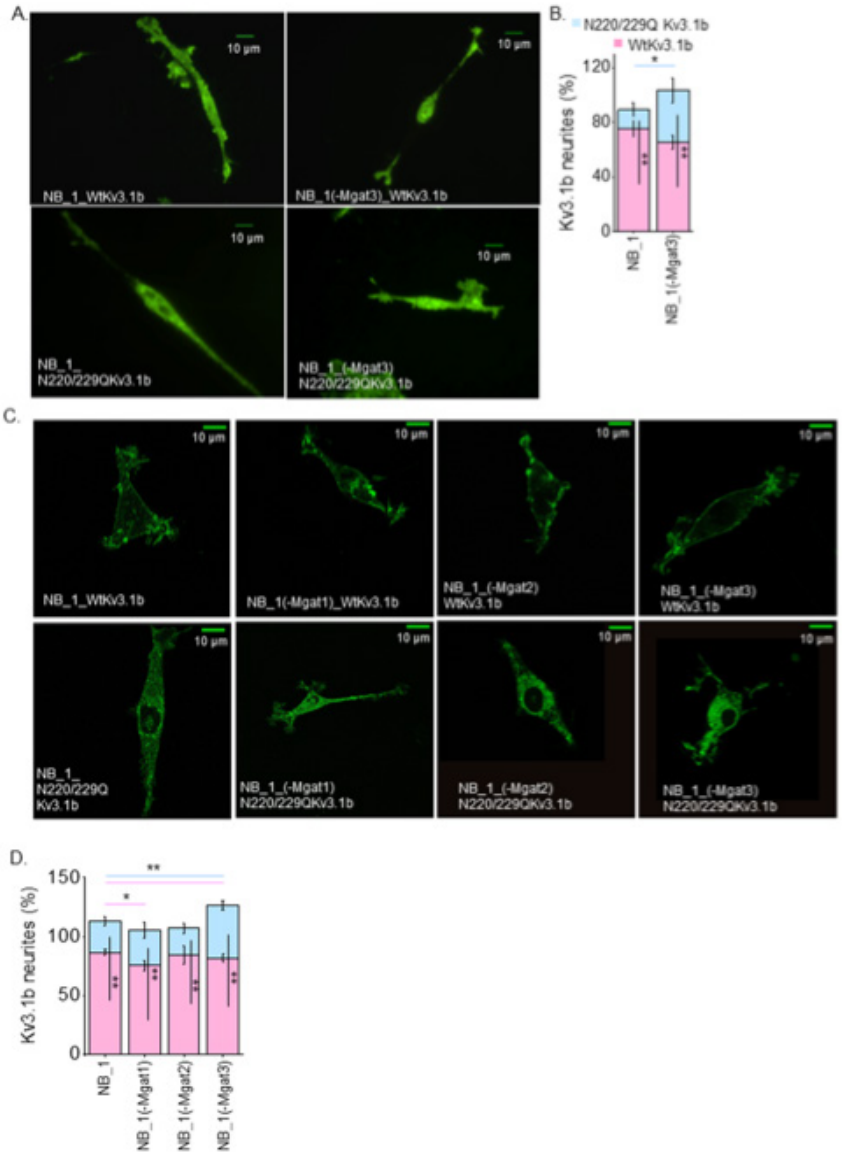
A.
10 µm
NB_1_WtKv3.1b
NB_1(-Mgat3)_WtKv3.1b
NB_1_
N220/229QKv3.1b
NB_1_(-Mgat3)
N220/229QKv3.1b
B.
N220/229Q Kv3.1b
WtKv3.1b
Kv3.1b neurites (%)
120
80
40
0
*
**
NB_1
NB_1(-Mgat3)
C.
NB_1_WtKv3.1b
NB_1(-Mgat1)_WtKv3.1b
NB_1_(-Mgat2)
WtKv3.1b
NB_1_(-Mgat3)
WtKv3.1b
NB_1_
N220/229Q
Kv3.1b
NB_1_(-Mgat1)
N220/229QKv3.1b
NB_1_(-Mgat2)
N220/229QKv3.1b
NB_1_(-Mgat3)
N220/229QKv3.1b
D.
Kv3.1b neurites (%)
150
100
50
0
*
**
NB_1
NB_1(-Mgat1)
NB_1(-Mgat2)
NB_1(-Mgat3)

Figure 2.8 Kv3.1b localization in outgrowths of rat neuroblastoma cell lines with atypical N-glycosylation. Representative TIRF (A) microscopy images acquired of glycosylated (WT) (upper panels) and glycosylated (N220/229Q) (lower panels) Kv3.1b proteins labeled with EGFP expressed in NB_1 (left columns) and NB_1(-*Mgat3*) (right columns) cells. Quantification of percent of Wt Kv3.1b (pink) and N220/229Q Kv3.1b (blue) localized in neurites of NB_1 and NB1_(-) cells as detected via TIRF ($n \geq 18$) (B). Confocal microscopy images (C) of glycosylated (WT) (upper panels) and unglycosylated (N220/229Q) (lower panels) Kv3.1b proteins. in cell lines as indicated. Bar graphs indicate % Kv3.1 detected in neurites via confocal microscopy ($n \geq 10$) (D) in NB cell lines as shown. The Wt Kv3.1 expressing NB cell line was compared to N220/229Q Kv3.1b expressing NB cell line by student t-test (*$p < 0.05$, **$p < 0.001$). Wt Kv3.1b or N220/229Q Kv3.1b expressing NB cell lines were compared by one-way ANOVA with Holm-Bonferroni mean comparison (*$p<0.1$, **$p<0.05$). Black lines inside the bars denote statistical differences between WT_Kv3.1b and N220/9Q Kv3.1b within each cell line. Corresponding color lines above the bar graph indicate statistical differences among the cell lines.

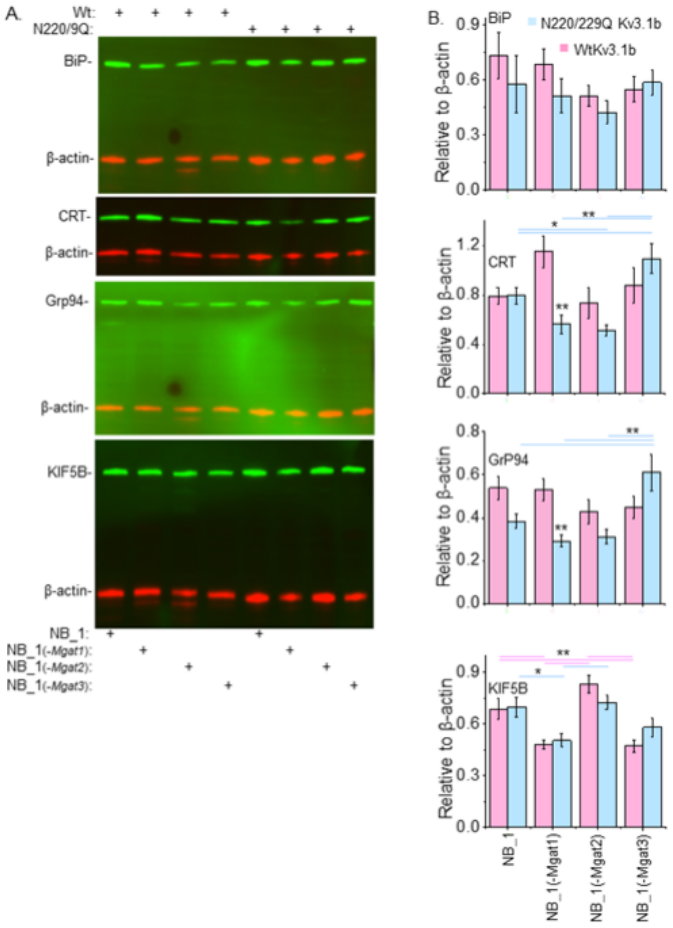
A.
Wt:
N220/9Q:
BiP-
β-actin-
CRT-
β-actin-
Grp94-
β-actin-
KIF5B-
β-actin-
NB_1:
NB_1(-Mgat1):
NB_1(-Mgat2):
NB_1(-Mgat3):
B.
BiP
N220/229Q Kv3.1b
WtKv3.1b
Relative to β-actin
CRT
GrP94
KIF5B
NB_1
NB_1(-Mgat1)
NB_1(-Mgat2)
NB_1(-Mgat3)

Figure 2.9 N-glycans and expression of ER chaperones in neuronal cells. Western blots of BiP (n=5), calreticulin (CRT) (n=4), Grp94 (n=4), and KIF5B (n=4) multiplexed with β-actin: rhodamine (A) and their quantification in NB cells (as shown) expressing WT KV3.1 (pink) or N220/9Q_Kv3.1 (blue)(B). Corresponding color lines above the bar graph indicate statistical differences among the cell lines. (*, ***) inset within the bar graph signified differences between WT_Kv3.1b and N220/9Q Kv3.1b within indicated cell line. Data are presented as mean±SEM. Wt. Kv3.1 expressing NB cell line was compared to non-transfected NB_1 cell line by student t-test (*$p<0.05$, **$p<0.001$). Wt. Kv3.1b or N220/9Q Kv3.1b expressing NB cell lines were all compared by one-way ANOVA with Holm-Bonferroni mean comparison (*$p < 0.1$, **$p < 0.05$).

CHAPTER III: Reduction in N-Acetylglucosaminyltransferase-I Activity Decreases Survivability and Delays Development of Zebrafish

This chapter is modified from Hall MK et. al., Reduction in N-Acetylglucosaminyltransferase-I Activity Decreases Survivability and Delays Development of Zebrafish. Curr Issues Mol Biol. 2023 Nov 15;45(11):9165-9180. doi: 10.3390/cimb45110575. PMID: 37998752; PMCID: PMC10669939.

Summary:

A lack of complex and hybrid types of N-glycans in mice is embryonically lethal due to neural tube maldevelopment. N-acetylglucosaminyltransferase-I (GnT-I; *mgat1*) catalyzes a required step for converting oligomannose N-glycans into hybrid and complex N-glycans. Unlike mice, zebrafish have two *mgat1a/b* genes. Herein, CRISPR/Cas9 technology was used to knockdown GnT-Ib activity in zebrafish, referred to as *mgat1b*$^{-/-}$, to examine the impact of a decrease in complex types of N-glycans on survival and development, and sensory and motor functions. Genotyping verified the occurrence of edited *mgat1b*, and LC-ESI-MS and lectin blotting identified higher levels of oligomannose and lower levels of complex N-glycans in *mgat1b*$^{-/-}$ relative to Wt AB. The microscopic visualization of developmental stages and locomotor studies using an automated tracking unit and manual touch assays revealed reduced survivability, and delayed motor and sensory functions in *mgat1b*$^{-/-}$. Moreover, embryonic staging linked reduced survivability of *mgat1b*$^{-/-}$ to disruption in brain anlagen formation. Birefringence measurements supported delayed skeletal muscle development, which corresponded with motor and sensory function impediments in *mgat1b*$^{-/-}$. Furthermore, GnT-Ib knockdown hindered cardiac activity onset. Collectively, *mgat1b*$^{-/-}$ displayed incomplete penetrance and variable expressivity, such that some died in early embryonic development, while others survived to adulthood, albeit, with developmental delays. Thus, the results reveal that reducing the amount of complex-type N-glycans is unfavorable for zebrafish survival and

development. Moreover, our results support a better understanding of human congenital disorders of glycosylation.

Introduction

Glycosylation, a complex co- and post-translational protein modification, is critical in the development and maintenance of an organism. There are three basic types of N-glycans—oligomannose, hybrid, and complex—each of which share a common pentasaccharide core and are processed sequentially (Stanley 2022). The various N-glycans result from the addition of different branch points via the action of N-acetylglucosaminyltransferases (GnTs, encoded by *MGAT* genes). The conversion of oligomannose-type *N*-glycans to the hybrid type is initiated via GnT-I (encoded by *MGAT1*), and the hybrid type is further processed to the complex type via GnT-II (encoded by *MGAT2*) (Wang, Tan et al. 2001). The consequences of aberrant N-glycosylation processing are well noted in the congenital disorders of glycosylation (CDG), an ever-growing disease family that encompasses almost every organ system and often results in neurological complications (Jaeken 2010, Ondruskova, Cechova et al. 2021).

The magnitude of N-glycan processing in organismal survival and development is well noted in past studies which show that the conditional inactivation of *mgat1* in neuronal tissue of mice causes severe neurological defects and early post-natal death at about embryonic day E13 (Ye and Marth 2004), while global *Mgat1* knockout mice did not survive beyond E10.5 due to maldevelopment of their neural tubes (Ioffe and Stanley 1994). Interestingly, although complex N-glycans were observed pre-implantation at around E3.5 in *mgat1* null embryos, these levels declined by E7.5, thus attributing the earlier levels to maternal derivation and further emphasizing the criticality of complex N-glycans in post-implantation development (Campbell, Metzler et al.

1995). Thus, these studies support the importance of complex-type N-glycans in the neurological development of mice. Moreover, expanding the glycan studies to zebrafish is ideal since they have two *mgat1* genes (*mgat1a* and *1b*), instead of a single *mgat1* gene like mice, thus allowing for an examination of how lowered levels of GnT-I activity affect development and survival, minus the lethality associated with mice.

The glycome of zebrafish (*Danio rerio*) is quite diverse, and all of the three N-glycan types are present as early as 6 h postfertilization (hpf), with an abundance of oligomannose-type N-glycans (Hanzawa, Suzuki et al. 2017). Although complex-type N-glycans are found in smaller amounts, a sharp increase in levels is noted in the segmentation to the pharyngula period (10–48 hpf) of embryonic development (Hanzawa, Suzuki et al. 2017). In adult zebrafish, although the proportion of complex- to oligomannose-type N-glycans varies among specific organs, most of the brain regions revealed a higher population of complex-relative to oligomannose-type N-glycans (Yamakawa, Vanbeselaere et al. 2018). Further, complex N-glycans found in the brain of adults were found to have the highest percentage of core fucose and highest overall sialyation pattern relative to other organs (Yamakawa, Vanbeselaere et al. 2018). It should also be noted that zebrafish, unlike mice and humans, have two genes (*mgat1a/b*) that encode GnTIa/b (Sprague, Doerry et al. 2001). Thus, the inactivation of one of the *mgat1* genes will likely result in lowered GnTI activities and thereby decrease the amount of complex-type N-glycans.

Zebrafish is a model organism for vertebrate development due to the rapid progression of developmental stages. Zebrafish development is initiated with a single cell, the zygote period, and progresses to the blastula stage within 3 hpf (Kimmel, Ballard et al. 1995). It is during the blastula phase when the embryo undergoes several important events, including the start of epiboly, a process of coordinated cell movement critical for body formation (Kimmel, Ballard et al. 1995).

Epiboly continues into gastrulation, during which the yolk is gradually internalized as cells continue to form. This is carried out through the thinning and spreading of the ectodermal layers while the endoderm layers move towards the inside of the embryo (Bruce and Heisenberg 2020). The portion of the yolk cell that is covered by the blastoderm is referred to as percent epiboly, with 75% epiboly occurring at around 8 hpf and 100% epiboly occurring around at 10.5 hpf (Bruce and Heisenberg 2020). During the segmentation phase (10–24 hpf), somites begin to form along with neural keel and neural crest migration. It is during the pharyngula stage (24–48 hpf) when the circulatory system is formed, and a heartbeat is initiated at the onset of this stage (Bruce and Heisenberg 2020). Therefore, by silencing one of the *mgat1* genes, the development of embryos can be monitored and compared with that in mice with conditional and global *mgat1* knockouts.

The objective of this study was to create a *mgat1b* mutant fish strain, *(mgat1b*$^{-/-}$), and to examine the impact of higher levels of oligomannose and less complex N-glycans in the survival and development of *mgat1b*$^{-/-}$ relative to Wt AB zebrafish. Survivability and developmental studies revealed that a reduction in complex-type N-glycans perturbs survivability and development. Embryonic developmental staging implicated disruptions of the brain anlagen, the precursor for brain formation, in the lower survivability of zebrafish with silenced *mgat1b*. Further, delayed skeletal muscle development coincides with a diminished amount of complex N-glycans, along with a reduction in motor and sensory functions. Likewise, cardiac muscle development is impeded in *mgat1b*$^{-/-}$. Taken together, the results of this study imply that a reduction in the amount of complex-type N-glycans is unfavorable in the survival and development of zebrafish.

2. Materials and Methods

2.1. Animal Husbandry, Staging, and Larva and Embryo Collections

All Zebrafish procedures were approved by the Institutional Animal Care & Use Committee (IACUC) of East Carolina University. The utilized adult wildtype Pseudoloma-free AB strain (Wt AB) was purchased from Sinnhuber Aquatic Research Laboratory (SARL), propagated at ECU, and utilized for the creation of mutant zebrafish with genetic editing of the *Mgat1b* gene. All zebrafish were maintained at 28 °C on a light/dark cycle of 14 h on and 10 h off in a Pseudoloma-free lab. Embryos collected from natural spawns were transferred to 100 × 15 mm Petri dishes containing egg water (5.03 mM NaCL, 0.17 mM KCl, 0.33 mM $CaCl_2$•$2H_2O$, 0.33 mM $MgSO_4$•$7H_2O$, and 0.05% methylene in 1 L system water) and developed in an incubator set at 28 °C. Embryos were staged based on morphological criteria and time post-fertilization as described by (Kimmel, Ballard et al. 1995, Bruce and Heisenberg 2020). Fish older than 96 h of age were fed a high-protein diet of Gemma Micro pellets (Skretting, Tooele, UT, USA) every morning and afternoon. Larvae (6 dpf and 24 dpf) and adult fish were euthanized using an ice slurry bath for 10 min prior to glycoprotein or RNA analysis. All experiments using live zebrafish were performed at 28 °C.

The CHOPCHOP program was employed to identify a guide RNA (gRNA) target sequence (ggccggtgaagtgatcagat) in zebrafish *mgat1b* (accession number: NM_001079971), along with forward (gccatggttcgcaagaaagg) and reverse (ccaattctggtcattgcctg) primers for amplification of the fragment of interest (Montague, Cruz et al. 2014, Labun, Montague et al. 2016, Labun, Montague et al. 2019). The target sequence has a BclI site which is shown in red font. The restriction sequence was selected to identify edited genomic DNA in the target sequence of an individual fish. Oligonucleotides were purchased from ThermoFisher, Waltham, MA, USA. The

gRNA target sequence also included a T7 promoter sequence added to the 5′ end and a 14 nucleotide overlap sequence added to the 3′ end for use of the EnGen® sgRNA Synthesis Kit, *S. pyogenes* (New England Biolabs, Ipswich, MA, USA). The transcribed nucleotide was purified using Monarch® Kits for RNA Cleanup (New England Biolabs, Ipswich, MA, USA).

2.2. Genotyping of Embryos, Larvae, and Adult Fish

After collection of embryos, larvae, or a small portion of the adult fish tail, genomic DNA was extracted by incubating embryos in 50 mM NaOH at 99 °C for 20 min. The NaOH solution containing genomic DNA was used directly for PCR. PCR forward (gccatggttcgcaagaaagg) and reverse (ccaattctggtcattgcctg) primers were designed around the gRNA target and used to amplify the target region. PCR conditions: Initial denaturation for 2 min at 94 °C; 32 cycles of denaturation at 95 °C for 30 s, annealing at 58 °C for 30 s, elongation at 72 °C for 30 s, then a final step at 70 °C for 10 min. Gene editing of the fragment was then identified by restriction enzyme (RE) digest reaction, followed by separation of band(s) on an agarose gel. The presence of an undigested band indicated that the DNA was edited for at least one of the *Mgat1b* alleles.

2.3. Generating the mgat1b$^{-/-}$ Mutant Line

Single-cell embryos were microinjected with an about 500-picoliter mixture solution containing 100 ng/µL of sgRNA and 360 pg/µL of EnGen Spy Cas9 NLS ®. Microinjection was driven by compressed N2 gas under the control of a PV820 Pneumatic PicoPump (World Precision Instruments, Sarasota, FL, USA), accomplished using a microcapillary pipette attached to a micromanipulator, under a Nikon microscope (Tokyo, Japan). About thirty microinjected embryos (F0) were collected for estimating gRNA efficiency at 24 h post-fertilization (hpf) via genotyping. If pooled F0 embryos had undigested bands after treatment with the restriction enzyme BclI (ThermoFisher, Waltham, MA, USA), then Cas9 successfully cut the targeted

region and the cell incorrectly repaired the damage, destroying the BclI site and possibly creating a frameshift mutation. The remaining microinjected F0 embryos were raised to adulthood and then checked for gene editing via fin clipping and restriction enzyme (RE) digest. Adult F0 fish had their DNA sequenced to verify a frameshift, and then, they were outcrossed with Wt AB. F1 embryos were screened for gene editing, and furthermore, mutations were confirmed by DNA sequencing. Notably, the mutation (Δ5) was identical in F0 and F1 adult fish. Fish that were heterozygous for the same mutation were paired for spawning. F2 and embryos from subsequent generations, e.g., F3, were collected and grown into adulthood, when they were screened by RE digestion.

2.4. Brain Dissections

Adult zebrafish were euthanized via an ice slurry bath for 10 min following operculum movement cessation in accordance with IACUC protocols. Euthanized fish were placed on a Sylgard (Sigma Aldrich, St. Louis, MO, USA)-coated 100 mm dish. Dissection pins were inserted through the mouth and extended through the ventral side of the fish to affix fish to the dish. Spring scissors were used to cut from the upper lip through the cranium, revealing the brain. Next, two perpendicular incisions were made behind the gills, running dorsal to ventral, starting at the initial cut. The optic nerves and brain stem were severed using spring scissors, and the brain was extracted with forceps. Dissected brains were placed in cryotubes, flash frozen in liquid nitrogen, and stored at −80 °C until ready for use.

2.5. Total Brain Membrane Preparations and Larval Homogenate

Total membranes of ten pooled adult zebrafish brains were isolated via ultracentrifugation, as previously described (Hall, Shajahan et al. 2023). Total membrane samples for glycan analysis were resuspended in 10 mM Tris, pH 7.4; 250 mM sucrose, 5 mM EDTA; protease inhibitor

cocktail set III (Calbiochem, San Diego, CA, USA). All samples were stored at −80 °C until needed. Wt AB and *Mgat1b*$^{-/-}$ larval zebrafish were pooled and collected for protein. About 90 larvae (6 dpf and 24 dpf) were resuspended in RIPA buffer (PBS, 1% Triton X-100, 0.5% sodium deoxycholate, and 0.1% SDS) plus protease inhibitor cocktail set III (EMD Biosciences, San Diego, CA, USA), followed by the addition of an SDS-PAGE sample buffer containing 200 mM DTT to reduce and denature the samples for lectin blotting and Coomassie blue staining.

2.6. Lectin Blots and Coomassie Blue-Stained Gels

The evaluation of total membrane proteins and larval homogenate was performed via Coomassie staining and lectin blotting. In brief, proteins were allowed to migrate on 10% SDS gels at 20 mA followed by incubation with Coomassie® Brilliant Blue (MP Biomedical, Solon, OH), or transferred to nitrocellulose membranes (Whatman, Dassel, Germany) at 250 mA for lectin blotting, as previously described (Hall, Shajahan et al. 2023). Transferred proteins were probed with biotin-conjugated E-PHA or GNL lectins (10 µg/mL; Vector Laboratories, Burlingame, CA, USA).

2.7. RNA Extraction

Approximately 95 larval zebrafish were collected in a microcentrifuge tube placed in an ice slurry and resuspended in TRIzol ®(Invitrogen, Carlsbad, CA, USA) and homogenized until sufficiently disrupted. Homogenized samples were allowed to sit at room temperature for five minutes to complete dissociation of samples, followed by the addition of chloroform. Samples were centrifuged at 12,000× *g* for 5 min at 4 °C. The upper aqueous phase was collected, RNA was precipitated via the addition of isopropanol, and the RNA pellet was washed with ethanol. Total RNA was resuspended in RNAse-free water. Total RNA cleanup was performed using the RNeasy mini kit (Qiagen, Hilden, Germany) per the manufacturer's protocol. The RNA quality

and quantity was assayed using a NanoDrop 1000 (ThermoFisher Scientific, Waltham, MA, USA).

2.8. RT-PCR

A total of 1 µg of RNA in a 20 µL reaction was reverse-transcribed utilizing the iScript™ cDNA Synthesis Kit (Bio-Rad Laboratories, Hercules, CA, USA) according to manufacturer's instructions. Quantitative real-time PCR was performed with a CFX96 Touch Real-Time PCR Detection System using IQ™SYBR Green SuperMix (Bio-Rad Laboratories, Hercules, CA, USA) and primers from ThermoFisher Scientific, Waltham, MA, USA. Primers for amplification were designed so the products would span at least one intron using Primer-Blast (Ye, Coulouris et al. 2012), except those for elfα (McCurley and Callard 2008); see (Table 3.1) for sequences. The amplification of a single product was confirmed via agarose gel visualization and/or melting curve analysis for all primer sets; see (Figure 3.S3). mRNA was quantified via ΔΔCT analysis using housekeeping genes β-actin and ELFα for normalization.

2.9. N-Glycan Analysis

Total membrane protein fractions from the brain of Wt AB and *mgat1b*$^{-/-}$ adult zebrafish were diluted with 100 µL of 50 mM ammonium bicarbonate buffer, followed by the addition of 25 µL of 25 mM Dithiothreitol (DTT) and incubated at 50 °C for 30 min (Shajahan, Supekar et al. 2020). The samples were subsequently desalted by centrifugal filtration using 10 k Amicon centrifuge filters (Millipore Sigma, Burlington, MA, USA, Cat. No. UFC501096) and then ultrasonicated to dissolve the proteins. The N-glycans were released from the samples by adding 5 µL of PNGaseF (New England Biolabs, Ipswich, MA, USA, Cat. No. P0709L) and incubating at 37 °C for 48 h. The released N-glycans were permethylated by using methyl iodide in the presence of NaOH-DMSO base. The permethylation reaction was quenched by the addition of

water, and the permethylated N-glycans were extracted with dichloromethane. The dichloromethane layer was washed with water four times and evaporated to dryness by nitrogen gas, and the permethylated N-glycans were mixed in a 1:1 methanol–water (plus 1 mM NaOH) mixture for the LC-ESI-MS/MS analysis. Samples were analyzed on an Orbitrap Fusion Tribrid mass spectrometer equipped with a nanospray ion source and connected to a nanoLC system (Thermo Ultimate 3000). A nano-LC column 15 cm in length with 75 μm internal diameter filled with 3 μm C18 material (reverse phase) was used for chromatographic separation of the glycans. LC-ESI-MS/MS runs were performed for 72 min gradients using a sodiated buffer system (Buffer A: 1 mM NaOAc in H_2O; Buffer B: 80% ACN, 0.1% formic acid, and 1 mM NaOAc). A precursor ion scan was acquired at 120,000 resolution in the Orbitrap analyzer, and precursors at a time frame of 3 s were selected for subsequent MS/MS fragmentation in the Orbitrap analyzer at 15,000 resolution. MS/MS fragmentation was conducted with fixed CID (collision energy 40%) using a data-dependent scan (DDS) program, which performs an MS/MS acquisition for the most abundant ions in the MS spectrum. Precursors with an unknown charge state or a charge state of +1 were excluded, and dynamic exclusion was enabled (30 s duration). LC-MS/MS data were analyzed using Thermo Xcalibur 4.2, Thermo FreeStyle 1.8 SP2, and GlycoWorkBench 2.1 software. The area under the curve of different charge states of each N-glycan peak were extracted from the LC-MS chromatogram and added, and the relative percentages of individual N-glycans were calculated.

2.10. Tactile-Evoked Escape Response

A touch-evoked escape response assay was performed with embryos and larvae at 2 and 3 dpf, respectively, (fish that appeared maldeveloped were not used) from male and female crossed using Wt AB or *mgat1b*$^{-/-}$. Two dpf fish were manually dechorionated using needles, as needed.

After at least 1 h, 15 larvae were put in a 100 mm dish with egg water and allowed to acclimate on a stereoscope for 10 min. A tactile stimulus was administered by a gentle tap with a P10 micropipette tip to the tail of the larvae. The escape behavior was scored according to the number of taps it took to get the larvae to swim away (response). All-points histograms were used to show the total number of larvae that responded to 1-9 taps and ≥10 taps. The mean ± S.D. was also determined from the total number of larvae tested for both groups and 2 and 3 dpf.

2.11. Vibrational Startle Response

Wt AB and *mgat1b*$^{-/-}$ zebrafish larvae (10 dpf) were placed individually into a well of a 6-well plate containing roughly 4 mL of system water and then placed in the chamber of the Zantiks MWP unit. An acclimation period of 5 min was followed by a 20 s tracking period to locate the fish. Pre-startle activity was then logged for 10 s, followed by a 1 s vibration. The machine then tracked post-startle for 20 more seconds. The vibration and post-startle were repeated 2 more times, with the combined startle activity averaged.

2.12. Swimming Locomotor Activity

Wt AB and the *mgat1b* homozygous mutant were maintained in 100 mm dishes containing egg water at 28 °C until 5 dpf, at which point the larvae (≥12) were housed in a 250 mL beaker containing a mixture of egg water and system water. The ratio of egg water to system water was adjusted incrementally as follows: 5 dpf (75:25), 6 dpf (50:50), 7 dpf (25:75), and ≥8 dpf (0:100). At 14 dpf, the larvae were transferred to a 1.8 L tank containing system water. For motor activity recordings, a single fish was placed in one well of a six-well plate containing 11 mL of egg water. The plate was transferred to the MWP unit (Zantiks, Cambridge, UK), and the fish was allowed to acclimate for 5 min. The motor activity of the larvae was tracked for five minutes (one minute intervals), with each one-minute interval followed by a 60 s acclimation

period and a 10 s target acquisition period. The protocol was run in triplicate for each plate. After the procedure, the fish were removed from the plate and transferred to a clean beaker or tank containing a clean larva medium and returned to the incubator. This process was repeated on the following days post-fertilization (dpf): 5, 7, 9, 14, 24, and 29.

2.13. Skeletal and Cardiac Muscle Developmental Assays

The skeletal muscle integrity of Wt AB and *mgat1b*$^{-/-}$ fish strains was monitored in embryos (58 hpf) and larvae (3 dpf and 4 dpf) via the employment of a birefringence assay (Smith, Beggs et al. 2013). The 58 hpf embryos were dechorionated with needles, if needed. Images were collected using a Leica M80 stereoscope and an attached Leica IC90 E camera at 2× magnification with two polarized lenses. One lens was stationary, and the other was rotated to adjust the polarizing light for muscle fiber illumination. Using image J, mean intensity measurements were taken from somites 12 through 20. The birefringence was normalized to Wt AB for each timepoint. Heart development was assayed by the direct visual observation of a heartbeat in zebrafish embryos at 25 hpf and 28 hpf using a Zeiss 47 50 52- 9901 stereoscope at 5× magnification. The number of embryos with a visually detectable heartbeat was recorded as the percent per plate. Experiments were set up on 2 occasions. Five and seven clutches were collected for Wt AB and *mgat1b*$^{-/-}$. Twenty embryos were added to each plate for Wt AB, and eight, sixteen, fifteen, ten, twenty-two, twenty-five, and thirty-two embryos were added per plate for Mgat1b$^{-/-}$. The percentage of embryos with a heartbeat was determined per plate.

2.14. Statistical Analysis

The N-glycan structures were assigned with the aid of GlycoworkBench 2.1 software based on precursor masses (sodium adduct) obtained by ESI-MS/MS and the common mammalian biosynthetic pathway (Shajahan, Supekar et al. 2020). Image J 1.54d software was used for

somite mean intensity measurements. Adobe Photoshop was employed to obtain agarose gel and lectin blot pictures. Origin 9.55 was used for graphics and statistics. Data are presented as the mean ± S.E., where n denotes the number of observations, as indicated. A statistical comparison of two groups was accomplished using unpaired Student's *t*-test.

3. Results

3.1. Generating the mgat1b$^{-/-}$ Mutant Line

Since *mgat1* (codes GnT-I) inactivation in mice was embryonically lethal due to defects in neural tube formation, we employed zebrafish as a model to examine whether reduced levels of complex N-glycans would disrupt development. Although zebrafish synthesize two N-acetylglucosaminyltrases (GnT-Ia and Ib) while mice and humans have a single GnT-I (Stanley 2022), zebrafish provides an excellent and useful model since we could introduce a premature termination codon in one *mgat1* gene (GnT-Ib), which enabled us to assess the impact of reduced GnT-I activity in both embryogenesis and development to adulthood, minus the lethality that is observed early in mice. These enzymes catalyze the conversion of oligomannose-type N-glycans to hybrid type N-glycans which in turn generates complex-type N-glycans (Figure 3.1A) (Stanley 2022). GnT-Ib is a type II single-pass transmembrane protein, composed of 524 amino acid residues, and resides in the Golgi apparatus (Sarkar, Hull et al. 1991, Sarkar, Pagny et al. 1998). Further, the catalytic domain is found in the C-terminal region of the protein (Sarkar, Hull et al. 1991). Adult fish with an indel in the *mgat1b* were identified by restriction enzyme digestion of an amplified fragment of the coding sequence (CDS) of *mgat1b* (Figure3.1b). The fragment in Wt AB contained a BclI site, as the digested amplified band produced two

fragments, while the mutant fish (*mgat1b*$^{-/-}$) generated a single larger band. Fish that were heterozygous for the mutation produced three bands, representing Wt and mutant *mgat1b* alleles. DNA sequencing of the mutant zebrafish line revealed five deleted nucleotides (Δ5) which generated a premature stop codon (Figure 3.2C). This deletion would result in a C-truncated protein of 70 amino acid residues lacking catalytic activity (Sarkar, Hull et al. 1991). Two N-truncated proteins of 381 and 377 residues in length could potentially be generated via two Met residues at positions 144 and 148. However, these N-truncated proteins would not be localized to the Golgi apparatus, since GnT-I is localized via its transmembrane segment (Sarkar, Pagny et al. 1998).

3.2. Glycomic Profiling of Wt AB and mgat1b$^{-/-}$ *Fish Lines Reveals Different Levels of Complex, Hybrid, and Oligomannose Types of N-Glycans*

To identify specific glycan structures, isolated permethylated N-glycans from the adult brains of Wt AB and *Mgat1b*$^{-/-}$ were analyzed by LC-ESI-MS. In both cases, detectable levels of the oligomannose, hybrid, and complex types of N-glycans were observed (Figure 3.2A). However, higher levels of Man5 and Man6 oligomannose N-glycans and lower levels of hybrid and complex types of N-glycans were in *mgat1b*$^{-/-}$ relative to Wt AB. In both fish strains, the levels of oligomannose and complex types of N-glycans were greater than 31%, while that of the hybrid type were much lower, ranging from 5 to 10% (Figure 3.2B). The rise in the oligomannose type corresponded to decreases in both complex and hybrid types. When comparing the levels of Man9 to Man5 oligomannose structures between *mgat1b*$^{-/-}$and Wt AB, there was about two-fold greater level of Man5 in the mutant line (Figure 3.2C). The accumulation of Man5 strongly supports

that *mgat1b* is at least partially inactive as this is the substrate utilized by GnT-Ib. Thus, the glycan population of adult brain from *mgat1b*$^{-/-}$ fish has less complex-type N-glycans than Wt AB fish.

3.3. Increased Levels of Oligomannose N-Glycans and Decreased mgat1b Expression in Mutant Strain of Adult and Larvae Fish

To verify that GnT-Ib activity was minimal in the adult brains (Figure 3.3A), as well as 24 dpf and 6 dpf larvae (Figure 3.3B) of *mgat1b*$^{-/-}$relative to Wt AB, glycosylated proteins from whole cell lysates of each strain were separated on a reducing SDS gel and probed with *Galanthus nivalis* lectin (GNL). This lectin has higher affinity for the oligomannose type than the hybrid or complex types of N-glycans (Patnaik and Stanley 2006). The overall band intensities of glycosylated proteins from the adult brains of *mgat1b*$^{-/-}$ were higher than those from Wt AB. Moreover, less *Phaseolus vulgaris* Erythroagglutinin (E-PHA), a lectin with very high affinity for complex-type N-glycans with bisecting N-acetylglucosamine (GlcNAc) relative to other N-glycan structures (Patnaik and Stanley 2006), bound to glycosylated proteins from the adult brain of *mgat1b*$^{-/-}$more often than that of Wt AB. GNL also had a preference for binding to glycosylated protein from whole larvae (24 dpf and 6dpf) of *mgat1b*$^{-/-}$ over those from Wt AB. In all cases, the amount of protein loaded for each sample was detected with Coomassie blue-stained SDS gels, indicating comparable levels of protein.

Since the *mgat1b* gene had an indel in the CDS and oligomannose N-glycans were reduced, it is likely that the abundance of the *mgat1b* transcript is lowered in fish from *mgat1b*$^{-/-}$ relative to Wt AB. The qRT-PCR assay showed significantly lower levels of *mgat1b* mRNA in adult brains from *Mgat1b*$^{-/-}$ using β-actin (Figure 3.3C) or ELFα (Figure 3.S1) as housekeeping genes. The levels of *Mgat1b*mRNA were also reduced in whole larvae zebrafish from 24 dpf and 6 dpf, as

well as embryos at 8 hpf of the mutant strain. The reduction in *mgat1b* transcripts was less in the entire organism than in the brain and, furthermore, was less reduced at the earlier post-fertilization timepoints. This decay in *mgat1b* mRNA throughout zebrafish development may be due to the non-sense mediated decay mechanism (Lejeune 2022), as mgat1b gene editing resulted in a premature termination codon. Taken together, the results indicate that *mgat1b*$^{-/-}$ fish have reduced GnT-I activity, and therefore, zebrafish from the *mgat1b*$^{-/-}$ strain have higher amounts of oligomannose N-glycans and lower levels of complex N-glycans.

3.4. Low Survival of Embryonic mgat1b$^{-/-}$ *Mutants after Reaching 75% Epiboly*

Survival of the *mgat1b*$^{-/-}$ and the Wt AB fish was tracked up to 72 hpf. *mgat1b*$^{-/-}$ survival was largely lowered at 12 hpf, and a smaller decrease was detected at 24 hpf while only minimal decreases in survival were observed after this time (Figure 3.4A). Next, we monitored the various stages of embryogenesis for *mgat1b*$^{-/-}$ and Wt AB (Figure 3.4B). By far, the majority of the Wt AB offspring survived while only about half of the *mgat1b*$^{-/-}$ embryos survived prior to reaching 90% epiboly. As such, most death from *mgat1b*$^{-/-}$ embryos occurred during the transition from 75% epiboly to 90% epiboly, a period heavy in coordinated cell migration, supporting that increased oligomannose-type N-glycans may hamper cell migration, thus proving to be detrimental in the progression of the later stages of epiboly.

3.5. Motor and Sensory Functions Were Hampered in mgat1b$^{-/-}$ *Mutants*

Since the inactivation of *mgat1* in mice had dramatic effects on neural structure (Ye and Marth 2004), the motor–sensory function of *mgat1b*$^{-/-}$embryos and larvae zebrafish was compared to those of Wt AB. The touch-evoked escape response assay was conducted to simultaneously determine the ability of Wt (2 dpf, 1.71 ± 1.92, n = 100; 3 dpf, 1.3 ± 0.99, n = 100) and mutant (2

dpf, 4.03 ± 3.63, n = 100; 3 dpf, 2.76 ± 2.90, n = 90) larval zebrafish to sense tactile stimuli on their tail region and to respond via locomotor activity (Figure 3.5A). Over 75% of Wt AB swam away immediately (1 touch) at 2 and 3 dpf. Less than 40% responded immediately for *mgat1b*$^{-/-}$ at 2 dpf but the response increased to about 50% at 3 dpf. *mgat1b*$^{-/-}$ larval zebrafish of 10 dpf also showed a decrease in the distance swam in response to vibration stimuli compared to those of Wt AB (Figure 3.5B). When observing spontaneous locomotor swimming from 5 dpf to 29 dpf, the *mgat1b*$^{-/-}$ larval zebrafish swam shorter distances than the Wt AB (Figure 3.5C). Notably, larvae from the *mgat1b*$^{+/-}$ mutant line had similar swimming locomotor activities to the *mgat1b*$^{+/+}$ and Wt AB lines, while that of the *mgat1b*$^{-/-}$ line was different, indicating that off-target effects were negligible; see (Figure 3.S4). Taken together, these results showed that the mutant embryos and larvae had impaired motor and sensory functions, demonstrating that diminished complex-type N-glycans causes sensory and movement inhibition and thus are critical components in zebrafish survival.

3.6. Delayed Development of Skeletal and Cardiac Muscle in mgat1b$^{-/-}$ *Mutants*

To examine muscle development, we evaluated skeletal muscle sarcomere organization and when heartbeat could be detected. Light intensity was lower in mutant embryo zebrafish at 58 hpf and larval zebrafish at 3 dpf and 4 dpf than in Wt AB, as indicated when birefringence was normalized to Wt AB (Figure 3.6A). The inhibition of light emitted is indicative of disorganized skeletal muscle; more organized tissue allows for more light emission. The birefringence for Wt AB was similar over the covered period while mutant fish had an increase and approached that of the Wt AB larval fish over the time course. The occurrence of a heartbeat in Wt AB embryos was greater at 25 hpf (90%), while it was about 50% in *mgat1b*$^{-/-}$ embryos (Figure 3.6B). In both cases, all embryos had heartbeats at 28 hpf. Thus, these experiments support that skeletal and cardiac

muscle development is hampered in the *mgat1b*$^{-/-}$ zebrafish, signifying the role of complex-type N-glycans in muscle formation.

4. Discussion

Previously, our lab utilized in vitro cell models to demonstrate that disruption in the N-glycosylation pathway alters aberrant cellular properties in neuronal-derived cells (Hall, Shajahan et al. 2023) (Hall, Weidner et al. 2018) and that the ectopic expression of incomplete N-glycosylation of a voltage-gated K^+ channel (Kv3.1b) in primary motor neurons (e.g., caudal primary, CaP) of zebrafish results in maldeveloped CaP neurons (Issa, Hall et al. 2021). Here, we extended those studies to reveal the deleterious consequences of a global knockdown of one of two GnT-I enzymes (GnT-Ib) in zebrafish. Genotyping confirmed an introduced frameshift in the *mgat1b*$^{-/-}$ strain. Additionally, swimming locomotor activity in the *mgat1b*$^{-/-}$ larvae was slower than that of Wt AB, as well as *mgat1b*$^{+/+}$ and *mgat1b*$^{+/-}$, minimizing the likelihood of off-target effects. The glycomic analysis supported an increase in the oligomannose type, along with decreases in the hybrid and complex types of N-glycans in the adult brains of the *mgat1b*$^{-/-}$ zebrafish strain compared to the Wt AB strain. Lectin blotting and qRT-PCR supported the knockdown in GnT-I activity in the adult brain, as well as the whole organism from 8 hpf to 24 dpf. Although prior glycomic studies have reported on the overall glycan populations of embryos and various zebrafish organs (Hanzawa, Suzuki et al. 2017, Yamakawa, Vanbeselaere et al. 2018) , our study investigated how reduced GnT-I activities contribute to the N-glycan population by altering the various types of N-glycans, such as lowering the levels of complex-type N-glycans. Moreover, our study investigated the negative consequences in the survival and development of zebrafish from this change in the N-glycan population.

N-glycomics is an important analytical technique that has been used in numerous different aspects of research to correlate glycan structure with cellular function (Shajahan, Heiss et al. 2017, Hall, Shajahan et al. 2023). Assaying *mgat1b*$^{-/-}$ in conjunction with Wt AB revealed that reduced complex-type N-glycans decreased the survivability of the mutant fish and, furthermore, delayed embryonic development. Embryonic survivability was about 50% for the *Mgat1b*$^{-/-}$ mutant strain. To elaborate, there was a drastic decline in embryonic survivability from 8 to 12 hpf and less decline after 12 hpf for the *mgat1b*$^{-/-}$ mutant strain. Further, various clutches had a similar survivability as the median value of percent viable embryos was like the mean value. Since embryonic development relies on maternal gene products (Abrams and Mullins 2009), it is of interest to evaluate the contribution of maternal mRNA. Our observations of developmental staging revealed that the *mgat1b*$^{-/-}$ mutant fish were lagging in development as they reached 75% epiboly at about 9 hpf and those that survived reached 90% epiboly at about 10–11 hpf, while the Wt AB embryos followed the developmental staging outlined by (Kimmel, Ballard et al. 1995). As such, the majority of *mgat1b*$^{-/-}$ embryos died during the transition from 75% to 90% epiboly, a stage of prominent cell movement, which transpires around 8–9 hpf in Wt AB zebrafish (Kimmel, Ballard et al. 1995). Given that at 90% epiboly, brain anlagen formation occurs (Mendelson 1986), it is plausible to associate the inability of the *mgat1b*$^{-/-}$ to transition from 75% to 90% epiboly with inefficient cell migration to the lessened complex-type N-glycans. Interestingly, the embryonic development of zebrafish at 12–15 hpf is equivalent to 9.5 to 10.5 embryonic days in mice (Takemoto, Natsuka et al. 2005), at which point GnT-I knockout is lethal due to maldevelopment of the neural tube (Ioffe and Stanley 1994), indicating that complex-type N-glycans are crucial even earlier in zebrafish development relative to mice since we observed a drastic decline in survival prior to 12 hpf. Taken together, our current study

implicates GnT-Ib knockdown as an impediment in zebrafish embryonic survivability and, specifically, supports that the developmental progression is halted due to possible inhibition of brain anlagen formation.

Complex-type N-glycans are present before brain anlagen development and during neuron development. Reports have shown that all three glycan types form as early as 6 hpf (Hanzawa, Suzuki et al. 2017). Moreover, glycomic studies indicated variable expression levels of complex-type N-glycans and a significant increase in the complex type at 12–15 hpf, (Takemoto, Natsuka et al. 2005), which is during the segmentation period when somites are formed and during the initiation of primary organs (Kimmel, Ballard et al. 1995). Our past studies supported the involvement of complex N-glycans in cell migration (Hall, Weidner et al. 2018, Issa, Hall et al. 2021, Hall, Shajahan et al. 2023) and, further, revealed the impact of partially N-glycosylated Kv3 channels, containing Kv3.1b protein, on primary motor neuron development and swimming locomotor activity in zebrafish (Issa, Hall et al. 2021). Together, the necessity of complex-type N-glycans is evident in embryonic development and neuronal function of zebrafish.

For the surviving *Mgat1b*$^{-/-}$ zebrafish, the influence of GnT-I knockdown in skeletal muscle organization and function was visible in the locomotion assays. Muscle performance during burst movements upon sensing external stimuli (Berger, Sztal et al. 2012, Smith, Beggs et al. 2013, Sztal, Ruparelia et al. 2016) was impaired at 2, 3, and 10 dpf in mutant fish relative to Wt AB. Further, spontaneous swimming distance, which is indicative of sustained muscle activity (Sztal, Ruparelia et al. 2016), was quite diminished in the *mgat1b*$^{-/-}$ mutant compared to Wt AB from 5 to 29 dpf. Organization of the muscle sarcomeres increased during skeletal muscle development (Berger, Sztal et al. 2012, Smith, Beggs et al. 2013). Here, we show that the organization of the sarcomeres was reduced in the embryos and larvae with GnT-I activity knocked down. Thus, the

delay in skeletal muscle development coincides with a reduction in motor and sensory functions. Likewise, past studies using the conditional inactivation of *mgat1* in mice corroborates the relevance of complex-type N-glycans in locomotor activity (Ye and Marth 2004). As such, our study implicates that inadequate levels of complex-type N-glycans can impair skeletal muscle development, thus coinciding with less efficient locomotor activity in zebrafish.

A range of diverse phenotypes from no marked clinical phenotype to severe disease is found in individuals with similar genetic variants (Kingdom and Wright 2022). Here, the indel introduced in both alleles of *mgat1b* showed incomplete penetrance and variable expressivity. As noted, embryonic survivability and developmental delays, including cardiac and skeletal muscle development, were observed in *mgat1b*$^{-/-}$ fish. Moreover, sensory and motor developmental delays were observed at 48 hpf in *mgat1b*$^{-/-}$ fish as less than 40% of embryos showed burst movements in response to one touch, while 65% of Wt AB had a response. Developmental delays in sensory and motor functions of the *mgat1b*$^{-/-}$ larvae were also noted at 3 dpf, which was supported by the delay in skeletal muscle development. Continued measurements of muscle performance via burst movements upon sensing external stimuli (Smith, Beggs et al. 2013), (Sztal, Ruparelia et al. 2016) and sustained muscle activity (Sztal, Ruparelia et al. 2016) revealed delays in motor function and sensory physiology throughout larval development. Thus, fish homozygous for the *mgat1b* mutation showed different degrees of disease, which support individuals suffering from congenital disorders of glycosylation, including disorders of N-glycosylation processing (Ondruskova, Cechova et al. 2021).

5. Conclusions

Defective N-glycan processing is a known deterrent in organismal survival and development, as noted in congenital orders of glycosylation (Ondruskova, Cechova et al. 2021). The impact of this rapidly growing disease family is devastating as it spans most organs and systems, yet minimal treatment options are available. Our study utilizing zebrafish reveals that increased oligomannose-type N-glycans concomitantly with reduced complex-type N-glycans diminishes overall survival, while those surviving exhibit significant developmental delays. It is of interest to note that the developmental delays traverse the nervous, cardiovascular, and skeletal systems. Moreover, developmental staging herein affords the opportunity to perhaps pinpoint specific periods of development in which certain N-glycan populations are crucial, particularly in terms of organ development. As such, these results suggest glycan populations as potential diagnostic targets/therapeutic options for a variety of human diseases, including congenital defects to adult onset. Our future direction is to engineer additional *mgat1* glycosylation mutant zebrafish strains, to perform similar developmental and behavioral studies, and to extend more diverse behavioral studies to juveniles and adults. Moreover, we will expand studies to include spinal cord morphology and microscopic evaluations of the neuronal structure, with the intent to corroborate the influence of complex-type N-glycans in organismal survival, development, and behavior. Although glycan studies that relate to survival and development in zebrafish are relatively minimal and we acknowledge our study could be enhanced by the creation of additional N-glycan knockout strains, as well as by performing a glycomic analysis of other tissues/organs, we believe that our study contributes to a better understanding of specific N-glycan populations in organismal development and function.

Contributions

For the work exhibited in this chapter I contributed to the genotyping, dissections for mass spec and lectin blotting, survivability, embryonic staging, vibrational startle, locomotor activity, heartbeat analysis and writing.

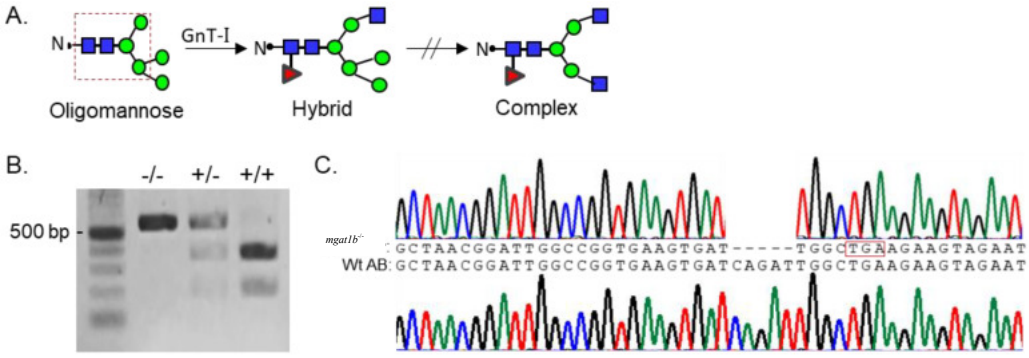
A.
N
GnT-I
N
N
Oligomannose
Hybrid
Complex
B.
-/-
+/-
+/+
500 bp
C.
mgat1b⁻
: GCTAACGGATTGGCCGGTGAAGTGAT-----TGGCTGAAGAAGTAGAAT
Wt AB: GCTAACGGATTGGCCGGTGAAGTGATCAGATTGGCTGAAGAAGTAGAAT

Figure 3.1 Generation and classification of the *mgat1b*$^{-/-}$ mutant line. Depiction of N-glycan types and the sequential processing initiated via GnT-I (*mgat1*) from the simplest N-glycan type (oligomannose) to more processed hybrid and complex types. The area encased within the dashed red box indicates the common pentasaccharide core (**A**). Products of BclI digest, which yield either homozygous *mgat1b*$^{-/-}$, heterozygous *mgat1b*$^{+/-}$, or Wt AB (*mgat1b*$^{+/+}$). Number adjacent to Kb ladder (500 bp) indicates band size (**B**). Chromatogram with coding sequence of a fragment of *mgat1b* from a Wt AB fish compared to that of *mgat1b*$^{-/-}$, revealing five nucleotide deletions (Δ5), which generated a premature stop codon (encased in red box) (**C**).

A.

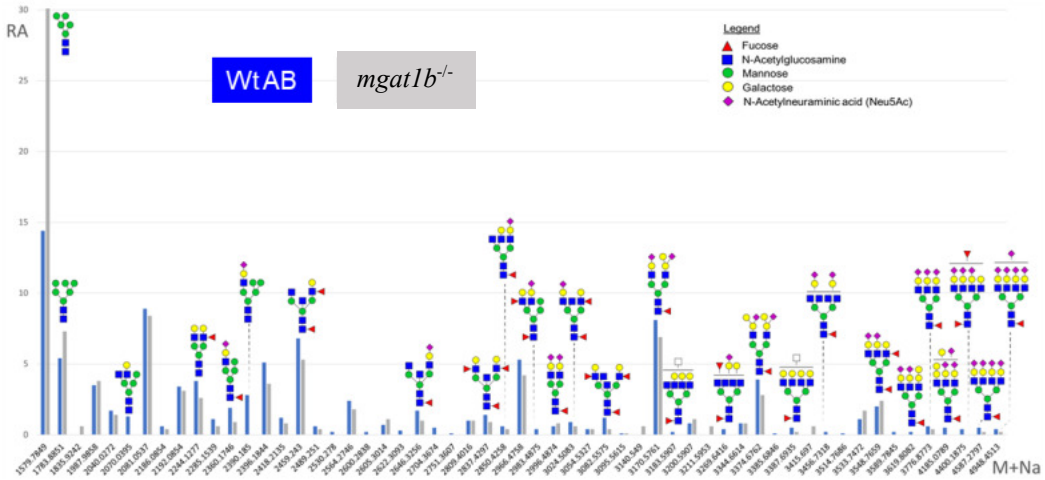
RA
WtAB
mgat1b-/-
Legend
Fucose
N-Acetylglucosamine
Mannose
Galactose
N-Acetylneuraminic acid (Neu5Ac)
M+Na

B.

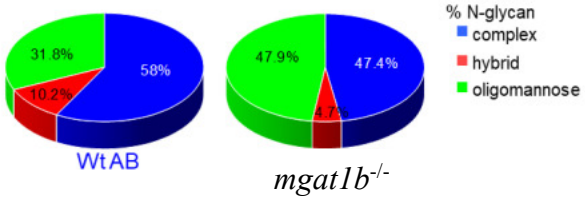
31.8%
58%
10.2%
WtAB
47.9%
47.4%
mgat1b-/-
% N-glycan
complex
hybrid
oligomannose

C.

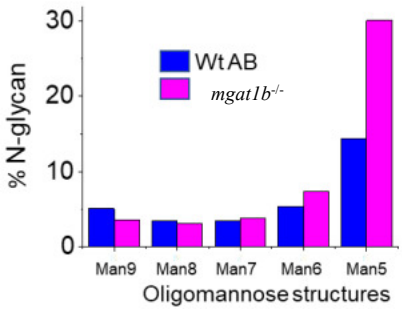
% N-glycan
30
20
10
0
WtAB
mgat1b-/-
Man9
Man8
Man7
Man6
Man5
Oligomannose structures

Figure 3.2 Comparison of LC-ESI-MS relative intensities of the permethylated N-glycans derived from Wt AB and the *mgat1b*$^{-/-}$ mutant line. LC-ESI-MS intensities of released N-glycans from Wt AB (blue bars) and *mgat1b*$^{-/-}$ (grey bars) (**A**). All molecular ions are present in sodiated form ([M + Na]+). N-glycan numbers correspond to **Figures S1 and S2**, and **Tables S2 and S3**. Breakdown of the percent of various detected N-glycan types (**B**) and types of oligomannose structures (**C**) identified by the ESI-MS spectra.

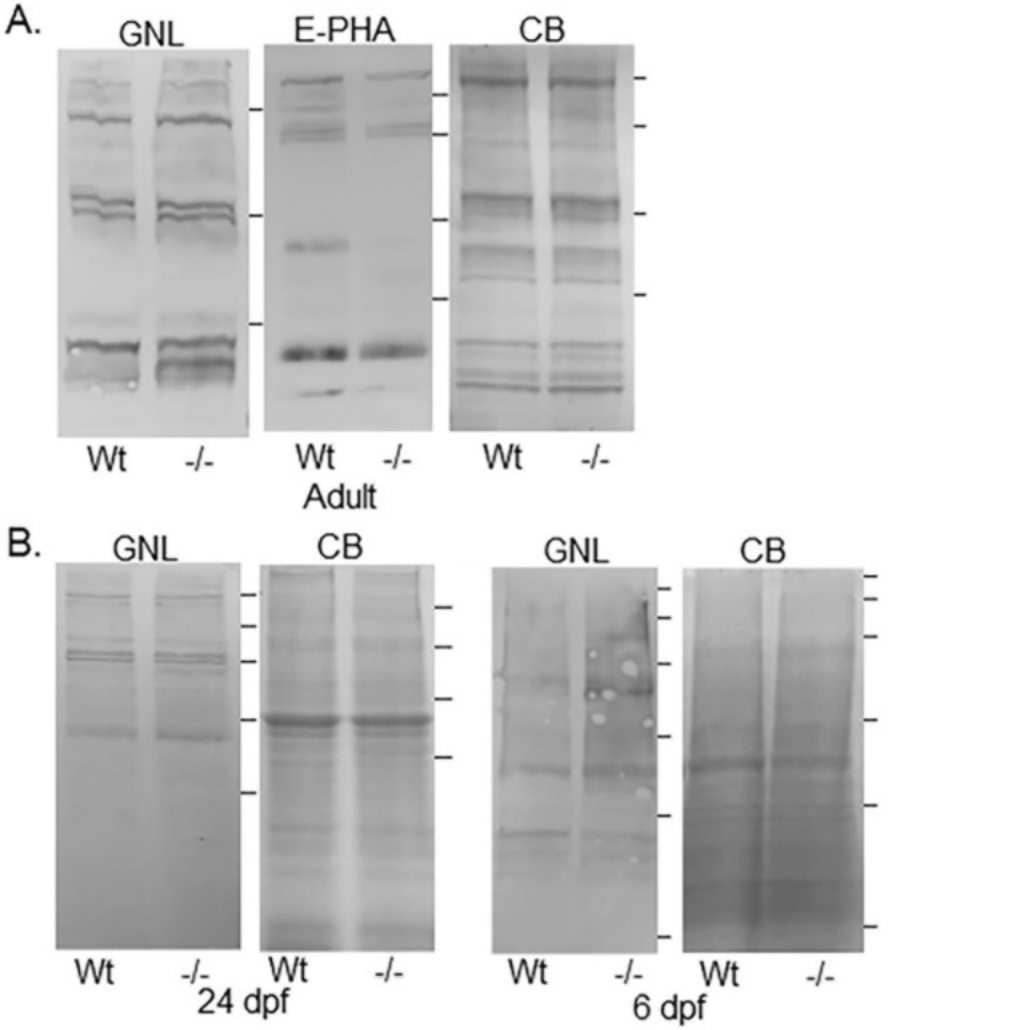
A.
GNL
E-PHA
CB
Wt
-/-
Wt
-/-
Wt
-/-
Adult
B.
GNL
CB
GNL
CB
Wt
-/-
Wt
-/-
Wt
-/-
Wt
-/-
24 dpf
6 dpf
C.
Wt AB
mgat1b-/-
Relative Mgat1b mRNA
1.2
0.8
0.4
0.0
**
**
**
*
Adult
24 dpf
6 dpf
8 hpf

Figure 3.3 Confirmation of decreased *mgat1b* expression, and an increase in oligomannose N-glycans in mutant strain of adult and larvae fish. Lectin blots of whole cell lysates of adult brain (**A**), and larvae at 24 dpf and 6 dpf from Wt AB and *mgat1b*$^{-/-}$ mutant zebrafish (**B**). Separated proteins were probed with Phaseolus vulgaris Erythroagglutinin (E-PHA) or Galanthus nivalis lectin (GNL). Coomassie blue (Rudy and McBain)-stained gel demonstrating equal protein loads among the samples. Lines adjacent to the blots denote protein markers (in KDa) 250, 150, 100, 75, 50, 37. Bar graphs represent *mgat1b* mRNA levels from Wt AB and *mgat1b*$^{-/-}$ mutant zebrafish relative to housekeeping genes β-actin (**C**) and ELFα (**Figure S1**). Data are presented as mean ± SEM, $n \geq 3$ and were all compared using Student's *t*-test (** $p < 0.005$, * $p < 0.02$).

A.

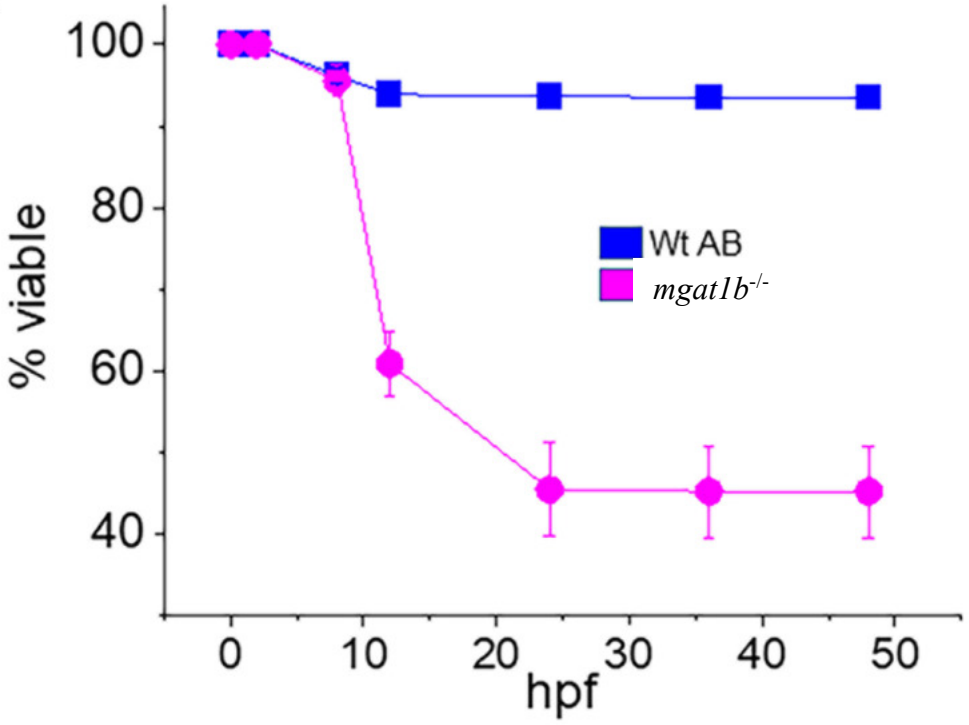
100
80
60
40
% viable
Wt AB
mgat1b-/-
0
10
20
30
40
50
hpf

B.

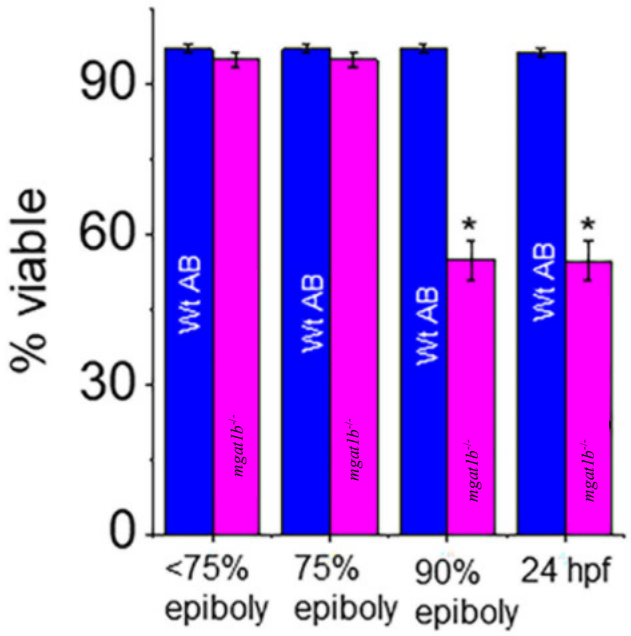
90
60
30
0
% viable
Wt AB
mgat1b-/-
*
<75% epiboly
75% epiboly
90% epiboly
24 hpf

Figure 3.4 Decline in survivability of *mgat1b*$^{-/-}$ mutants post 75% epiboly relative to Wt AB. Survivability of Wt AB and *mgat1b*$^{-/-}$ zebrafish tracked up to 48 hpf (**A**). Percent of viable embryos at the various stages of embryogenesis (**B**). Data are presented as mean ± SEM, $n \geq 8$ clutches, and were all compared using Student's *t*-test (* $p < 0.0001$).

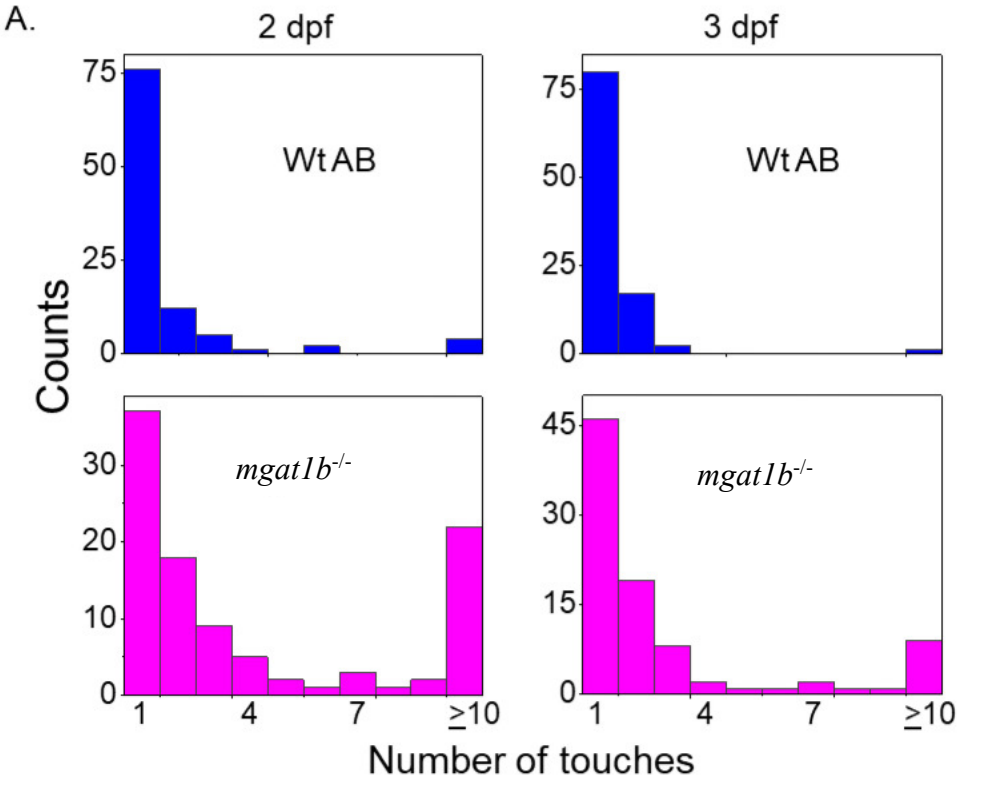
A.
2 dpf
3 dpf
Wt AB
Wt AB
mgat1b-/-
mgat1b-/-
Counts
Number of touches
1
4
7
≥10

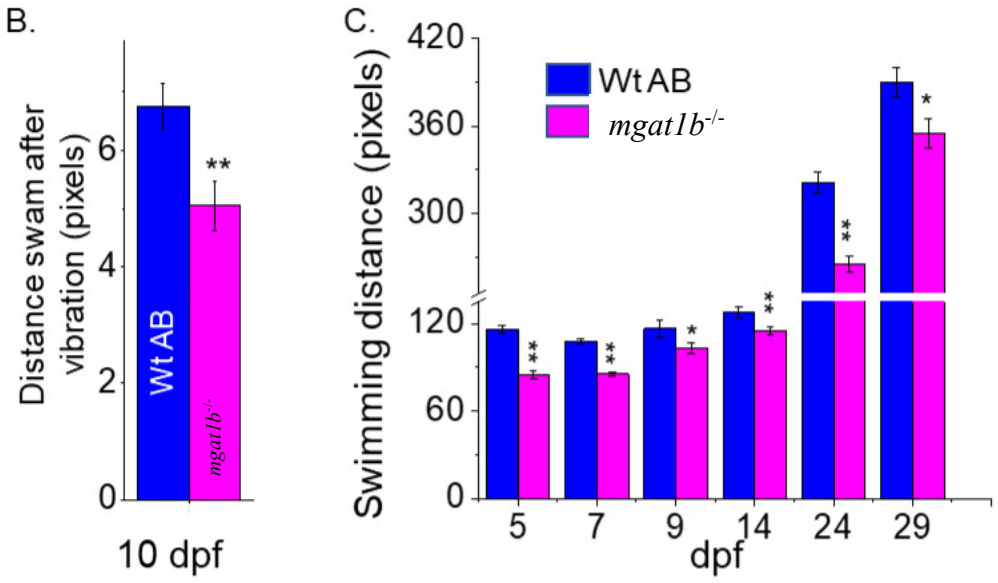
B.
Distance swam after vibration (pixels)
Wt AB
mgat1b-/-
10 dpf
C.
Swimming distance (pixels)
Wt AB
mgat1b-/-
dpf
5
7
9
14
24
29

Figure 3.5 Inhibition of motor and sensory functions in *mgat1b*$^{-/-}$ mutants. Touch-evoked response of Wt AB (upper panels) and *mgat1b*$^{-/-}$ (lower panels) at 2 and 3 dpf, as indicated (**A**). Data are presented as mean ± SEM, $n \geq 90$ larvae. Distance swam in response to vibrational stimuli exhibited in 10 dpf larvae, $n \geq 45$ larvae (**B**). Spontaneous locomotor swimming distance recorded in 5–29 dpf larvae, $n \geq 6$ fish (**C**). Data are presented as mean ± SEM and were compared using Student's *t*-test (** $p < 0.005$, * $p < 0.05$).

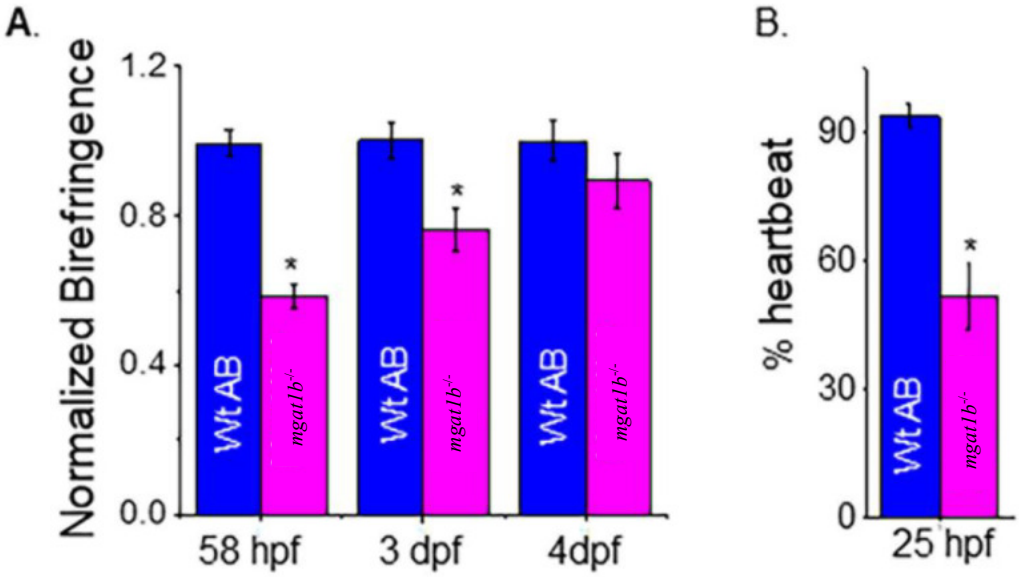
A.
Normalized Birefringence
1.2
0.8
0.4
0.0
Wt AB
mgat1b-/-
58 hpf
3 dpf
4dpf
B.
% heartbeat
90
60
30
0
25 hpf

Figure 3.6 Maldevelopment of skeletal and cardiac muscle in *mgat1b*$^{-/-}$ mutants. Normalized birefringence of Wt AB (n = 26, 31, 22 as 58 hpf, 3 dpf, and 4 dpf) and *mgat1b*$^{-/-}$ (n = 30, 25, and 22, at 58 hpf, 3 dpf, and 4 dpf); n denotes number of examined embryos or larvae (**A**). Percent of Wt AB and *mgat1b*$^{-/-}$ zebrafish with detected heartbeat at 25 hpf, n = 5 and n = 7 for Wt AB and *mgat1b*$^{-/-}$, respectively (**B**). Data are presented as mean ± SEM and were compared using Student's t-test (* $p < 0.003$).

Table S1. Zebrafish primers used for real time PCR.

Gene	Forward	Reverse
mgat1a	GGTTGTTGTTGTGGAGGACGA	TTGTCATTCCAGGCAGACACG
mgat1a	ACAAGATCGCCAGGCACTAC	ACAGCGCACGGAAATACTCA
β-actin	AGTTGTCTAACAGGGGAGAGC	TTGTGAGGAGGGCAAAGTGG
elfα	CTTCTCAGGCTGACTGTGC	CCGCTAGCATTACCCTCC

CHAPTER IV: Lowered GnT-I Activity Decreases Complex Type N-glycans and Results in Aberrant Primary Motor Neuron Structure in the Spinal Cord

- *This chapter is modified from Hatchett et al.,* Lowered GnT-I Activity Decreases Complex Type N-glycans and Results in Aberrant Primary Motor Neuron Structure in the Spinal Cord*; (188):e64534. 2024 August 11. doi:10.3390/jdb12030021*
  PMID: 39189261, PMCID: PMC11348029

Summary: The attachment of sugar to proteins and lipids is a basic modification needed for organismal survival, and perturbations in glycosylation cause severe developmental and neurological difficulties. Here, we investigated the neurological consequences of N-glycan populations in the spinal cord of Wt AB and *mgat1b* mutant zebrafish. Mutant fish have reduced N-acetylglucosaminyltransferase-I (GnT-I) activity as *mgat1a* remains intact. GnT-I converts oligomannose N-glycans to hybrid N-glycans, which is needed for complex N-glycan production. MALDI-TOF MS profiles identified N-glycans in the spinal cord for the first time and revealed reduced amounts of complex N-glycans in mutant fish, supporting a lesion in *mgat1b*. Further lectin blotting showed that oligomannose N-glycans were more prevalent in the spinal cord, skeletal muscle, heart, swim bladder, skin, and testis in mutant fish relative to WT AB, supporting lowered GnT- I activity in a global manner. Developmental delays were noted in hatching and in the swim bladder. Microscopic images of caudal primary (Sur, Wang et al.) motor neurons of the spinal cord transiently expressing EGFP in mutant fish were abnormal with significant reductions in collateral branches. Further motor coordination skills were impaired in mutant fish. We conclude that identifying the neurological consequences of aberrant N-glycan processing will enhance our understanding of the role of complex N-glycans in development and nervous system health.

1. Introduction

N-Glycosylation, the combination of sugars with proteins, is a basic process in organismal survival, as N-glycans in proteins have vital biological roles (Varki 1993). Perturbations in N-glycosylation have been associated with both neurodegenerative (Lee, Grigorian et al. 2007, Fajersztajn, Cordeiro et al. 2008, Schedin-Weiss, Winblad et al. 2014, Wajda and Sosnoff 2015, Moustafa, Chakravarthy et al. 2016, Kizuka, Kitazume et al. 2017, Videira and Castro-Caldas 2018, Cho, Veillon et al. 2019, Cvetko, Kifer et al. 2020, Conroy, Hawkinson et al. 2021, Xu, Jin et al. 2022, Pradeep, Kang et al. 2023) and neurodevelopmental (Pivac, Knezevic et al. 2011, Barone, Sturiale et al. 2016, Dwyer and Esko 2016, Cast, Boesch et al. 2021)diseases, and, therefore, it is of utmost importance to elucidate the contributions of specific N-glycans to nervous system health. Although the contribution of N-glycans to neurologic abnormalities is uncertain, congenital disorders of glycosylation (CDG) are a rapidly growing group of metabolic diseases in which patients manifest profound global developmental delays and defects, including neurologic difficulties (Chang, He et al. 2018, Verheijen, Tahata et al. 2020, Paprocka, Jezela-Stanek et al. 2021). All three types of N-glycans, including oligomannose, hybrid, and complex, have a common pentasaccharide core (Stanley 2022). The action of N-acetylglucosaminyltransferases (GnTs) on the core gives rise to all three types of N-glycans. The initial type of N-glycans biosynthesized is oligomannose, which is converted to the hybrid type via the action of GnT-I (encoded by *MGAT1*), and subsequently the hybrid type is further processed into the complex type via GnT-II (encoded by *MGAT2*). Zebrafish (*Danio rerio*) have two *mgat1* genes (*mgat1a/b*) which are ubiquitously expressed at varied levels (Sur, Wang et al. 2023), while other vertebrates, e.g., humans and mice, have a single *MGAT1* gene.

Prevention of N-glycan branching via GnT-I and GnT-II was detrimental in mice. *Mgat1* knockout mice died at embryonic day 9.5 (E9.5) due to maldeveloped neural tubes (Ioffe and Stanley 1994). While initial attempts to knockout *Mgat2* resulted in death during early post-natal development, a later effort using a specific genetic background produced some survivors which reiterated *MGAT2*-CDG (Wang, Tan et al. 2001, Wang, Schachter et al. 2002). Further, these *Mgat* genes were inactivated in the neurological tissue of mice at about E13. It was observed that the inactivation of *Mgat1* caused severe neurological defects and early post-natal death, while the inactivation of *Mgat2* supported viable and developed neurons (Ye and Marth 2004). These results suggested that complex N-glycans were dispensable in the development of neurons. However, patients with *MGAT2*-CDG have major neurological problems suggesting that complex N-glycans are essential for neurological processes (Tan, Dunn et al. 1996). It was the aim of this investigation to clarify the role of complex-type N-glycans in neuron development.

All three N-glycan types are biosynthesized as early as 6 hpf in zebrafish (Hanzawa, Suzuki et al. 2017). However, the level of oligomannose is much higher at 6 hpf, with a sharp increase in complex N-glycans occurring in the segmentation to the pharyngula period (10–48 hpf) (Hanzawa, Suzuki et al. 2017). The N-glycan population of adult zebrafish (*Danio rerio*) is quite diverse as 95 complex and hybrid types, and 5 of the oligomannose type of N-glycans were identified in 8 different tissues, including 20 N-glycans in the brain (Yamakawa, Vanbeselaere et al. 2018). A later study identified up to 48 complex and hybrid N-glycans, and furthermore showed that the amount of complex N-glycans to oligomannose N-glycans was significantly higher in the brain (Hall, Hatchett et al. 2023). The N-glycan populations of other neural tissues in zebrafish, such as the spinal cord, has yet to be deciphered.

The increase in complex-type N-glycans overlaps with the development of the primary motor neurons of the spinal cord. Zebrafish spinal cord neurons are broken into two types of neurons, including primary and secondary motor neurons. There are three variants of primary motor neurons found in the spinal cord: rostral primary (Aamodt, Waligorska et al.), middle primary (MiP), and caudal primary (Sur, Wang et al.) motor neurons, which first appear between 9 and 11 hpf (Kimmel, Ballard et al. 1995, Ahmed, Amin et al. 2018). The primary motor neurons per each hemi-segment are named and identified by their soma location when viewing the fish from the rostral end to the caudal end, and are further identified by the fast twitch muscles innervated by their axons (Wen and Brehm 2005, Moreno and Ribera 2009). This architecture of the zebrafish spinal cord is consistent between segments and in different zebrafish. Upon the exiting of their axons from the spinal cord, the primary motor neurons extend towards the horizontal myoseptum, and then their paths differentiate (Myers, Eisen et al. 1986, Lewis and Eisen 2003). CaP is the first axon to leave the spinal cord ventrally where it crosses the horizontal myoseptum, moves downward, and hooks around the ventral trunk musculature. RoP extends rostrally and ventrally along the horizontal myoseptum over the lateral surface of the axial muscles. MiP turns dorsally and caudally and extends over the dorsal axial muscle. During the first day of development, primary spinal neurons undergo axogenesis and then within a few hours, synaptic connections begin to be established (Myers, Eisen et al. 1986, Sainath and Granato 2013). The branching patterns to specific regions of the muscle are established by 3 dpf and are accompanied by changes in firing properties (Westerfield, Liu et al. 1990, Moreno and Ribera 2009). Hence, the spinal cord primary motor neurons of zebrafish offer an excellent approach for investigating whether the development of neurons depends on N-glycan branching.

In the present study, we identified 3 hybrid and 17 complex types of N-glycans, along with 4 oligomannose N-glycans, in the spinal cords of Wt AB zebrafish using MALDI-TOF MS. By far, the majority of the N-glycans were capped with sialic acid and were fucosylated. Previously, we engineered a *mgat1b* mutant fish strain, *(mgat1b*$^{-/-}$), which had higher levels of oligomannose and fewer complex N-glycans relative to Wt AB zebrafish (Hall, Hatchett et al. 2023). The oligomannose with five Man residues was more abundant in the spinal cord of the *mgat1b* mutant than in Wt AB, and furthermore, two of the three hybrid N-glycans were increased, and bi-antennary and tetra-antennary N-glycans were reduced in the mutant fish. GnT-I activity was globally reduced as the brain (Hall, Hatchett et al. 2023), spinal cord, skin, skeletal muscle, heart, swim bladder, and testis all had a higher affinity for a lectin which prefers binding oligomannose rather than hybrid and complex N-glycans. Examination of the spinal cord primary motor neurons in embryos revealed that the CaP motor neurons were defective, as they had diminished collateral branching innervating the ventral trunk musculature. Swimming locomotion of mutant larvae (8 dpf) was jerky and unsmooth, and furthermore, adult mutant fish had markedly reduced motor coordination and resistance. Thus, our investigation shows the N-glycan population in the spinal cord of Wt AB zebrafish, and that the reduction in the amount of complex-type N-glycans in the mutant fish results in an aberrant CaP motor neuron structure in embryos and larvae, along with deficits in motor resistance and coordination in adult zebrafish.

Materials and Methods

Zebrafish

The Institutional Animal Care and Use Committee (IACUC) of East Carolina University approved all zebrafish procedures within this study. The adult wildtype Pseudoloma-free AB

strain (Wt AB) was purchased from Sinnhuber Aquatic Research Laboratory (SARL) (Corvallis, OR, USA). The Wt AB was utilized for the creation of the *mgat1b*$^{-/-}$mutant zebrafish, and genetic edits were verified as previously described (Hall, Hatchett et al. 2023).

The *mgat1b*$^{-/-}$ mutant zebrafish used for studies herein were offspring from genotyped, fertile adult mutants, tested alongside the Wt AB. All zebrafish were maintained on a light/dark cycle of 14 h on and 10 h off at 28 °C. Fish were fed a high-protein diet of Gemma Micro pellets (Skretting, Tooele, UT, USA) every morning and afternoon beginning at 96 hpf to adulthood. Assays utilizing live zebrafish were performed at 28 °C.

Dissections of Tissue

Adult zebrafish were euthanized in an ice slurry bath for 10 min following operculum movement cessation following IACUC protocols. Euthanized fish were affixed on a Sylgard (Sigma Aldrich, St. Louis, MO, USA)-coated 100 mm dish with dissection pins via their insertion through the mouth, and extension through the ventral side of the fish. An incision from the upper lip through the cranium was made using spring scissors. Two perpendicular incisions were made running behind the gills, running dorsal to ventral, beginning at the initial cut. A ventral cut was added along the belly of the fish from the gills to just above the cloaca. The skin was pulled back along the fish's side until the skin peeled off with the organs visible. The heart, swim bladder, skin, and testis were then collected. The skeletal muscle was cut from the fish using spring scissors to reveal the spinal column. The spinal column was extricated by severing it from the brain and the tail. The vertebrae were removed by pulling apart the vertebrae using two forceps as the spinal cord was freed. Dissected tissues were placed in cryotubes, flash-frozen in liquid nitrogen, and stored at −80 °C until ready for use.

Total Membrane Preparations and Homogenate

Total membranes of about 100 pooled adult zebrafish spinal cords, 60 hearts, 50–60 swim bladders, and 8–10 skeletal muscle slices were isolated via ultracentrifugation, as previously described (Hall, Hatchett et al. 2023). Total membranes for glycan analysis (spinal cord) and lectin blots (spinal cord, heart, swim bladder, and skeletal muscle) were resuspended in 10 mM of Tris, pH 7.4; 250 mM of sucrose; 5 mM of EDTA; and protease inhibitor cocktail set III (Calbiochem, San Diego, CA, USA). Samples were kept at −80 °C until needed. Additionally, to minimize the number of fish euthanized, and since homogenates are adequate for lectin blotting, Wt AB and *mgat1b* zebrafish testis (20–24) and skin (slices from 3 adult fish) samples were pooled per tissue type, resuspended in the RIPA buffer (PBS, 1% Triton X-100, 0.5% sodium deoxycholate, and 0.1% SDS) plus protease inhibitor cocktail set III (EMD Biosciences, San Diego, CA, USA), pulse sonicated, and homogenates were resuspended in the SDS-PAGE sample buffer for protein evaluation. Samples were reduced and denatured by the addition of 200 mM of DTT.

Coomassie Blue-Stained Gels and Lectin Blots

Coomassie staining and lectin blotting were used to examine total membrane proteins and whole cell lysates. Samples were loaded on 10% SDS gels and allowed to migrate at 20 mA for 90 min. Then, the gel was placed directly in Coomassie® Brilliant Blue (MP Biomedical, Solon, OH, USA) for protein visualization, or migrated proteins were transferred to PVDF membranes (Whatman, Dassel, Germany) at 250 mA and used for lectin blotting, as previously described (Hall, Weidner et al. 2013). Biotin-conjugated GNL (Vector Laboratories, Burlingame, CA, USA) was used to probe transferred proteins.

N-Glycan Profiling

N-glycan profiling of total membrane protein fractions from the spinal cords of Wt AB and *mgat1b* adult zebrafish was performed using Creative Proteomics (Shirley, NY, USA). Details of the protocol can be viewed at https://www.creative-proteomics.com/resource/support-documents.html (accessed on 20 June 2024).

Spinner Task Assay

Motor coordination and resistance were measured in adult fish (Blazina, Vianna et al. 2013)with modifications. Briefly, zebrafish were acclimated in groups (25–30), with male and females separated, of an average size (3.2 cm) in tanks (6 L) for several weeks prior to the start of the assay. For the study, a 1000 mL beaker filled with 800 mL of rack system water was placed onto a Thermolyne Cimarec® 2 magnetic stir plate (Barnstead International, Dubuque, IA, USA) that was isolated within a box with blackened walls to reduce external stimuli and minimize fear. Zebrafish were placed individually into the beaker and allowed a habituation period of two minutes to lessen the effect of stress/anxiety. Following the habituation period, the stirrer speed was gradually increased incrementally for 30 s until the desired speed was reached, during which time the fish would move toward the wall and toward bottom of the beaker. Our determined desired speed was represented by the setting of 4.5 which corresponds to 540 rpm according to the manufacturer's specifications. Upon the attainment of the set speed, a timer was started and the ability of the fish to swim without being swept into the current was observed. As soon as the fish was swept into the whirlpool, the beaker was immediately removed from the stir plate and the sustained swimming time (seconds) was recorded. Assay was performed on four separate

days (two days were assayed blindly) for both males and females, but given no statistical differences being present between the sexes, the data were combined.

Zebrafish Hatching and Swim Bladder Developmental Evaluations

Hatching and swim bladder inflation (5 dpf) of Wt AB and *mgat1b*$^{-/-}$ embryos were examined by direct visual observation using a Zeiss 47 50 52- 9901 stereoscope at 5× magnification. Hatching was followed up to 78 hpf on 4 and 3 different experimental days, using 9 and 8 clutches from Wt AB and *mgat1b*$^{-/-}$ fish, respectively. The number of fish per clutch at about 24 hpf was 118, 83, 16, 36, 43, 90, 158, 62, and 128 for Wt AB fish, and 51, 36, 58, 105, 27, 44, 42, and 40 for *mgat1b*$^{-/-}$ fish. The percentage of hatched embryos was recorded at 72 and 78 hpf. Assessment of swim bladder inflation was followed on 3 and 4 different experimental days, using 5 and 4 clutches from Wt AB and *mgat1b*$^{-/-}$ fish, respectively. The number of fish per clutch at about 24 hpf was 50, 126, 71, 72, and 91 for Wt AB fish, and 12, 27, 60, and 115 for *mgat1b*$^{-/-}$ fish. The percentage of inflated swim bladders was recorded at 5 dpf.

Motor Skill Measurements via Mean Square Difference Analysis

The mean square difference (MSD) was assayed using the Zantiks MWP (Zantiks, Cambridge, UK). The apparatus is set to record 30 frames per 1 s time bin. As the protocol runs, one frame is subtracted from the following, thus generating a pixel difference between the two frames. The data were then squared to remove any negative values and reported as the mean pixel value for each arena with a bin of 1 s. Video noise was eliminated using a threshold set so that in an empty arena under constant lighting, the MSD value will be equal to 0. The threshold setting for this experiment was set at five, meaning any pixel difference recording under five was eliminated. It is expected that zebrafish with more “erratic” movements, e.g., twitching, tics, and unsmoothed

movements, will have a higher MSD value as they will cause more pixels with each movement. Fish were placed into six-well plates that were then moved to the Zantiks box, which was preheated to a temperature of 28 °C, and allowed to acclimate for 5 min. The assay was then run for 3 min with a time bin every 1 s. The overall average of the total fish movement was recorded.

Microscopy of Primary Motor Neurons in Live Embryos

Wt AB and *mgat1b*$^{-/-}$ zebrafish embryos with EGFP-expressing primary motor neurons were placed in 0.03% MS-222 for 3 m and then transferred to a microscope depression slide. Residual water surrounding the embryo was removed using a transfer pipet. A drop of warm 1% agarose was placed on top of the embryo and the slide was transferred to an ice pack for 5 s to hasten the solidification of the agar. Images were captured using a 40x water immersion objective with an upright Leica DM6 B epifluorescence microscope (Leica, Deer Park, IL, USA), with a set Z-step interval of 1 μm, 1 s of exposure time, and a numerical aperture of 0.80 au. CaP neuron images were processed using Leica Microsystems LAS X office 1.4.6.28433 software with the resulting z-stack compressed using ImageJ software version 1.54d. Compressed z-stacks of CaP neuron axons and collateral branches were traced in Adobe Photoshop and overlaid onto transmitted light images.

Statistical Analysis

The *N*-glycan structures were assigned via GlycoworkBench version 2.0 software. Agarose gel and lectin blot figures were created using Adobe Photoshop version 7.0. ImageJ software was used to obtain lectin blot band intensities. Origin version 9.55 was used for graphics and statistics. Data are presented as the mean ± S.E., where *n*denotes the number of observations, as

indicated. Statistical comparison was accomplished using an unpaired Student's *t*-test and a one-way ANOVA with Holm-Bonferroni adjustments.

Results

3.1. N-Glycan Profiles of Spinal Cords from Wt AB Zebrafish Lines

The N-glycan populations in spinal cords from adult zebrafish were examined for the first time. Isolated permethylated N-glycans from spinal cords of Wt AB zebrafish were analyzed by MALDI-TOF MS. The relative abundances, compositions, and proposed structures of N-glycans can be viewed in the supplementary section (Tables S1 and S2). N-glycans of the oligomannose to complex types with four extended branches were identified (Figure 1A). All three types of N-glycans were detected, but the oligomannose and complex types of N-glycans were much more prevalent than the hybrid type. Both Man5 oligomannose and bi-antennary N-glycans with sialic acid capping and core fucosylation had the highest percent values. The N-glycan population in the spinal cord consisted of 4 oligomannose, 3 hybrid, and 17 complex N-glycan structures (Figure 1B, left panel). A high majority of the complex N-glycans were capped with sialic acid while all hybrid N-glycans were sialylated (Figure 1B, middle panel). Further, most complex and hybrid types of N-glycans were fucosylated (Figure 1B, right panel). Complex N-glycans were quite diverse as six, two, and five structures with bi-antennary, tri-antennary, and tetra-antennary, respectively, were observed (Figure 1C). Four complex N-glycans were undefined regarding the number of antennae as three N-glycans could have been either bi-antennary with bisecting GlcNAc or tri-antennary, while another was either tri-antennary with bisecting GlcNAc or tretra-antennary. These results reveal that the N-glycan population is quite diverse in the spinal cord of adult zebrafish.

3.2. Differences in the N-Glycan Populations in Spinal Cords from Adult Wt AB and mgat1b$^{-/-}$ Zebrafish

Complex N-glycans in the spinal cords of adult Wt AB fish made up most N-glycan structures, followed by oligomannose N-glycans, and then low levels of the hybrid type, while significant differences between complex and oligomannose types were undetected for the mutant fish (Figure 2A). Further the relative abundance of the hybrid type was increased in mutant fish relative to Wt AB fish. Evaluation of the various N-glycans types showed that the 5Man oligomannose structure was seen markedly more in the mutant than in the Wt fish (Figure 2B). This finding supports that GnT-I activity is reduced due to lowered GnT-I levels in the mutant fish, as the 5Man oligomannose structure is the substrate used by GnT-I to convert oligomannose N-glycans into complex N-glycans. The rise in the hybrid type of N-glycans for the *mgat1b* mutant fish was due to an increase in two of the three hybrid N-glycans (Figure 2C). The decline in the complex type of N-glycans for the mutant fish was due to decreases in the levels of five of the seventeen complex N-glycans (Figure 2D). Two of the six bi-antennary, and three of the five tetra-antennary complex types of N-glycans were decreased, while the amounts of all tri-antennary N-glycans were quite similar between the two fish lines. The relative abundance for the various branched complex N-glycans, along with the fucosylated and sialylated N-glycans of the Wt AB and *mgat1b* mutant fish strains are summarized in Table 1. While the capping by sialylated N-glycans was quite similar, the level of fucosylated N-glycans for the *mgat1b* mutant fish was significantly reduced. Thus, lowered activity of GnT-I resulted in more Man5 oligomannose N-glycans which was accompanied by markedly reduced N-glycan branching and sialylated N-glycans in the spinal cord of the *mgat1b* mutant fish.

3.3. Oligomannose-Type N-Glycans Were Increased in Various Tissues of the mgat1b Mutant Relative to the Wt AB Zebrafish

Previously, we showed that the adult brain of *mgat1b* mutant zebrafish had increased amounts of oligomannose N-glycans relative to Wt AB via ESI-MS, and furthermore, lectin blotting confirmed this finding, along with there being more oligomannose N-glycans in young and old larvae (Hall, Hatchett et al. 2023). The lectin used was the *Galanthus nivalis* lectin (GNL) as it has a higher affinity for oligomannose relative to hybrid and complex types of N-glycans (Patnaik and Stanley 2006). Here, we compared the levels of oligomannose N-glycans in various tissues from adults of Wt AB (Wt) and the *mgat1b* mutant fish. The total band intensities of GNL binding to glycosylated proteins from adult spinal cords of the *mgat1b* mutants were higher than those of Wt AB (Figure 3A), verifying that oligomannose N-glycans were more prevalent in the mutant fish. The Coomassie blue-stained SDS gel (Rudy and McBain) shows that the amounts of proteins loaded for each sample were comparable. Skeletal muscles (Figure 3B), swim bladders (Figure 3C), hearts (Figure 3D), skin (Figure 3E), and testis (Figure 3F), were analyzed in a similar manner. In all cases, more GNL bound to the glycosylated protein from tissue obtained from the *mgat1b* mutant fish. Overall, the increased level of oligomannose N-glycans in seven different tissues from the *mgat1b* mutant compared to the Wt AB support that the reduction in GnT-I activity was global.

3.4. Primary Motor Neurons in the Spinal Cord of mgat1b Mutant Fish Are Maldeveloped

Previously, our data supported that the structure/function of fast-spiking neurons depends on the N-glycosylation processing of proteins, e.g., Kv3 voltage-gated K channels (Rudy and McBain 2001). Here, we investigated the role of reduced GnT-I activity on the development of caudal

primary (Sur, Wang et al.) motor neurons, fast-spiking cells, of the spinal cord. This choice was based on their early time (24–52 hpf) of development and maturation and well-characterized morphology (Myers, Eisen et al. 1986). As we previously described (Issa, Hall et al. 2021), the expression of EGFP in the motor neurons of zebrafish embryos was accomplished using a recombinant pTol2 vector which contained a motor neuron enhancer from the mouse Mnx1 (Hb9) gene. Although the motor neuron enhancer from the mouse Mnx1 (Hb9) gene is not specific for any one type of motoneuron, herein, our focus was on CaP neurons. The Leica thunder imaging system with an upright epifluorescence microscope was employed to acquire images of CaP neurons expressing EGFP in live images from 48 to 52 hpf (Figure 4A) and 72 to 76 hpf (Figure 4B). In all cases, fluorescence micrographs overlaid with transmitted microscope images show the positioning of the fluorescent CaP neuron relative to the spinal cord, notochord, and ventral myotome in Wt AB and *mgat1b*$^{-/-}$ mutant zebrafish embryos (upper panels). Further tracings of the neurons are depicted below the microscope images to clearly show the axon and collateral branching (lower panels). These images show that the *mgat1b*$^{-/-}$ mutant embryos clearly display the characteristic axon hook of CaP neurons by 52 hpf in live mgat1b mutant embryos like the Wt AB embryos. However, the CaP neurons from the mutant embryos have greatly reduced amounts of collateral branching relative to Wt AB embryos (Figure 4C). The reduced amount of collateral branching was observed in mutant fish (0.3 ± 0.1, n = 12; 0.6 ± 0.2, n = 10) relative to Wt AB fish (4.5 ± 0.3, n = 8; 6.1 ± 0.3, n = 12) at 48–52 hpf and 72–76 hpf, respectively. Further, there was a significant increase in the number of collateral branches for Wt AB fish from 48 to 72 hpf while the number of branches for *mgat1b* fish was not significant. These results support that CaP primary motor neuron development is aberrant in the *mgat1b* mutant.

3.5. Hatching and Swim Bladder Development Is Delayed

Previously, we showed that skeletal muscle development up to 4 dpf and the inception of heartbeat were delayed in the *mgat1b* mutant fish relative to the Wt AB fish (Hall, Hatchett et al. 2023). Since these delays were identified during the embryo period, we evaluated the hatching of the embryos at 72 and 78 hpf (Figure 5A). It was observed that close to 100% of the Wt AB embryos hatched at 72 hpf while only half of the *mgat1b* mutant embryos hatched. All embryos for both fish lines were hatched at 78 hpf. Close to all the Wt AB larvae had inflated swim bladders at 5 dpf, while only half of the *mgat1b*mutant larvae had inflated swim bladders (Figure 5B). Hence, development in the *mgat1b* zebrafish line shows developmental delays in embryonic, hatching, and larval periods.

3.6. Motor Coordination and Resistance Are Impaired in the mgat1b Mutant Fish

Previously, we showed that the total swimming distance per time period was greater for Wt AB than mgat1b mutant fish (Hall, Hatchett et al. 2023). Here, “erratic” movements, e.g., twitching, tics, and unsmoothed movements, in larvae and motor coordination in adult fish were studied. The MSD assay was used to assess twitching, and unsmooth movements in the *mgat1b* mutant larvae (8 dpf) compared to Wt AB larvae (Figure 5C). There was a substantial increase in the MSD values for the mutant larvae, indicating that the swimming locomotion was unsmooth, unlike that of the Wt AB larvae. Thus, the mutant larvae appear to have less motor coordination skills than the Wt AB larvae.

To measure motor coordination and resistance in adult fish, the spinning task protocol was employed (Blazina, Vianna et al. 2013). In short, individual adult fish with an average length of 3.2 cm were placed in a 1000 mL beaker filled with 800 mL of system water on top of a

magnetic stirrer. A current was gradually produced by spinning the stir bar until a speed of about 540 rpm was reached. The total amount of time Wt AB and *mgat1b*$^{-/-}$ fish could swim in the current before being swept into the vortex was recorded (Figure 5D). Wt AB fish could swim in the current much longer than the *mgat1b*$^{-/-}$ fish. When observing Wt AB fish, they tended to move towards the wall and the mid-bottom of the beaker and oriented themselves against the current. As time passed, the current moved them backwards, then the fish would resist and begin to swim against the current, but eventually the fish would move in the backwards direction and be swept into the whirlpool. They could fight the current for close to 75 s. In contrast, the *mgat1b*$^{-/-}$ fish had difficulty orienting themselves with the current and did not stay on the sides of the beaker; however, they could resist the current for about 30 s. Of note, since significant differences were not detected between the male and female lines, the data were combined. Taken together, the results support that motor coordination was defective in the *mgat1b* mutant fish.

Discussion

It has been shown that nullifying *Mgat1* in mice was embryonically lethal due to poor development, particularly in neural tissue, and mice died after a period between 9.5 and 10.5 days (Ioffe and Stanley 1994). Mice, like humans, have a single *Mgat1* gene. Since zebrafish have two *mgat1* genes (*mgat1a/b*) and are vertebrates, we created a *mgat1b* mutant fish model with reduced complex and increased oligomannose types of N-glycans to investigate how disruptions in the N-glycosylation pathway, resulting in lowered levels of complex-type N-glycans, cause defects and delays in development (Hall, Hatchett et al. 2023). It was verified that amounts of oligomannose N-glycans were increased in early and late-developed larvae, and adult brains. In the current study, oligomannose N-glycans were shown to be in higher amounts in six additional tissues, including spinal cords, hearts, skeletal muscles, skin, swim bladders, and testis from adults in the *mgat1b* mutant fish relative to the Wt AB fish. This systematic approach of profiling various organs for oligomannose N-glycans in adult fish supports that the mutation in *mgat1b* is reducing GnT-I activity in a global manner. It also substantiates that there are differences in N-glycan populations between tissues, such as those of the brain and the spinal cord which resulted in defective CaP neurons of the spinal cord. Additionally, the results indicate that identified delays in the development of the heart (Hall, Hatchett et al. 2023) , skeletal muscle (Hall, Hatchett et al. 2023), and swim bladder, including that in the hatching period, were caused by the perturbed N-glycosylation processing of proteins in the *mgat1b* mutant fish.

In the current study, the N-glycan structures of the spinal cord were identified for the first time in Wt AB zebrafish. The number of N-glycan structures were 17, 3, and 4 for complex, hybrid, and oligomannose N-glycans, respectively, and the majority of hybrid and complex N-glycan structures were sialylated and fucosylated. Further, the numbers of bi- and tetra-antennary N-

glycan structures identified were higher than the number of tri-antennary N-glycans, while in rat spinal cords, bi- and tri-antennary N-glycans were more abundant than tetra-antennary N-glycans (Ronan, Kshirsagar et al. 2022). We also observed that the abundance of oligomannose N-glycans (36 ± 3%) was lower than the abundance of complex (57 ± 4%) types of N-glycans in spinal cords, and these abundancies of the N-glycan types were comparable to those in zebrafish brains (Yamakawa, Vanbeselaere et al. 2018, Hall, Hatchett et al. 2023). However, hybrid-type N-glycan amounts were decreased in the brain (Hall, Hatchett et al. 2023)and increased in the spinal cord. Significant levels of oligomannose N-glycans were also obtained in rat spinal cords (Ronan, Kshirsagar et al. 2022), as observed in rat brains (Chen, Wing et al. 1998), but based on the ratio of complex to oligomannose types of N-glycans, it appeared that the amount of oligomannose N-glycans was higher in zebrafish. Taken together, complex N-glycans in zebrafish appeared to be more heavily branched than those in rat spinal cords, and furthermore, zebrafish tend to favor more oligomannose N-glycans in neural tissues than rats do.

Lessened GnT-Ib activity in the spinal cord causes attenuation in the later N-glycan-processing steps. Evidence for reduced GnT-Ib activity in the *mgat1b* mutant fish was shown via changes in the N-glycan populations in larvae (Hall, Hatchett et al. 2023) and various tissues of adults, including an increase in oligomannosylated N-glycans with 5 Man residues in the brain (Hall, Hatchett et al. 2023)and spinal cord compared to Wt AB fish. Unexpectedly, two of the three hybrid N-glycan amounts (m/z 1565, 1727) were significantly increased while the amounts of the other was unchanged. The diminution of the later steps of N-glycosylation processing was evident as the N-glycans in the spinal cord of the *mgat1b* mutant fish had significant reductions in the levels of fucosylated N-glycans and tetra-antennary N-glycans relative to those in the WT AB fish. Comparing the individual complex N-glycan structures of the *mgat1b* mutant fish to the

Wt AB fish, two sulfated tetra-antennary N-glycans (m/z 2840, 2954) showed significantly decreased levels, and furthermore, the amount of the lighter sulfated tetra-antennary N-glycan (m/z 2840) was reduced by roughly 50%. The other two sulfated N-glycans were bi-antennary and their levels were unmodified. It should be noted that seven complex N-glycans with sulfate were observed in rat spinal cords (Ronan, Kshirsagar et al. 2022), suggesting a role for these less-common N-glycans in the spinal cord. We also observed reduced levels of two bi-antennary N-glycans (m/z 2221, 2367) and a tri-antennary N-glycan (m/z 3024). These results argue that enhanced branching was reduced when the N-glycosylation pathway was disrupted at the initial branch site by decreased GnT-Ib activity.

Deciphering the role of hybrid and complex N-glycans in neural tissue development and maintenance is of utmost importance in therapeutics for neurodegenerative (Lee, Grigorian et al. 2007, Fajersztajn, Cordeiro et al. 2008, Schedin-Weiss, Winblad et al. 2014, Wajda and Sosnoff 2015, Moustafa, Chakravarthy et al. 2016, Kizuka, Kitazume et al. 2017, Videira and Castro-Caldas 2018, Cho, Veillon et al. 2019, Cvetko, Kifer et al. 2020, Conroy, Hawkinson et al. 2021, Xu, Jin et al. 2022, Pradeep, Kang et al. 2023) and neurodevelopmental (Pivac, Knezevic et al. 2011, Barone, Sturiale et al. 2016, Dwyer and Esko 2016, Cast, Boesch et al. 2021) diseases, as disruptions in N-glycosylation have been linked to these diseases. Past studies demonstrated that *Mgat1*knockout in mice was lethal at embryonic day 9.5 (E9.5), resulting from aberrant neural tube formation (Ioffe and Stanley 1994). Moreover, the inactivation of *Mgat1* in the neurological tissue of mice at about E13 caused serious neurological defects and early post-natal death, while the inactivation of *Mgat2* produced viable and developed neurons, indicating that hybrid N-glycans, not complex N-glycans, are required for the development of neurons (Ye and Marth 2004). However, patients with *MGAT2*-CDG have major neurological difficulties,

suggesting that complex-type N-glycans are essential for the development of neurons (Tan, Dunn et al. 1996). Additionally, replacement of complex N-glycans with hybrid N-glycans linked to a voltage-gated K channel, Kv3.1b, of the central nervous system which enables neurons to fire repetitively at high frequencies, produced Kv3 channels with slowed opening and closing rates in neuronal-derived cells (Hall, Weidner et al. 2017) , as did substitution with oligomannose, but the latter substitution had a more dramatic effect on the Kv3 channels (Issa, Hall et al. 2021). Further expression of Kv3.1b with only one of the two glycosylation sites occupied with complex N-glycans produced maldeveloped CaP motor neurons in zebrafish (Issa, Hall et al. 2021). The maldeveloped neurons had reduced branching, and in several cases, the characteristic hook was incomplete. Here, the amount of hybrid N-glycans increased while the amount of complex N-glycans decreased in the spinal cords of *mgat1b* mutant fish compared to those of Wt AB fish, and furthermore, CaP motor neurons were aberrant in the mutant fish. It was observed that CaP motor neurons had at least four branches at 48–52 hpf and that the number of branches increased to six at 72–76 hpf in Wt AB fish, while mutant fish developed the characteristic hook of CaP motor neurons with up to one branch at these time periods. Our current study, along with the discussed past studies, underlines the importance of complex N-glycans in the development of spinal cord neurons, specifically CaP motor neurons. Future studies will address whether other primary neurons or secondary neurons of the spinal cord have delays or defects in development.

Here, the CaP neurons were shown to be aberrant in embryos and larvae. We suspect that the CaP neurons are defective in structure and function throughout the life cycle of the fish since peripheral arbors of primary motor neurons in embryos were shown to be similar in adult fish (Myers, Eisen et al. 1986). Collateral branches of CaP neurons in Wt fish start at about 30 hpf and end at about 38 hpf (Sainath and Granato 2013). Our results showed that only 25% and 50%

of the embryos/larvae had a collateral branch at 2 and 3 dpf, respectively. When delays in development for other tissue were observed, they were much less pronounced, as shown for the onset of a heart beat (Hall, Hatchett et al. 2023), skeletal muscle organization (Hall, Hatchett et al. 2023), hatching, and the inflation of the swim bladder. Additionally, the deficiencies in motor activity in embryos(Hall, Hatchett et al. 2023) , larvae (Hall, Hatchett et al. 2023), and adults support that CaP neurons, and possibly other spinal cord primary motor neurons, may be defective as they innervate fast-twitch muscles and control fast, large-amplitude locomotion(Eisen, Myers et al. 1986, Liu and Westerfield 1988, Fetcho, Higashijima et al. 2008). Interestingly, our past study showed that when Kv3.1b lacked the attachment of one of the two N-glycans, CaP neurons were maldeveloped, causing larvae to have deficient amounts of locomotor activity (Issa, Hall et al. 2021). Since electrical properties of CaP neurons are established and modified in embryos at 24 hpf and 48 hpf, respectively (Moreno and Ribera 2009), and N-glycosylated Kv3 channels (Moreno and Ribera 2009, Issa, Mazzochi et al. 2011, Issa, Hall et al. 2021)are expressed in CaP neurons at about 24 hpf with significant increases thereafter, it may be that these channels have an impact on CaP neuron development. Taken together, our results showed that the structure of CaP neurons is abnormal in embryos and early developing larvae, and they suggest that the abnormality continues in the later developmental stages of the mutant fish. However, future studies will have to confirm the maturity of CaP neurons at later ages of the fish, and the involvement of Kv3 channels.

The impact of reduced GnT-I activity in the spinal cord on CaP motor neurons was evident in gross motor activity measurements. Since CaP motor neurons innervate trunk musculature (Moreno and Ribera 2009), reduced branching and incomplete axon formation would be expected to reduce swimming movements. Evoked and spontaneous swimming locomotion was

reduced in the embryos and larvae of *mgat1b* mutant fish relative to Wt AB fish (Hall, Hatchett et al. 2023). Here, we showed that *mgat1b* mutant larvae movements are jerky and unsmooth. Additionally, motor coordination and resistance were markedly reduced in adult *mgat1b* mutant fish. Taken together, the deficient gross motor activities implicate that CaP motor neurons, and possibly other spinal cord neurons, were underdeveloped, and spinal cord neuron function was deficient in adult *mgat1b* fish.

Conclusions

The relevance of N-glycosylation in the development and survival of organisms has been well established. The consequences of aberrant N-glycan processing are observed in individuals afflicted with symptoms resulting from congenital disorders of glycosylation, as the field currently offers little in terms of treatment. Moreover, given the severe neurological impact of this disease class, it is of great interest to expand studies that may also benefit those suffering from neurodevelopmental and neurodegenerative diseases. It is plausible that our results using a mutant *mgat1b*zebrafish strain as our model, combined with the novel assignment of N-glycans in the spinal cords of zebrafish, the microscopic evaluations of CaP motor neurons, and the examination of motor coordination, will enhance the understanding of the role of specific N-glycans in development and neurologic system health.

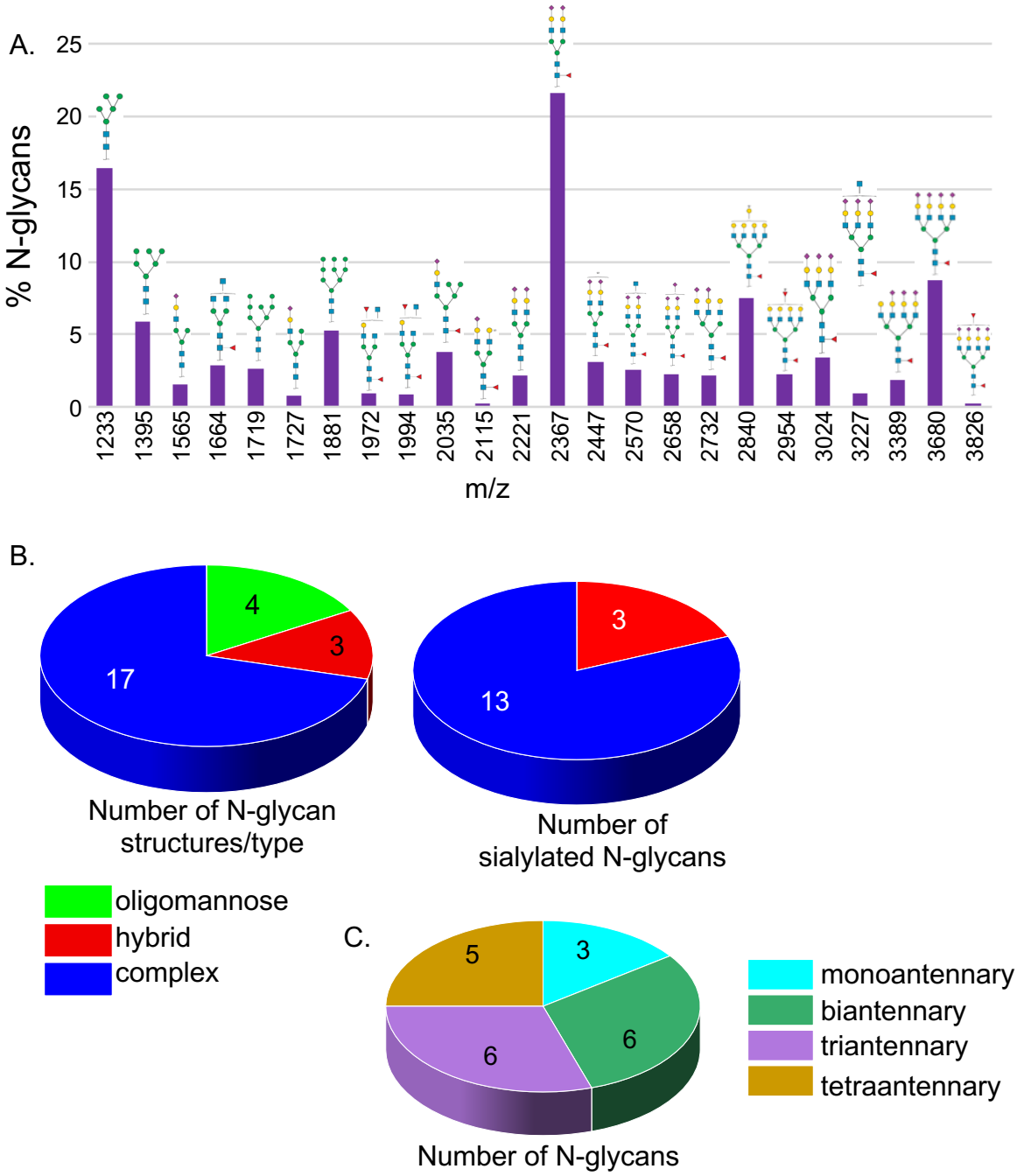
A.
% N-glycans
25
20
15
10
5
0
1233
1395
1565
1664
1719
1727
1881
1972
1994
2035
2115
2221
2367
2447
2570
2658
2732
2840
2954
3024
3227
3389
3680
3826
m/z
B.
4
3
17
Number of N-glycan structures/type
oligomannose
hybrid
complex
3
13
Number of sialylated N-glycans
C.
5
3
6
6
Number of N-glycans
monoantennary
biantennary
triantennary
tetraantennary

Figure 4.1 MALDI-TOF MS profiles of the N-glycans derived from Wt AB spinal cords. MALDI-TOF MS spectra of released *N*-glycan structures (%) from Wt AB spinal cords (**A**). The relative abundance is the average of four separate runs. *N*-Glycan numbers correlate to **Supplementary Tables S1 and S2**. Pie charts denote the number of *N*-glycan structures per type, and the number of sialylated and fucosylated hybrid and complex *N*-glycan structures (**B**). The breakdown of complex-type *N*-glycan structures by the number of antennae (**C**).

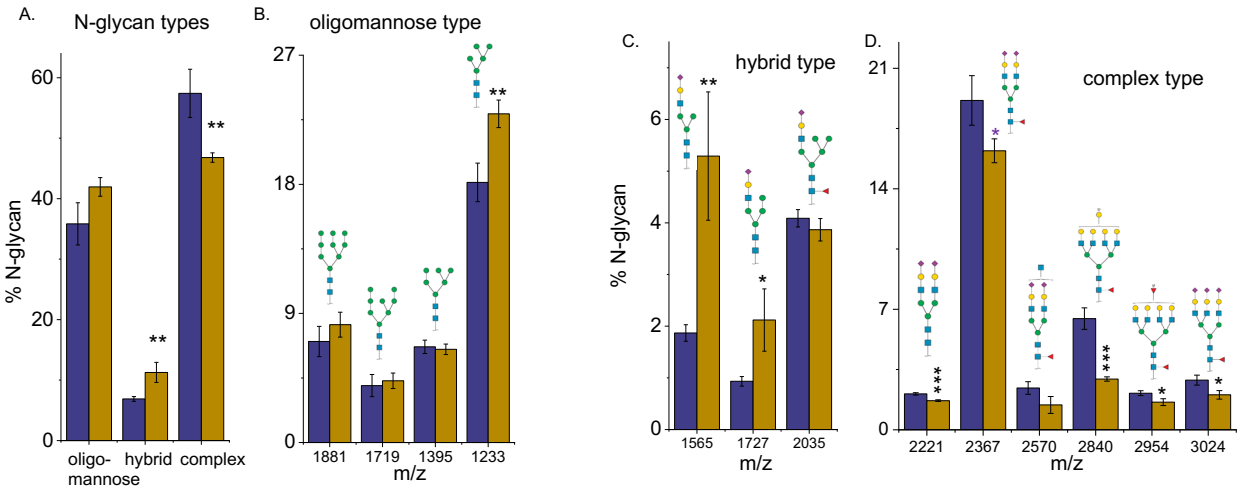
A.
N-glycan types
% N-glycan
60
40
20
0
**
**
oligo-
mannose
hybrid
complex
B.
oligomannose type
27
18
9
0
**
1881
1719
1395
1233
m/z
C.
hybrid type
% N-glycan
6
4
2
0
**
*
1565
1727
2035
m/z
D.
complex type
21
14
7
0
***
*
***
*
2221
2367
2570
2840
2954
3024
m/z

Figure 4.2 Comparison of N-glycan structures derived from adult Wt AB and *mgat1b*$^{-/-}$ mutant zebrafish. Averaged MS spectra of released N-glycan types (%) from Wt AB (purple bars) and *mgat1b*$^{-/-}$ (gold bars) zebrafish (**A**). Representative bar graphs showing the percents of oligomannose (**B**), hybrid (**C**), and complex (**D**) structures with the corresponding m/z value of the structures. Data are presented as mean ± SEM, $n = 4$, where n signifies the number of technical replicates, and Wt AB to mutant zebrafish were compared using Student's *t*-test (* $p < 0.11$, * $p < 0.08$, ** $p < 0.05$, *** $p < 0.01$).

N-glycan	Wt AB	mgat1b$^{-/-}$
sialylated	49.0 ± 4.8	45.6 ± 2.7
fucosylated	59.4 ± 3.8	49.0 ± 0.7**
bi-antennary	27.6 ± 1.6	25.3 ± 1.1
tri-antennary	4.8 ± 0.5	3.9 ± 0.4
tetra-antennary	15.3 ± 4.0	7.8 ± 0.9*

Table 4.1 N-glycan structures of spinal cords from Wt AB ($n = 4$) and *mgat1b*$^{-/-}$ ($n = 4$) adult fish. Values are expressed as mean ± S.E, where *n* denotes replicates. * and ** denote $p > 0.12$, 0.035.

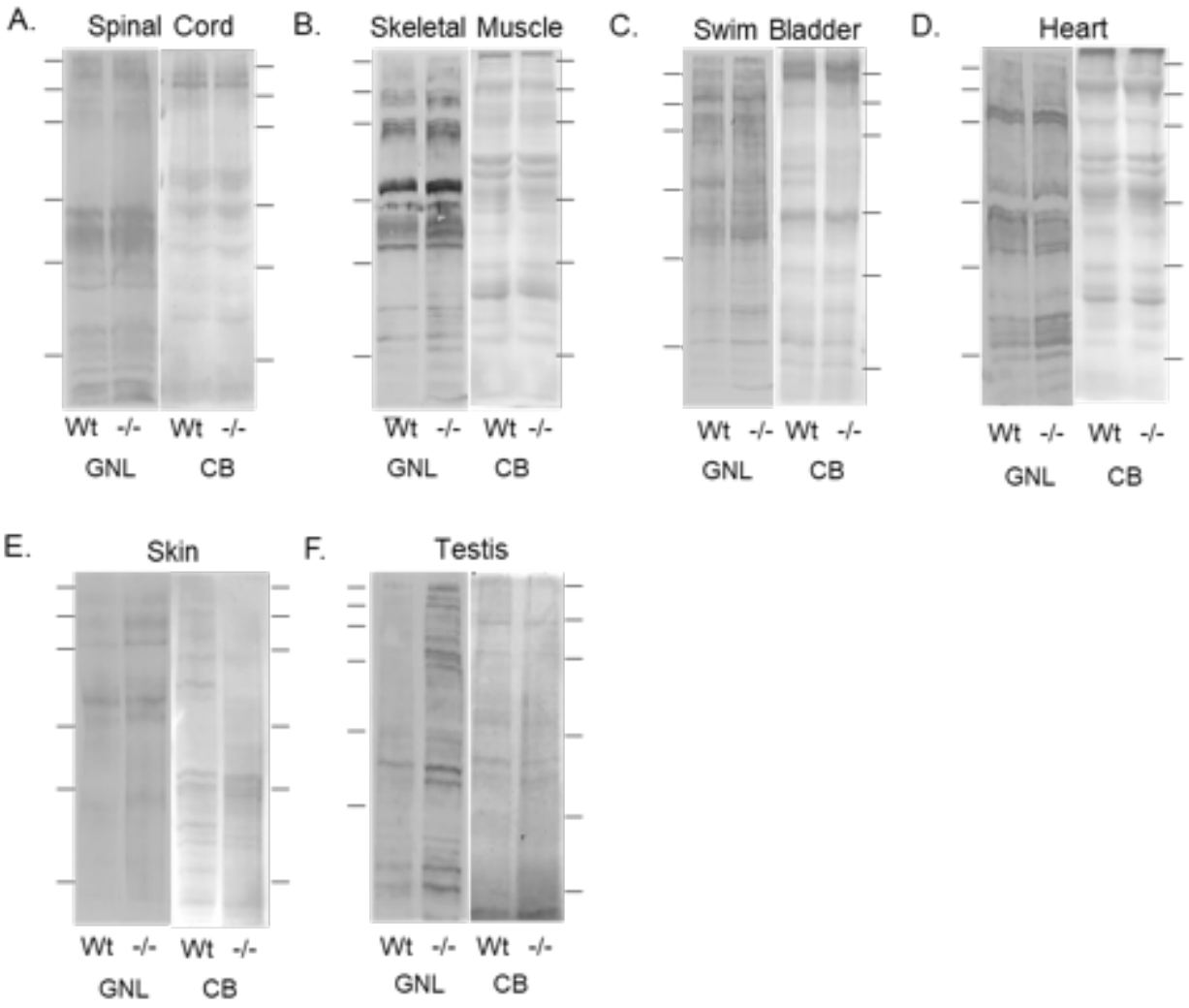
A.
Spinal Cord
B.
Skeletal Muscle
C.
Swim Bladder
D.
Heart
Wt -/- Wt -/-
GNL CB
E.
Skin
F.
Testis

Figure 4.3 Validation of diminished mgat1b expression and a concomitant increase in oligomannose N-glycans in various tissues. Lectin blots of total membranes from spinal cords (**A**), skeletal muscles (**B**), swim bladders (**C**), hearts (**D**), and whole cell lysates of skin (**E**), and testis (**F**) harvested from adult Wt AB and *mgat1b*$^{-/-}$ mutant zebrafish. Separated proteins were probed with Galanthus nivalis lectin (GNL). In all cases, lectin blots were reproducible (n = 3); see **Figure S1**. For the quantification of lectin band intensities relative to protein loads, see **Table S3**. Coomassie blue (Rudy and McBain)-stained gel adjacent to each lectin demonstrated equal protein loads among the samples. Lines adjacent to the blots denote protein markers (in kDa) 250, 150, 100, 75, 50, and 37.

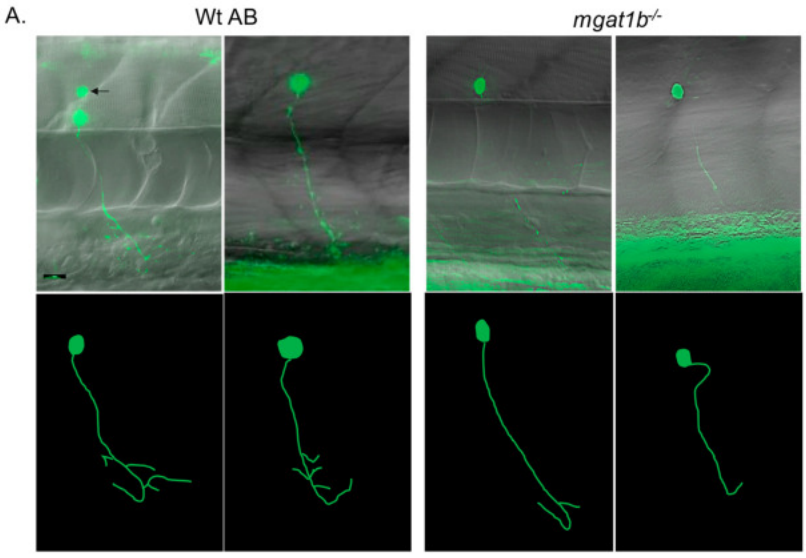
A.
Wt AB
mgat1b-/-

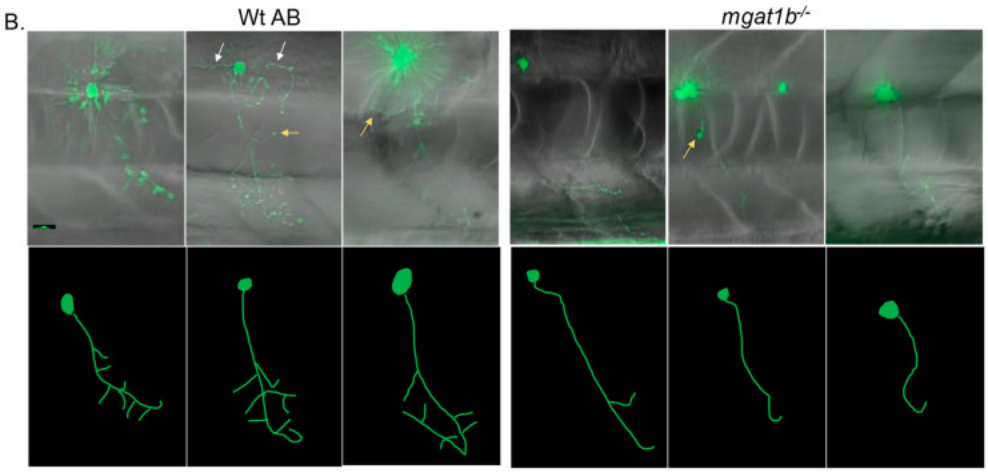
B.
Wt AB
mgat1b-/-

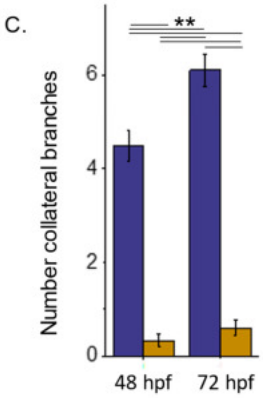
C.
**
Number collateral branches
0
2
4
6
48 hpf
72 hpf

Figure 4.4 Mutant fish show maldeveloped primary motor neurons in the spinal cord relative to Wt AB fish. EGFP-expressing CaP primary motor neuron images captured at 48–52 hpf (**A**) and 72–76 hpf (**B**) using a 40X objective. Upper panels depict images captured, overlaid with bright field images. Black arrows denote secondary, white arrows signify middle primary (MiP), and yellow arrows show rostral primary (Aamodt, Waligorska et al.) motor neurons. For clarity, the lower panels are tracings of CaP neurons from reconstructed images. The tracings do not include MiP, RoP, or secondary neurons. Scale bar represents 25 μm in all cases. Assessment of the number of collateral branches in Wt AB (purple) and *mgat1b*$^{-/-}$ (gold bars) fish (**C**). Wt AB (n = 20); *mgat1b*$^{-/-}$(n = 22); n denotes a neuron. Data are presented as mean ± SEM and were compared using one-way ANOVA at $p < 0.01$, **.

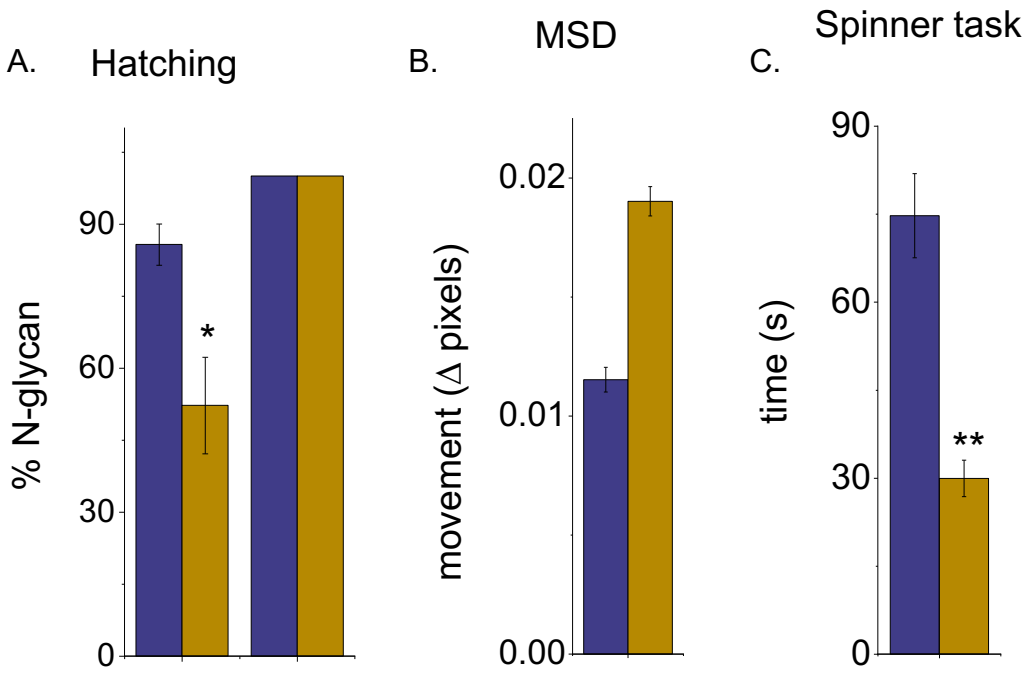
A.
Hatching
% N-glycan
90
60
30
0
*
B.
MSD
movement (Δ pixels)
0.02
0.01
0.00
C.
Spinner task
time (s)
90
60
30
0
**

Figure 4.5 Mutant fish demonstrate delayed hatching and swim bladder development, and motor skill impairment. Bar graphs representing the percent (%) of embryos hatched at 72 hpf (left bars) and 78 hpf (right bars), while *n* denotes number of clutches (**A**), and the percent of swim bladders inflated at 5 dpf, while *n* signifies number of clutches (**B**). Movement in pixels acquired via the mean square difference (MSD) assay at 8 dpf, while *n* denotes the number of fish (**C**). Time in seconds that adult zebrafish could efficiently swim without being swept into the whirlpool as observed in the spinner task assay, *n* represents the number of fish (**D**). In all cases, Wt AB are shown in purple bars, and *Mgat1b*$^{-/-}$ in gold bars. Data are presented as mean ± SEM and were compared using Student's *t*-test (*** $p < 0.0001$; ** $p < 0.01$; * $p < 0.04$).

Figure S1. Lectin blots (GNL) of tissue from zebrafish

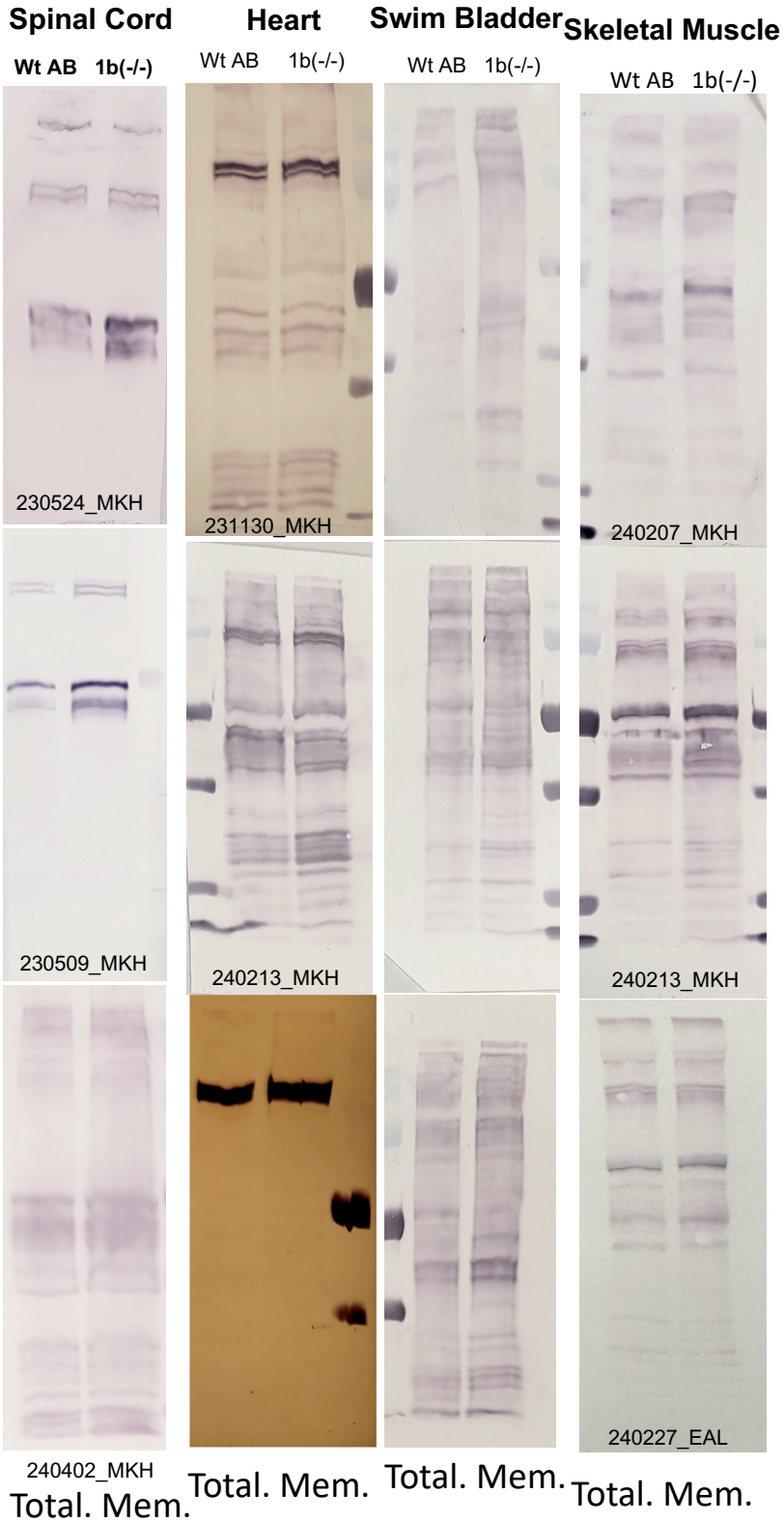

Figure 4. S1

Lectin blots (GNL) of tissue from zebrafish

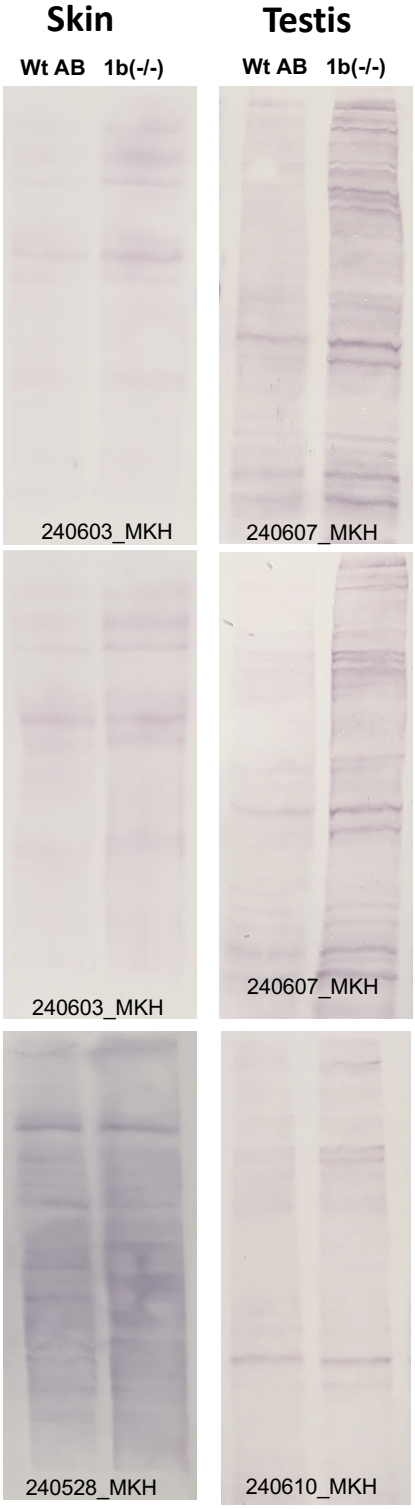

Coomassie blue stained gels f from zebrafish

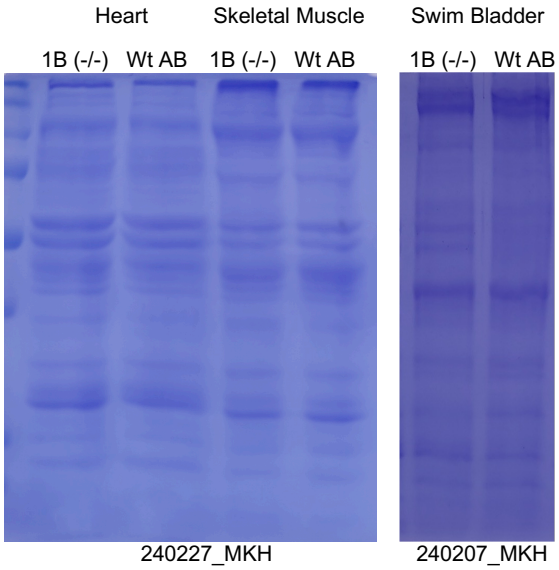

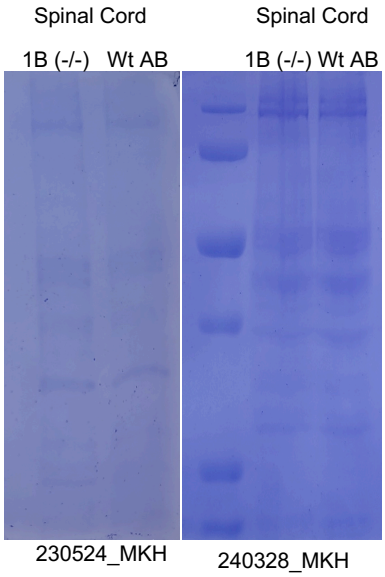

Table 4. S1 The following table summarizes the N-glycan profiled of replicate of the 3 and 4, including monoisotopic mass, compositions, proposed structures, and relative abundance.

m/z	Composition	Proposed Structure	WT Rep 1	WT Rep 2	1b Rep 1	1b Rep 2
1233.43	(Hex)2 + (Man)3(GlcNAc)2	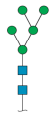	11.26%	14.35%	19.72%	19.15%
1395.48	(Hex)3 + (Man)3(GlcNAc)2	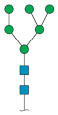	4.44%	4.71%	5.22%	5.01%
1565.55	(Hex)1 (HexNAc)1 (NeuAc)1 + (Man)3(GlcNAc)2		1.21%	1.28%	2.96%	6.12%
1664.62	(HexNAc)3 (Deoxyhexose)1 + (Man)3(GlcNAc)2	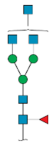	1.77%	2.67%	2.98%	3.17%
1719.58	(Hex)5 + (Man)3(GlcNAc)2	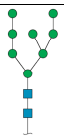	1.79%	2.33%	2.62%	2.92%
1727.60	(Hex)2 (HexNAc)1 (NeuAc)1 + (Man)3(GlcNAc)2	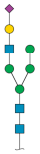	0.68%	0.54%	0.90%	2.55%
1840.61	(Hex)7 + (Man)3 (GlcNAc)1	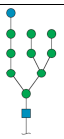	9.12%	11.25%	10.52%	6.96%
1881.64	(Hex)6 + (Man)3(GlcNAc)2	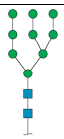	3.82%	4.31%	5.26%	5.75%
1972.73	(HexNAc)3 (Hex)1 (Deoxyhexose)2 + (Man)3(GlcNAc)2	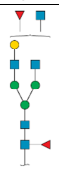	0.00%	1.44%	2.33%	2.55%

1994.64	(HexNAc)2 (Hex)1 (NeuAc)1 (Deoxyhexose)1 (Sulph)1 + (Man)3(GlcNAc)2		0.66%	0.71%	0.00%	2.83%
2002.66	(Hex)8 + (Man)3(GlcNAc)1		8.47%	9.36%	9.47%	6.70%
2035.71	(HexNAc)1 (Hex)3 (NeuAc)1 (Deoxyhexose)1 + (Man)3 (GlcNAc)2		2.86%	3.09%	3.11%	2.75%
2115.67	(HexNAc)2 (Hex)2 (NeuAc)1 (Sulph)1 + (Man)3 (GlcNAc)2		0.46%	0.00%	0.00%	1.19%
2205.74	(Hex)8 + (Man)3(GlcNAc)2		0.69%	0.47%	0.48%	1.23%
2221.77	(Hex)2 (HexNAc)2 (NeuAc)2 + (Man)3(GlcNAc)2		1.69%	1.72%	1.41%	1.36%
2367.83	(Hex)2 (HexNAc)2 (NeuAc)2 (Deoxyhexose)1 + (Man)3(GlcNAc)2		17.27%	16.31%	14.14%	12.47%
2447.79	(Hex)2 (HexNAc)2 (NeuAc)2 (Deoxyhexose)1 (Sulph)1 + (Man)3(GlcNAc)2		2.24%	2.61%	2.30%	2.24%

2529.85	(Hex)10 + (Man)3(GlcNAc)2		2.61%	2.22%	1.71%	1.70%
2570.91	(Hex)2 (HexNAc)3 (NeuAc)2 (Deoxyhexose)1 + (Man)3(GlcNAc)2		1.34%	2.65%	0.00%	1.78%
2658.93	(Hex)2 (HexNAc)2 (NeuAc)3 (Deoxyhexose)1 + (Man)3(GlcNAc)2		1.31%	2.23%	2.18%	1.87%
2732.97	(Hex)3 (HexNAc)3 (NeuAc)2 (Deoxyhexose)1 + (Man)3(GlcNAc)2		1.77%	1.60%	1.87%	1.59%
2840.01	(HexNAc)4 (Hex)6 (Deoxyhexose)1 + (Man)3(GlcNAc)2		6.29%	5.33%	2.59%	2.31%
2954.08	(HexNAc)4 (Hex)4 (Deoxyhexose)4 + (Man)3(GlcNAc)2		1.51%	1.95%	1.70%	1.13%
3024.06	(Hex)3 (HexNAc)3 (NeuAc)3 (Deoxyhexose)1 + (Man)3(GlcNAc)2		2.57%	2.68%	2.16%	1.47%
3227.14	(Hex)3 (HexNAc)4 (NeuAc)3 (Deoxyhexose)1 + (Man)3(GlcNAc)2		0.84%	0.58%	0.53%	0.35%

3389.19	(Hex)4 (HexNAc)4 (NeuAc)3 (Deoxyhexose)1 + (Man)3(GlcNAc)2		1.53%	1.34%	1.49%	1.08%
3680.29	(Hex)4 (HexNAc)4 (NeuAc)4 (Deoxyhexose)1 + (Man)3(GlcNAc)2	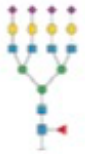	11.81%	1.87%	2.09%	1.60%
3826.34	(Hex)4 (HexNAc)4 (NeuAc)4 (Deoxyhexose)2 + (Man)3(GlcNAc)2		0.00%	0.42%	0.27%	0.20%

Table 4. S2 The following table summarizes the N-glycan profiled of replicate of the 3 and 4, including monoisotopic mass, compositions, proposed structures, and relative abundance.

m/z	Composition	Proposed Structure	WT Rep 3	WT Rep 4	1b Rep 3	1b Rep 4
1233.43	(Hex)2 + (Man)3(GlcNAc)2		15.13%	15.77%	18.23%	17.01%
1395.48	(Hex)3 + (Man)3(GlcNAc)2		5.73%	5.90%	5.97%	4.82%
1565.55	(Hex)1 (HexNAc)1 (NeuAc)1 + (Man)3(GlcNAc)2		1.61%	1.72%	2.06%	6.14%
1664.62	(HexNAc)3 (Deoxyhexose)1 + (Man)3(GlcNAc)2		5.14%	5.14%	5.51%	4.39%
1719.58	(Hex)5 + (Man)3(GlcNAc)2		4.17%	4.07%	4.53%	3.89%
1727.60	(Hex)2 (HexNAc)1 (NeuAc)1 + (Man)3(GlcNAc)2		0.86%	0.83%	0.80%	2.69%
1840.61	(Hex)7 + (Man)3 (GlcNAc)1		10.44%	10.92%	8.95%	7.85%
1881.64	(Hex)6 + (Man)3(GlcNAc)2		7.04%	6.78%	8.36%	7.25%
1972.73	(HexNAc)3 (Hex)1 (Deoxyhexose)2 + (Man)3(GlcNAc)2		2.56%	2.32%	3.86%	0.89%

1994.64	(HexNAc)2 (Hex)1 (NeuAc)1 (Deoxyhexose)1 (Sulph)1 + (Man)3(GlcNAc)2		1.02%	0.39%	0.00%	2.69%
2002.66	(Hex)8 + (Man)3(GlcNAc)1		8.60%	9.03%	8.42%	7.69%
2035.71	(HexNAc)1 (Hex)3 (NeuAc)1 (Deoxyhexose)1 + (Man)3 (GlcNAc)2		3.40%	3.38%	3.48%	3.16%
2115.67	(HexNAc)2 (Hex)2 (NeuAc)1 (Sulph)1 + (Man)3 (GlcNAc)2		0.48%	0.00%	0.38%	1.16%
2205.74	(Hex)8 + (Man)3(GlcNAc)2		0.55%	0.56%	0.58%	0.30%
2221.77	(Hex)2 (HexNAc)2 (NeuAc)2 + (Man)3(GlcNAc)2		1.52%	1.56%	1.39%	1.32%
2367.83	(Hex)2 (HexNAc)2 (NeuAc)2 (Deoxyhexose)1 + (Man)3(GlcNAc)2		12.91%	13.09%	12.89%	12.89%
2447.79	(Hex)2 (HexNAc)2 (NeuAc)2 (Deoxyhexose)1 (Sulph)1 + (Man)3(GlcNAc)2		2.05%	2.01%	1.85%	2.23%

2529.85	(Hex)10 + (Man)3(GlcNAc)2		2.00%	1.83%	1.80%	1.77%
2570.91	(Hex)2 (HexNAc)3 (NeuAc)2 (Deoxyhexose)1 + (Man)3(GlcNAc)2		1.78%	1.78%	1.53%	1.43%
2658.93	(Hex)2 (HexNAc)2 (NeuAc)3 (Deoxyhexose)1 + (Man)3(GlcNAc)2		2.04%	1.72%	1.25%	1.82%
2732.97	(Hex)3 (HexNAc)3 (NeuAc)2 (Deoxyhexose)1 + (Man)3(GlcNAc)2		1.00%	1.61%	1.33%	1.30%
2840.01	(HexNAc)4 (Hex)6 (Deoxyhexose)1 + (Man)3(GlcNAc)2	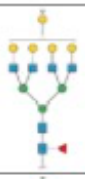	4.37%	4.13%	2.29%	2.35%
2954.08	(HexNAc)4 (Hex)4 (Deoxyhexose)4 + (Man)3(GlcNAc)2	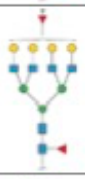	1.55%	1.61%	1.08%	1.26%
3024.06	(Hex)3 (HexNAc)3 (NeuAc)3 (Deoxyhexose)1 + (Man)3(GlcNAc)2		1.82%	1.91%	1.44%	1.48%
3227.14	(Hex)3 (HexNAc)4 (NeuAc)3 (Deoxyhexose)1 + (Man)3(GlcNAc)2		0.22%	0.00%	0.41%	0.23%

3389.19	(Hex)4 (HexNAc)4 (NeuAc)3 (Deoxyhexose)1 + (Man)3(GlcNAc)2		0.62%	0.64%	0.58%	0.63%
3680.29	(Hex)4 (HexNAc)4 (NeuAc)4 (Deoxyhexose)1 + (Man)3(GlcNAc)2	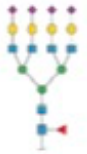	1.14%	1.13%	0.78%	1.10%
3826.34	(Hex)4 (HexNAc)4 (NeuAc)4 (Deoxyhexose)2 + (Man)3(GlcNAc)2		0.23%	0.18%	0.24%	0.24%

Table 4. S3 The following table outlines the lectin blot band intensities of the various tissues (*n*=3 per tissue). Numbers highlighted in blue signify the ratio (*mgat1b*$^{-/-}$: Wt) of the blot shown in figure 3. Band intensities of Wt and *mgat1b-/-* were quantified relative to Coomassie blue load controls. Band intensities were quantified using ImageJ software. *P* values were determined from one sample t-test using a designated value of 1.

Spinal Cord					**Skin**				
Date	Wt	*mgat1b*$^{-/-}$	*1b*/wt	*P*	Date	Wt	*mgat1b*$^{-/-}$	*1b*/wt	*P*
230509	166736	238960	1.43	0.015	240603	135082	170001	1.26	0.077
240403	63574	104427	1.64		240603	335978	406602	1.21	
230524	311476	424354	1.36		240528	886985	904871	1.02	
Skeletal muscle					**Heart**				
Date	Wt	*mgat1b*$^{-/-}$	*1b*/wt	*P*	Date	Wt	*mgat1b*$^{-/-}$	*1b*/wt	*P*
240213	386905	422736	1.09	0.014	240212	168269	192268	1.14	0.081
240207	1073597	1169672	1.09		231120	600051	617547	1.03	
240227	219106	229709	1.05		231130	73221	92081	1.26	
Swim Bladder					**Testis**				
Date	Wt	*mgat1b*$^{-/-}$	*1b*/wt	*P*	Date	Wt	*mgat1b*$^{-/-}$	*1b*/wt	*P*
240207	691321	807469	1.17	0.071	240610	397967	483232	1.21	0.046
240228	523017	606158	1.16		240607	476678	502631	1.05	
240212	229426	349288	1.52		240607	459815	538614	1.17	

CHAPTER V: General Discussion and Conclusions

Zebrafish N-Glycosylation

N-glycosylation profiles are currently established for the brain, skin, gills, heart, liver, intestine, testis, and ovary of zebrafish. Though, this is the first study to show the N-glycosylation profile of zebrafish spinal cord. It was shown that the spinal cord of Wt AB zebrafish consisted primarily of complex N-glycans followed by oligomannose which was found to be like zebrafish brain (Hall, Hatchett et al. 2023, Hatchett, Hall et al. 2024). This is likely because both the brain and spinal cord originate from the neural tube of zebrafish (Harrington, Chalasani et al. 2010). In the spinal cord there were several different structural types found with complex type consisting of over 17 unique structures while hybrid and oligomannose types only consisted of three and four structures (Hall, Hatchett et al. 2023). When comparing N-glycan profiles of neural tissue from other vertebrate, such as the rat spinal cord and brain (Osimanjiang, Roballo et al. 2020), zebrafish had a higher percentage of oligomannose type N-glycans (Osimanjiang, Roballo et al. 2020, Hatchett, Hall et al. 2024). Regardless though the complex and hybrid N-glycans present in zebrafish were more sialylated and fucosylated than those found in rats (Osimanjiang, Roballo et al. 2020, Hall, Hatchett et al. 2023, Hatchett, Hall et al. 2024). It is of interest to determine how increased sialylation and fucosylation of N-glycans contribute to vertebrate development.

mgat1b Knockout Zebrafish

A knockout of *Mgat1* appears lethal in vertebrates as mice only survived for around 9.5 embryonic days (Ioffe and Stanley 1994). Zebrafish though have two copies of the *mgat1* gene known as *mgat1a/b* (Sprague, Doerry et al. 2001). This research illustrated a successful knockout

of *mgat1b* using CRISPR/Cas9 (Hall, Hatchett et al. 2023). This knockout resulted in a premature stop codon that resulted in a truncated C terminal region which would remove the catalytic domain (Sarkar, Hull et al. 1991). It is possible to generate two different shortened versions of GnTI using more downstream start sites however these versions would not function correctly due to inappropriate localization of the protein (Hall, Hatchett et al. 2023). While the catalytic domain is located towards the C-terminus, subcellular localization is performed by the transmembrane domain of GnT-I (Sarkar, Hull et al. 1991). The *mgat1b* knockout is supported by sequencing, lectin blotting, qt-PCR, mass spectroscopy, and restriction enzyme digests of amplified genomic DNA (Hall, Hatchett et al. 2023, Hatchett, Hall et al. 2024) . Glycan analysis of *mgat1b* mutant brains and spinal cords showed a reduction in complex type N-glycans and an increase in oligomannose type N-glycans (Cho, Veillon et al.). The increase in the $GlcNAc_2Man_5$ structure abundance in *mgat1b* knockout fish suggests that GnT-I activity is reduced when only one *mgat1* gene is active (Hall, Hatchett et al. 2023, Hatchett, Hall et al. 2024). Levels of *mgat1b* transcripts were shown to reduce further with age (Hall, Hatchett et al. 2023). Lectin blotting of various tissues showing increased oligomannose type N-glycans indicated that the knockout was also organismal-wide(Hatchett, Hall et al. 2024). The *mgat1b* knockout zebrafish line was overall viable as the penetrance of the mutation showed some functional overlap between *mgat1a* and *mgat1b.* However, there was a steep decline in survivability during the later stages of gastrulation (Cho, Veillon et al.). Many surviving embryos though did still suffer from developmental delays (Cho, Veillon et al.). These studies argue that lowered activity of GnT-I perturbs vertebrate survivability and development.

***mgat1b* Zebrafish Development**

Zebrafish N-glycosylation begins early with all three types present at around 6 hpf (Hanzawa, Suzuki et al. 2017). These early zebrafish glycans are primarily oligomannose in type followed by complex and hybrid N-glycans (Cho, Veillon et al.). During embryonic development, the reduction in survivability occurred between 8-10 hpf for the *mgat1b*$^{-/-}$ zebrafish. This time frame aligns with gastrulation, which is a period of heavy cell migration and rearrangement when the blastula becomes a gastrula and the embryo forms the three embryonic germ layers known as endoderm, mesoderm, ectoderm and begins to form the bi-lateral body plan (Rohde and Heisenberg 2007). Gastrulation heavily utilizes the activity of glycoproteins such as fibronectin, laminin, matrix metalloproteinases, and cadherins (Winklbauer and Keller 1996, Pedersen, Vuong et al. 2015). These proteins are responsible for regulating cell migration, adhesion, signaling, and differentiation. An *MGAT1* knockout in human skin cells resulted in reduced adhesion to fibronectin, laminin and the absence of α5 integrin expression at the surface (Dabelsteen, Pallesen et al. 2020). This along with our own previous studies (Hall, Weidner et al. 2017, Hall 2023) show the importance of N-glycosylation in protein localization which can alter migration and adhesion. Survivability stabilized after 24 hpf for the *mgat1b* mutant fish line but embryos still suffered from delays in several further stages of development (Cho, Veillon et al.). Mutant fish had developmental delays in all three types of muscle tissue: cardiac, skeletal, and smooth, resulting in impaired movement, compromised heart function, and defective swim bladder formation (Cho, Veillon et al.). Though complex N-glycosylation does not spike until the late segmentation to pharyngula period (10- 48 hpf) (Cho, Veillon et al.), the reduction in

survivability shows the importance of complex N-glycans to the early stages of development especially during periods of heavy migration, cell differentiation.

Cardiac inception in mutant fish was delayed approximately 4 hours from that of Wt AB fish (Cho, Veillon et al.). In zebrafish cardiac inception is a result of an action potential propagated by $Ca_V1.2$ (Jia, Qi et al. 2023). The cardiac L-type $Ca_V1.2$ subunits are heavily N-glycosylated with some subunits having as many as sixteen N-glycosylation sites. It has been shown that alteration of the N-glycosylation levels reduced L-type Ca_v subunits to the surface. (Ednie, Deng et al. 2019). Cardiac studies performed in *Mgat1* knockout mice, indicated left ventricle dilatation attributed to the depolarization of Ca_V channels (Tetreault, Bourdin et al. 2016). These N-glycans are usually either complex or hybrid type as they possess terminal sialic acid residues, and the loss of those hybrid and complex resulted in asynchronous beating. The *mgat1b* fish also suffer from other lagging developmental checkpoints that include hatching and swim bladder inflation (Cho, Veillon et al.).

Motor Neuron Development

N-glycosylation has been shown to play a crucial role in primary neuron structure. Our previous studies showed that removal of an N-glycosylation site on Kv3.1b when expressed in zebrafish primary motor neurons resulted in truncated axon structure and branching was greatly reduced (Issa, Hall et al. 2021). The *mgat1b* zebrafish mutant had similar effects with CaP motor neuron collateral branching reduced to almost no branches (Hatchett, Hall et al. 2024). These branches are what would be responsible for the innervation of the ventral axial muscle (Cho, Veillon et al.) and allow for proper movement. N-glycosylation was also shown to alter Rat NB_1 morphology, resulting in shortened neurite length and increased width (Hall 2023). The change

in neuron morphology could be due to Kv3 channels being improperly localized or unable to correctly regulate the membrane potential which leads to improper cytoskeletal structure (Hall, Weidner et al. 2017, Hall, Shajahan et al. 2023).

Motor Activity

Alteration of the zebrafish motor neurons and muscle organization had a serious and lasting impact on the locomotor activity. The *mgat1b* zebrafish had reduced responses to startle stimulus such as touch evoked response and a delayed response to a vibrational startle (Hatchett, Hall et al. 2024). This delay or lack of startle response could be due to alterations in the glycosylation of voltage gated ion channels such as Kv3 channels. These channels when glycosylated with complex N-glycans help with rapid repolarization of the membrane potential of neurons (Cho, Veillon et al.). The rapid repolarization allows the fish to respond more rapidly to initiate an escape response. Further, cellular studies of NB_1(-*Mgat1*) expressing Kv3.1b with almost no complex and hybrid N-glycans showed reduced activation and deactivation rates of Kv3 channels which would have reduced the ability of a neuron to fire repetitive action potentials (Issa, Hall et al. 2021). The reduction in repolarization rate likely explains the reduced or lack of response from the mutant fish. Muscle coordination of the mutant line was greatly reduced with the reduction in complex N-glycans which could be attributed to altered primary neuron branching(Hatchett, Hall et al. 2024). These motor function discrepancies continued throughout adulthood where stamina was reduced with the *mgat1b* mutant fish (Hatchett, Hall et al. 2024). Thus, delays in development and maldeveloped primary motor neurons appear to strongly correlate with motor locomotion in zebrafish.

Conclusion

The research findings here demonstrated the different roles of N-glycosylation using both *in vivo* and *in vitro* models. These roles included cell morphology, protein localization, and cell motility in neuronal-derived cell models. These studies also showed the effects of reduced levels of complex N-glycans on zebrafish development, as well as provide the first N-glycan profiling on zebrafish spinal cord. Overall, the reduction in complex N-glycans resulted in discrepancies such as delayed development, reduced sensory-motor response, and truncated neuron structure. A better understanding of N-glycosylation processing and its roles in development will help bring to light new target areas for study and, eventually, therapies for those suffering from CDGs and other neurological diseases, such as Alzheimer's and Parkinson's disease.

Here, the research studies developed a vertebrate model organism for study of CDGs that are embryonically lethal in humans and identified a vital role of complex N-glycans in neuron development. A past study reported no change in neuron development due to lowered complex N-glycans; however, the report only looked at cell number, not at neuron structure. This current study was more in-depth and demonstrated that a reduction in complex N-glycans caused considerable reduction in axonal branching of primary motor neurons. This study also showed key stages of development that were impacted by reduced complex N-glycans which could correlate with aberrant organ development in humans with lowered complex N-glycans.

References

Aamodt, W. W., T. Waligorska, J. Shen, T. F. Tropea, A. Siderowf, D. Weintraub, M. Grossman, D. Irwin, D. A. Wolk, S. X. Xie, J. Q. Trojanowski, L. M. Shaw and A. S. Chen-Plotkin (2021). "Neurofilament Light Chain as a Biomarker for Cognitive Decline in Parkinson Disease." Mov Disord **36**(12): 2945-2950.

Abrams, E. W. and M. C. Mullins (2009). "Early zebrafish development: it's in the maternal genes." Curr Opin Genet Dev **19**(4): 396-403.

Ahmed, K. T., M. R. Amin, P. Shah and D. W. Ali (2018). "Motor neuron development in zebrafish is altered by brief (5-hr) exposures to THC (Δ(9)-tetrahydrocannabinol) or CBD (cannabidiol) during gastrulation." Sci Rep **8**(1): 10518.

Alfonso, S., M. Peyrafort, X. Cousin and M. L. Begout (2020). "Zebrafish Danio rerio shows behavioural cross-context consistency at larval and juvenile stages but no consistency between stages." J Fish Biol **96**(6): 1411-1421.

Arduini, B. L. and P. D. Henion (2004). "Melanophore sublineage-specific requirement for zebrafish touchtone during neural crest development." Mechanisms of Development **121**(11): 1353-1364.

Barone, R., L. Sturiale, A. Fiumara, A. Palmigiano, R. O. Bua, R. Rizzo, M. Zappia and D. Garozzo (2016). "CSF N-glycan profile reveals sialylation deficiency in a patient with GM2 gangliosidosis presenting as childhood disintegrative disorder." Autism Res **9**(4): 423-428.

Berger, J., T. Sztal and P. D. Currie (2012). "Quantification of birefringence readily measures the level of muscle damage in zebrafish." Biochem Biophys Res Commun **423**(4): 785-788.

Blazina, A. R., M. R. Vianna and D. R. Lara (2013). "The spinning task: a new protocol to easily assess motor coordination and resistance in zebrafish." Zebrafish **10**(4): 480-485.

Breitling, J. and M. Aebi (2013). "N-linked protein glycosylation in the endoplasmic reticulum." Cold Spring Harb Perspect Biol **5**(8): a013359.

Bruce, A. E. E. and C.-P. Heisenberg (2020). Chapter Eleven - Mechanisms of zebrafish epiboly: A current view. Current Topics in Developmental Biology. L. Solnica-Krezel, Academic Press. **136:** 319-341.

Bruce, A. E. E. and C. P. Heisenberg (2020). "Mechanisms of zebrafish epiboly: A current view." Curr Top Dev Biol **136**: 319-341.

Burke, J., J. M. Pettitt, D. Humphris and P. A. Gleeson (1994). "Medial-Golgi retention of N-acetylglucosaminyltransferase I. Contribution from all domains of the enzyme." J Biol Chem **269**(16): 12049-12059.

Campbell, R. M., M. Metzler, M. Granovsky, J. W. Dennis and J. D. Marth (1995). "Complex asparagine-linked oligosaccharides in Mgat1-null embryos." Glycobiology **5**(5): 535-543.

Cantagrel, V. and D. J. Lefeber (2011). "From glycosylation disorders to dolichol biosynthesis defects: a new class of metabolic diseases." J Inherit Metab Dis **34**(4): 859-867.

Cartwright, T. A. and R. A. Schwalbe (2009). "Atypical sialylated N-glycan structures are attached to neuronal voltage-gated potassium channels." Biosci Rep **29**(5): 301-313.

Cast, T. P., D. J. Boesch, K. Smyth, A. E. Shaw, M. Ghebrial and S. Chanda (2021). "An Autism-Associated Mutation Impairs Neuroligin-4 Glycosylation and Enhances Excitatory Synaptic Transmission in Human Neurons." J Neurosci **41**(3): 392-407.

Chang, I. J., M. He and C. T. Lam (2018). "Congenital disorders of glycosylation." Ann Transl Med **6**(24): 477.

Chen, K. Z., S. X. Liu, Y. W. Li, T. He, J. Zhao, T. Wang, X. X. Qiu and H. F. Wu (2023). "Vimentin as a potential target for diverse nervous system diseases." Neural Regen Res **18**(5): 969-975.

Chen, Q., Z. Tan, F. Guan and Y. Ren (2020). "The Essential Functions and Detection of Bisecting GlcNAc in Cell Biology." Front Chem **8**: 511.

Chen, Y. J., D. R. Wing, G. R. Guile, R. A. Dwek, D. J. Harvey and S. Zamze (1998). "Neutral N-glycans in adult rat brain tissue--complete characterisation reveals fucosylated hybrid and complex structures." Eur J Biochem **251**(3): 691-703.

Cho, B. G., L. Veillon and Y. Mechref (2019). "N-Glycan Profile of Cerebrospinal Fluids from Alzheimer's Disease Patients Using Liquid Chromatography with Mass Spectrometry." J Proteome Res **18**(10): 3770-3779.

Chu, J. and K. C. Sadler (2009). "New school in liver development: lessons from zebrafish." Hepatology **50**(5): 1656-1663.

Conroy, L. R., T. R. Hawkinson, L. E. A. Young, M. S. Gentry and R. C. Sun (2021). "Emerging roles of N-linked glycosylation in brain physiology and disorders." Trends Endocrinol Metab **32**(12): 980-993.

Cvetko, A., D. Kifer, O. Gornik, L. Klaric, E. Visser, G. Lauc, J. F. Wilson and T. Stambuk (2020). "Glycosylation Alterations in Multiple Sclerosis Show Increased Proinflammatory Potential." Biomedicines **8**(10).

Dabelsteen, S., E. M. H. Pallesen, I. N. Marinova, M. I. Nielsen, M. Adamopoulou, T. B. Romer, A. Levann, M. M. Andersen, Z. Ye, D. Thein, E. P. Bennett, C. Bull, S. J. Moons, T. Boltje, H. Clausen, S. Y. Vakhrushev, I. Bagdonaite and H. H. Wandall (2020). "Essential Functions of Glycans in Human Epithelia Dissected by a CRISPR-Cas9-Engineered Human Organotypic Skin Model." Dev Cell **54**(5): 669-684 e667.

Dent, E. W., S. L. Gupton and F. B. Gertler (2011). "The growth cone cytoskeleton in axon outgrowth and guidance." Cold Spring Harb Perspect Biol **3**(3).

Dong, Y. Y., H. Wang, A. C. W. Pike, S. A. Cochrane, S. Hamedzadeh, F. J. Wyszynski, S. R. Bushell, S. F. Royer, D. A. Widdick, A. Sajid, H. I. Boshoff, Y. Park, R. Lucas, W. M. Liu, S. S. Lee, T. Machida, L. Minall, S. Mehmood, K. Belaya, W. W. Liu, A. Chu, L. Shrestha, S. M. M. Mukhopadhyay, C. Strain-Damerell, R. Chalk, N. A. Burgess-Brown, M. J. Bibb, C. E. Barry Iii, C. V. Robinson, D. Beeson, B. G. Davis and E. P. Carpenter (2018). "Structures of DPAGT1 Explain Glycosylation Disease Mechanisms and Advance TB Antibiotic Design." Cell **175**(4): 1045-1058 e1016.

Dorner, A. J., D. G. Bole and R. J. Kaufman (1987). "The relationship of N-linked glycosylation and heavy chain-binding protein association with the secretion of glycoproteins." J Cell Biol **105**(6 Pt 1): 2665-2674.

Dwyer, C. A. and J. D. Esko (2016). "Glycan susceptibility factors in autism spectrum disorders." Mol Aspects Med **51**: 104-114.

Echeazarra, L., M. P. Hortigon-Vinagre, O. Casis and M. Gallego (2020). "Adult and Developing Zebrafish as Suitable Models for Cardiac Electrophysiology and Pathology in Research and Industry." Front Physiol **11**: 607860.

Ednie, A. R., W. Deng, K. P. Yip and E. S. Bennett (2019). "Reduced myocyte complex N-glycosylation causes dilated cardiomyopathy." FASEB J **33**(1): 1248-1261.

Eisen, J. S., P. Z. Myers and M. Westerfield (1986). "Pathway selection by growth cones of identified motoneurones in live zebra fish embryos." Nature **320**(6059): 269-271.

Ezgu, F. (2016). Chapter Seven - Inborn Errors of Metabolism. Advances in Clinical Chemistry. G. S. Makowski, Elsevier. **73:** 195-250.

Fajersztajn, L., R. C. Cordeiro, S. Andreoni and J. T. Garcia (2008). "Effects of functional physical activity on the maintenance of motor function in Alzheimer's disease." Dement Neuropsychol **2**(3): 233-240.

Fetcho, J. R., S. Higashijima and D. L. McLean (2008). "Zebrafish and motor control over the last decade." Brain Res Rev **57**(1): 86-93.

Fletcher, D. A. and R. D. Mullins (2010). "Cell mechanics and the cytoskeleton." Nature **463**(7280): 485-492.

Fucikova, J., R. Spisek, G. Kroemer and L. Galluzzi (2021). "Calreticulin and cancer." Cell Res **31**(1): 5-16.

Gazulla, J. and J. Berciano (2024). "Potential Benefit of Channel Activators in Loss-of-Function Primary Potassium Channelopathies Causing Heredoataxia." Cerebellum **23**(2): 833-837.

Giraldez, A. J., Y. Mishima, J. Rihel, R. J. Grocock, S. Van Dongen, K. Inoue, A. J. Enright and A. F. Schier (2006). "Zebrafish MiR-430 promotes deadenylation and clearance of maternal mRNAs." Science **312**(5770): 75-79.

Grissmer, S., S. Ghanshani, B. Dethlefs, J. D. McPherson, J. J. Wasmuth, G. A. Gutman, M. D. Cahalan and K. G. Chandy (1992). "The Shaw-related potassium channel gene, Kv3.1, on human chromosome 11, encodes the type l K+ channel in T cells." J Biol Chem **267**(29): 20971-20979.

Gunthorpe, M. J. (2022). "Timing is everything: structural insights into the disease-linked Kv3 channels controlling fast action-potential firing in the brain." Nat Commun **13**(1): 4086.

Hall, M. K., Asif Shajahan, Cody J Hatchett, Adam P Burch, Parastoo Azadi, and Ruth A Schwalbe. (2023). "Kv3-Expressing Cells Present More Elaborate N-Glycans with Changes in Cytoskeletal Proteins, Neurite Structure and Cell Migration." COJ Biomed Sci Res. **2**(3).

Hall, M. K., A. P. Burch and R. A. Schwalbe (2021). "Functional analysis of N-acetylglucosaminyltransferase-I knockdown in 2D and 3D neuroblastoma cell cultures." PLoS One **16**(11): e0259743.

Hall, M. K., T. A. Cartwright, C. M. Fleming and R. A. Schwalbe (2011). "Importance of glycosylation on function of a potassium channel in neuroblastoma cells." PLoS One **6**(4): e19317.

Hall, M. K., C. J. Hatchett, S. Shalygin, P. Azadi and R. A. Schwalbe (2023). "Reduction in N-Acetylglucosaminyltransferase-I Activity Decreases Survivability and Delays Development of Zebrafish." Curr Issues Mol Biol **45**(11): 9165-9180.

Hall, M. K., A. Shajahan, A. P. Burch, C. J. Hatchett, P. Azadi and R. A. Schwalbe (2023). "Limited N-Glycan Processing Impacts Chaperone Expression Patterns, Cell Growth and Cell Invasiveness in Neuroblastoma." Biology (Basel) **12**(2).

Hall, M. K., D. A. Weidner, J. Chen, C. J. Bernetski and R. A. Schwalbe (2013). "Glycan structures contain information for the spatial arrangement of glycoproteins in the plasma membrane." PLoS One **8**(9): e75013.

Hall, M. K., D. A. Weidner, S. Dayal, E. Pak, A. K. Murashov and R. A. Schwalbe (2017). "Membrane Distribution and Activity of a Neuronal Voltage-Gated K+ Channel is Modified by Replacement of Complex Type N-Glycans with Hybrid Type." J Glycobiol **6**(3).

Hall, M. K., D. A. Weidner, M. A. Edwards and R. A. Schwalbe (2015). "Complex N-Glycans Influence the Spatial Arrangement of Voltage Gated Potassium Channels in Membranes of Neuronal-Derived Cells." PLoS One **10**(9): e0137138.

Hall, M. K., D. A. Weidner, A. A. Whitman and R. A. Schwalbe (2018). "Lack of complex type N-glycans lessens aberrant neuronal properties." PLoS One **13**(6): e0199202.

Hall, M. K., A. A. Whitman, D. A. Weidner and R. A. Schwalbe (2020). "Knockdown of N-Acetylglucosaminyltransferase-II Reduces Matrix Metalloproteinase 2 Activity and Suppresses Tumorigenicity in Neuroblastoma Cell Line." Biology (Basel) **9**(4).

Halperin, L., J. Jung and M. Michalak (2014). "The many functions of the endoplasmic reticulum chaperones and folding enzymes." IUBMB Life **66**(5): 318-326.

Hanneman, E. and M. Westerfield (1989). "Early expression of acetylcholinesterase activity in functionally distinct neurons of the zebrafish." J Comp Neurol **284**(3): 350-361.

Hanzawa, K., N. Suzuki and S. Natsuka (2017). "Structures and developmental alterations of N-glycans of zebrafish embryos." Glycobiology **27**(3): 228-245.

Harrington, M. J., K. Chalasani and R. Brewster (2010). "Cellular mechanisms of posterior neural tube morphogenesis in the zebrafish." Developmental Dynamics **239**(3): 747-762.

Hatchett, C. J. (2021). Impaired N-Glycosylation Processing Impacts Neuronal Function. Masters of Biolemdical Science East Carolina University.

Hatchett, C. J., M. K. Hall, A. R. Messer and R. A. Schwalbe (2024). "Lowered GnT-I Activity Decreases Complex-Type N-Glycan Amounts and Results in an Aberrant Primary Motor Neuron Structure in the Spinal Cord." J Dev Biol **12**(3).

Hirano, H., J. S. Gootenberg, T. Horii, O. O. Abudayyeh, M. Kimura, P. D. Hsu, T. Nakane, R. Ishitani, I. Hatada, F. Zhang, H. Nishimasu and O. Nureki (2016). "Structure and Engineering of Francisella novicida Cas9." Cell **164**(5): 950-961.

Hirata, E., K. T. Sakata, G. I. Dearden, F. Noor, I. Menon, G. N. Chiduza and A. K. Menon (2024). "Molecular characterization of Rft1, an ER membrane protein associated with congenital disorder of glycosylation RFT1-CDG." J Biol Chem **300**(8): 107584.

Hirokawa, N. (1982). "Cross-linker system between neurofilaments, microtubules, and membranous organelles in frog axons revealed by the quick-freeze, deep-etching method." J Cell Biol **94**(1): 129-142.

Hirokawa, N. and Y. Noda (2008). "Intracellular transport and kinesin superfamily proteins, KIFs: structure, function, and dynamics." Physiol Rev **88**(3): 1089-1118.

Huang, C. Y., C. C. Lien, C. F. Cheng, T. Y. Yen, C. J. Chen and M. L. Tsaur (2017). "K(+) Channel Kv3.4 Is Essential for Axon Growth by Limiting the Influx of Ca(2+) into Growth Cones." J Neurosci **37**(17): 4433-4449.

Ioffe, E. and P. Stanley (1994). "Mice lacking N-acetylglucosaminyltransferase I activity die at mid-gestation, revealing an essential role for complex or hybrid N-linked carbohydrates." Proc Natl Acad Sci U S A **91**(2): 728-732.

Issa, F. A., M. K. Hall, C. J. Hatchett, D. A. Weidner, A. C. Fiorenza and R. A. Schwalbe (2021). "Compromised N-Glycosylation Processing of Kv3.1b Correlates with Perturbed Motor Neuron Structure and Locomotor Activity." Biology (Basel) **10**(6).

Issa, F. A., C. Mazzochi, A. F. Mock and D. M. Papazian (2011). "Spinocerebellar ataxia type 13 mutant potassium channel alters neuronal excitability and causes locomotor deficits in zebrafish." J Neurosci **31**(18): 6831-6841.

Jaeken, J. (2010). "Congenital disorders of glycosylation." Ann N Y Acad Sci **1214**: 190-198.

Jia, B. Z., Y. Qi, J. D. Wong-Campos, S. G. Megason and A. E. Cohen (2023). "A bioelectrical phase transition patterns the first vertebrate heartbeats." Nature **622**(7981): 149-155.

Jinek, M., K. Chylinski, I. Fonfara, M. Hauer, J. A. Doudna and E. Charpentier (2012). "A programmable dual-RNA-guided DNA endonuclease in adaptive bacterial immunity." Science **337**(6096): 816-821.

Kaczmarek, L. K. (2006). "Non-conducting functions of voltage-gated ion channels." Nat Rev Neurosci **7**(10): 761-771.

Kaczmarek, L. K. and Y. Zhang (2017). "Kv3 Channels: Enablers of Rapid Firing, Neurotransmitter Release, and Neuronal Endurance." Physiol Rev **97**(4): 1431-1468.

Kanemasa, T., L. Gan, T. M. Perney, L. Y. Wang and L. K. Kaczmarek (1995). "Electrophysiological and pharmacological characterization of a mammalian Shaw channel expressed in NIH 3T3 fibroblasts." J Neurophysiol **74**(1): 207-217.

Kimelman, D., M. Kirschner and T. Scherson (1987). "The events of the midblastula transition in Xenopus are regulated by changes in the cell cycle." Cell **48**(3): 399-407.

Kimmel, C. B., W. W. Ballard, S. R. Kimmel, B. Ullmann and T. F. Schilling (1995). "Stages of embryonic development of the zebrafish." Dev Dyn **203**(3): 253-310.

Kingdom, R. and C. F. Wright (2022). "Incomplete Penetrance and Variable Expressivity: From Clinical Studies to Population Cohorts." Front Genet **13**: 920390.

Kizuka, Y., S. Kitazume and N. Taniguchi (2017). "N-glycan and Alzheimer's disease." Biochim Biophys Acta Gen Subj **1861**(10): 2447-2454.

Konietzny, A., J. Bar and M. Mikhaylova (2017). "Dendritic Actin Cytoskeleton: Structure, Functions, and Regulations." Front Cell Neurosci **11**: 147.

Labun, K., T. G. Montague, J. A. Gagnon, S. B. Thyme and E. Valen (2016). "CHOPCHOP v2: a web tool for the next generation of CRISPR genome engineering." Nucleic Acids Res **44**(W1): W272-276.

Labun, K., T. G. Montague, M. Krause, Y. N. Torres Cleuren, H. Tjeldnes and E. Valen (2019). "CHOPCHOP v3: expanding the CRISPR web toolbox beyond genome editing." Nucleic Acids Res **47**(W1): W171-W174.

Lee, S. U., A. Grigorian, J. Pawling, I. J. Chen, G. Gao, T. Mozaffar, C. McKerlie and M. Demetriou (2007). "N-glycan processing deficiency promotes spontaneous inflammatory demyelination and neurodegeneration." J Biol Chem **282**(46): 33725-33734.

Lejeune, F. (2022). "Nonsense-Mediated mRNA Decay, a Finely Regulated Mechanism." Biomedicines **10**(1).

Leterrier, C., P. Dubey and S. Roy (2017). "The nano-architecture of the axonal cytoskeleton." Nat Rev Neurosci **18**(12): 713-726.

Lewis, K. E. and J. S. Eisen (2003). "From cells to circuits: development of the zebrafish spinal cord." Prog Neurobiol **69**(6): 419-449.

Li, P., R. M. White and L. I. Zon (2011). Chapter 17 - Transplantation in Zebrafish. Methods in Cell Biology. H. W. Detrich, M. Westerfield and L. I. Zon, Academic Press. **105:** 403-417.

Link-Lenczowski, P., M. Bubka, C. I. A. Balog, C. A. M. Koeleman, T. D. Butters, M. Wuhrer and A. Litynska (2018). "The glycomic effect of N-acetylglucosaminyltransferase III overexpression in metastatic melanoma cells. GnT-III modifies highly branched N-glycans." Glycoconj J **35**(2): 217-231.

Liu, D. W. and M. Westerfield (1988). "Function of identified motoneurones and co-ordination of primary and secondary motor systems during zebra fish swimming." J Physiol **403**: 73-89.

Liu, S. Q. and L. K. Kaczmarek (1998). "Depolarization selectively increases the expression of the Kv3.1 potassium channel in developing inferior colliculus neurons." J Neurosci **18**(21): 8758-8769.

Marzec, M., D. Eletto and Y. Argon (2012). "GRP94: An HSP90-like protein specialized for protein folding and quality control in the endoplasmic reticulum." Biochim Biophys Acta **1823**(3): 774-787.

McCurley, A. T. and G. V. Callard (2008). "Characterization of housekeeping genes in zebrafish: male-female differences and effects of tissue type, developmental stage and chemical treatment." BMC Mol Biol **9**: 102.

Mendelson, B. (1986). "Development of reticulospinal neurons of the zebrafish. I. Time of origin." J Comp Neurol **251**(2): 160-171.

Mikolajczyk, K., R. Kaczmarek and M. Czerwinski (2020). "How glycosylation affects glycosylation: the role of N-glycans in glycosyltransferase activity." Glycobiology **30**(12): 941-969.

Mollenhauer, B., M. Dakna, N. Kruse, D. Galasko, T. Foroud, H. Zetterberg, S. Schade, R. G. Gera, W. Wang, F. Gao, M. Frasier, L. M. Chahine, C. S. Coffey, A. B. Singleton, T. Simuni, D. Weintraub, J. Seibyl, A. W. Toga, C. M. Tanner, K. Kieburtz, K. Marek, A. Siderowf, J. M. Cedarbaum, S. J. Hutten, C. Trenkwalder and D. Graham (2020). "Validation of Serum Neurofilament Light Chain as a Biomarker of Parkinson's Disease Progression." Mov Disord **35**(11): 1999-2008.

Montague, T. G., J. M. Cruz, J. A. Gagnon, G. M. Church and E. Valen (2014). "CHOPCHOP: a CRISPR/Cas9 and TALEN web tool for genome editing." Nucleic Acids Res **42**(Web Server issue): W401-407.

Moreno, R. L. and A. B. Ribera (2009). "Zebrafish motor neuron subtypes differ electrically prior to axonal outgrowth." J Neurophysiol **102**(4): 2477-2484.

Moustafa, A. A., S. Chakravarthy, J. R. Phillips, A. Gupta, S. Keri, B. Polner, M. J. Frank and M. Jahanshahi (2016). "Motor symptoms in Parkinson's disease: A unified framework." Neurosci Biobehav Rev **68**: 727-740.

Myers, P. Z., J. S. Eisen and M. Westerfield (1986). "Development and axonal outgrowth of identified motoneurons in the zebrafish." J Neurosci **6**(8): 2278-2289.

Nagae, M., Y. Yamaguchi, N. Taniguchi and Y. Kizuka (2020). "3D Structure and Function of Glycosyltransferases Involved in N-glycan Maturation." Int J Mol Sci **21**(2).

Nixon, R. A. and T. B. Shea (1992). "Dynamics of neuronal intermediate filaments: a developmental perspective." Cell Motil Cytoskeleton **22**(2): 81-91.

O'Farrell, P. H., J. Stumpff and T. T. Su (2004). "Embryonic cleavage cycles: how is a mouse like a fly?" Curr Biol **14**(1): R35-45.

Ondruskova, N., A. Cechova, H. Hansikova, T. Honzik and J. Jaeken (2021). "Congenital disorders of glycosylation: Still "hot" in 2020." Biochim Biophys Acta Gen Subj **1865**(1): 129751.

Osimanjiang, W., K. C. S. Roballo, B. D. Houck, M. Ito, A. Antonopoulos, A. Dell, S. M. Haslam and J. S. Bushman (2020). "Analysis of N- and O-Linked Glycosylation: Differential Glycosylation after Rat Spinal Cord Injury." J Neurotrauma **37**(18): 1954-1962.

Ousingsawat, J., M. Spitzner, S. Puntheeranurak, L. Terracciano, L. Tornillo, L. Bubendorf, K. Kunzelmann and R. Schreiber (2007). "Expression of voltage-gated potassium channels in human and mouse colonic carcinoma." Clin Cancer Res **13**(3): 824-831.

Panousopoulou, E., C. Hobbs, I. Mason, J. B. Green and C. J. Formstone (2016). "Epiboly generates the epidermal basal monolayer and spreads the nascent mammalian skin to enclose the embryonic body." J Cell Sci **129**(9): 1915-1927.

Paprocka, J., A. Jezela-Stanek, A. Tylki-Szymanska and S. Grunewald (2021). "Congenital Disorders of Glycosylation from a Neurological Perspective." Brain Sci **11**(1).

Parkinson, W., M. L. Dear, E. Rushton and K. Broadie (2013). "N-glycosylation requirements in neuromuscular synaptogenesis." Development **140**(24): 4970-4981.

Patnaik, S. K. and P. Stanley (2006). "Lectin-resistant CHO glycosylation mutants." Methods Enzymol **416**: 159-182.

Pedersen, M. E., T. T. Vuong, S. B. Rønning and S. O. Kolset (2015). "Matrix metalloproteinases in fish biology and matrix turnover." Matrix Biology **44-46**: 86-93.

Pivac, N., A. Knezevic, O. Gornik, M. Pucic, W. Igl, H. Peeters, A. Crepel, J. Steyaert, M. Novokmet, I. Redzic, M. Nikolac, V. N. Hercigonja, K. D. Curkovic, M. Curkovic, G. Nedic, D. Muck-Seler, F. Borovecki, I. Rudan and G. Lauc (2011). "Human plasma glycome in attention-deficit hyperactivity disorder and autism spectrum disorders." Mol Cell Proteomics **10**(1): M110 004200.

Pobre, K. F. R., G. J. Poet and L. M. Hendershot (2019). "The endoplasmic reticulum (ER) chaperone BiP is a master regulator of ER functions: Getting by with a little help from ERdj friends." J Biol Chem **294**(6): 2098-2108.

Pradeep, P., H. Kang and B. Lee (2023). "Glycosylation and behavioral symptoms in neurological disorders." Transl Psychiatry **13**(1): 154.

Rajkovic, J., V. Djokic, M. Gostimirovic, L. Gojkovic-Bukarica, M. Martorell, J. Sharifi-Rad and R. Novakovic (2020). "Potassium channels on smooth muscle as a molecular target for plant-derived Resveratrol." Cell Mol Biol (Noisy-le-grand) **66**(4): 133-144.

Ramirez, A. S. and K. P. Locher (2023). "Structural and mechanistic studies of the N-glycosylation machinery: from lipid-linked oligosaccharide biosynthesis to glycan transfer." Glycobiology **33**(11): 861-872.

Rohde, L. A. and C. P. Heisenberg (2007). Zebrafish Gastrulation: Cell Movements, Signals, and Mechanisms. International Review of Cytology, Academic Press. **261:** 159-192.

Rombough, P. J. (2007). "Ontogenetic changes in the toxicity and efficacy of the anaesthetic MS222 (tricaine methanesulfonate) in zebrafish (Danio rerio) larvae." Comp Biochem Physiol A Mol Integr Physiol **148**(2): 463-469.

Ronan, R., A. Kshirsagar, A. L. Rebelo, A. Sunny, M. Kilcoyne, R. O. Flaherty, P. M. Rudd, G. Schlosser, R. Saldova, A. Pandit and S. S. McMahon (2022). "Distinct Glycosylation Responses to Spinal Cord Injury in Regenerative and Nonregenerative Models." J Proteome Res **21**(6): 1449-1466.

Rudy, B. and C. J. McBain (2001). "Kv3 channels: voltage-gated K+ channels designed for high-frequency repetitive firing." Trends Neurosci **24**(9): 517-526.

Sainath, R. and M. Granato (2013). "Plexin A3 and turnout regulate motor axonal branch morphogenesis in zebrafish." PLoS One **8**(1): e54071.

Sarkar, M., E. Hull, Y. Nishikawa, R. J. Simpson, R. L. Moritz, R. Dunn and H. Schachter (1991). "Molecular cloning and expression of cDNA encoding the enzyme that controls conversion of high-mannose to hybrid and complex N-glycans: UDP-N-acetylglucosamine: alpha-3-D-mannoside beta-1,2-N-acetylglucosaminyltransferase I." Proc Natl Acad Sci U S A **88**(1): 234-238.

Sarkar, M., S. Pagny, U. Unligil, D. Joziasse, J. Mucha, J. Glossl and H. Schachter (1998). "Removal of 106 amino acids from the N-terminus of UDP-GlcNAc: alpha-3-D-mannoside beta-1,2-N-acetylglucosaminyltransferase I does not inactivate the enzyme." Glycoconj J **15**(2): 193-197.

Schedin-Weiss, S., B. Winblad and L. O. Tjernberg (2014). "The role of protein glycosylation in Alzheimer disease." FEBS J **281**(1): 46-62.

Schnapp, B. J. and T. S. Reese (1982). "Cytoplasmic structure in rapid-frozen axons." J Cell Biol **94**(3): 667-669.

Schroder, M. and R. J. Kaufman (2005). "The mammalian unfolded protein response." Annu Rev Biochem **74**: 739-789.

Schwalbe, R. A., M. J. Corey and T. A. Cartwright (2008). "Novel Kv3 glycoforms differentially expressed in adult mammalian brain contain sialylated N-glycans." Biochem Cell Biol **86**(1): 21-30.

Seifert, A., D. Glanz, N. Glaubitz, R. Horstkorte and K. Bork (2012). "Polysialylation of the neural cell adhesion molecule: interfering with polysialylation and migration in neuroblastoma cells." Arch Biochem Biophys **524**(1): 56-63.

Shah, N., D. A. Kuntz and D. R. Rose (2008). "Golgi alpha-mannosidase II cleaves two sugars sequentially in the same catalytic site." Proc Natl Acad Sci U S A **105**(28): 9570-9575.

Shajahan, A., C. Heiss, M. Ishihara and P. Azadi (2017). "Glycomic and glycoproteomic analysis of glycoproteins-a tutorial." Anal Bioanal Chem **409**(19): 4483-4505.

Shajahan, A., N. T. Supekar, D. Chapla, C. Heiss, K. W. Moremen and P. Azadi (2020). "Simplifying Glycan Profiling through a High-Throughput Micropermethylation Strategy." SLAS Technol **25**(4): 367-379.

Singleman, C. and N. G. Holtzman (2014). "Growth and maturation in the zebrafish, Danio rerio: a staging tool for teaching and research." Zebrafish **11**(4): 396-406.

Smith, L. L., A. H. Beggs and V. A. Gupta (2013). "Analysis of skeletal muscle defects in larval zebrafish by birefringence and touch-evoke escape response assays." J Vis Exp(82): e50925.

Snowden, C. J., N. Leborgne-Castel, L. J. Wootton, J. L. Hadlington and J. Denecke (2007). "In vivo analysis of the lumenal binding protein (BiP) reveals multiple functions of its ATPase domain." Plant J **52**(6): 987-1000.

Solnica-Krezel, L. (2020). Chapter Thirteen - Maternal contributions to gastrulation in zebrafish. Current Topics in Developmental Biology. F. L. Marlow, Academic Press. **140:** 391-427.

Song, P. and L. K. Kaczmarek (2006). "Modulation of Kv3.1b potassium channel phosphorylation in auditory neurons by conventional and novel protein kinase C isozymes." J Biol Chem **281**(22): 15582-15591.

Sprague, J., E. Doerry, S. Douglas and M. Westerfield (2001). "The Zebrafish Information Network (ZFIN): a resource for genetic, genomic and developmental research." Nucleic Acids Res **29**(1): 87-90.

Stanley, P. (2022). Essentials of Glycobiology. Essentials of Glycobiology. A. Varki, R. D. Cummings, J. D. Esko et al. Cold Spring Harbor (NY).

Stanley, P., N. Taniguchi and M. Aebi (2015). N-Glycans. Essentials of Glycobiology. rd, A. Varki, R. D. Cummings et al. Cold Spring Harbor (NY), Cold Spring Harbor Laboratory Press

Strahle, U. and S. Jesuthasan (1993). "Ultraviolet irradiation impairs epiboly in zebrafish embryos: evidence for a microtubule-dependent mechanism of epiboly." Development **119**(3): 909-919.

Strasser, R., J. Stadlmann, B. Svoboda, F. Altmann, J. Glossl and L. Mach (2005). "Molecular basis of N-acetylglucosaminyltransferase I deficiency in Arabidopsis thaliana plants lacking complex N-glycans." Biochem J **387**(Pt 2): 385-391.

Sur, A., Y. Wang, P. Capar, G. Margolin and J. A. Farrell (2023). "Single-cell analysis of shared signatures and transcriptional diversity during zebrafish development." bioRxiv.

Sur, A., Y. Wang, P. Capar, G. Margolin, M. K. Prochaska and J. A. Farrell (2023). "Single-cell analysis of shared signatures and transcriptional diversity during zebrafish development." Dev Cell **58**(24): 3028-3047 e3012.

Sztal, T. E., A. A. Ruparelia, C. Williams and R. J. Bryson-Richardson (2016). "Using Touch-evoked Response and Locomotion Assays to Assess Muscle Performance and Function in Zebrafish." J Vis Exp(116).

Takemoto, T., S. Natsuka, S. Nakakita and S. Hase (2005). "Expression of complex-type N-glycans in developmental periods of zebrafish embryo." Glycoconj J **22**(1-2): 21-26.

Tan, J., J. Dunn, J. Jaeken and H. Schachter (1996). "Mutations in the MGAT2 gene controlling complex N-glycan synthesis cause carbohydrate-deficient glycoprotein syndrome type II, an autosomal recessive disease with defective brain development." Am J Hum Genet **59**(4): 810-817.

Tetreault, M. P., B. Bourdin, J. Briot, E. Segura, S. Lesage, C. Fiset and L. Parent (2016). "Identification of Glycosylation Sites Essential for Surface Expression of the CaValpha2delta1 Subunit and Modulation of the Cardiac CaV1.2 Channel Activity." J Biol Chem **291**(9): 4826-4843.

Trimmer, J. S. (2015). "Subcellular localization of K+ channels in mammalian brain neurons: remarkable precision in the midst of extraordinary complexity." Neuron **85**(2): 238-256.

Tucker, J. A., K. A. Mintzer and M. C. Mullins (2008). "The BMP signaling gradient patterns dorsoventral tissues in a temporally progressive manner along the anteroposterior axis." Dev Cell **14**(1): 108-119.

Vallee, R. B., G. E. Seale and J.-W. Tsai (2009). "Emerging roles for myosin II and cytoplasmic dynein in migrating neurons and growth cones." Trends in Cell Biology **19**(7): 347-355.

Varki, A. (1993). "Biological roles of oligosaccharides: all of the theories are correct." Glycobiology **3**(2): 97-130.

Verheijen, J., S. Tahata, T. Kozicz, P. Witters and E. Morava (2020). "Therapeutic approaches in Congenital Disorders of Glycosylation (CDG) involving N-linked glycosylation: an update." Genet Med **22**(2): 268-279.

Vicente, P. C., J. Y. Kim, J. J. Ha, M. Y. Song, H. K. Lee, D. H. Kim, J. S. Choi and K. S. Park (2018). "Identification and characterization of site-specific N-glycosylation in the potassium channel Kv3.1b." J Cell Physiol **233**(1): 549-558.

Videira, P. A. Q. and M. Castro-Caldas (2018). "Linking Glycation and Glycosylation With Inflammation and Mitochondrial Dysfunction in Parkinson's Disease." Front Neurosci **12**: 381.

Wajda, D. A. and J. J. Sosnoff (2015). "Cognitive-motor interference in multiple sclerosis: a systematic review of evidence, correlates, and consequences." Biomed Res Int **2015**: 720856.

Wallace, K. N. and M. Pack (2003). "Unique and conserved aspects of gut development in zebrafish." Dev Biol **255**(1): 12-29.

Wang, Y., H. Schachter and J. D. Marth (2002). "Mice with a homozygous deletion of the Mgat2 gene encoding UDP-N-acetylglucosamine:alpha-6-D-mannoside beta1,2-N-acetylglucosaminyltransferase II: a model for congenital disorder of glycosylation type IIa." Biochim Biophys Acta **1573**(3): 301-311.

Wang, Y., J. Tan, M. Sutton-Smith, D. Ditto, M. Panico, R. M. Campbell, N. M. Varki, J. M. Long, J. Jaeken, S. R. Levinson, A. Wynshaw-Boris, H. R. Morris, D. Le, A. Dell, H. Schachter and J. D. Marth (2001). "Modeling human congenital disorder of glycosylation type IIa in the mouse: conservation of asparagine-linked glycan-dependent functions in mammalian physiology and insights into disease pathogenesis." Glycobiology **11**(12): 1051-1070.

Waters, M. F., N. A. Minassian, G. Stevanin, K. P. Figueroa, J. P. Bannister, D. Nolte, A. F. Mock, V. G. Evidente, D. B. Fee, U. Muller, A. Durr, A. Brice, D. M. Papazian and S. M. Pulst (2006). "Mutations in voltage-gated potassium channel KCNC3 cause degenerative and developmental central nervous system phenotypes." Nat Genet **38**(4): 447-451.

Wen, H. and P. Brehm (2005). "Paired motor neuron-muscle recordings in zebrafish test the receptor blockade model for shaping synaptic current." J Neurosci **25**(35): 8104-8111.

Westerfield, M., D. W. Liu, C. B. Kimmel and C. Walker (1990). "Pathfinding and synapse formation in a zebrafish mutant lacking functional acetylcholine receptors." Neuron **4**(6): 867-874.

Williams, M. L. and L. Solnica-Krezel (2020). "Nodal and planar cell polarity signaling cooperate to regulate zebrafish convergence and extension gastrulation movements." Elife **9**.

Winklbauer, R. and R. E. Keller (1996). "Fibronectin, mesoderm migration, and gastrulation in Xenopus." Dev Biol **177**(2): 413-426.

Xu, M., H. Jin, Z. Wu, Y. Han, J. Chen, C. Mao, P. Hao, X. Zhang, C. F. Liu and S. Yang (2022). "Mass Spectrometry-Based Analysis of Serum N-Glycosylation Changes in Patients with Parkinson's Disease." ACS Chem Neurosci **13**(12): 1719-1726.

Yabe, J. T., W. K. Chan, F. S. Wang, A. Pimenta, D. D. Ortiz and T. B. Shea (2003). "Regulation of the transition from vimentin to neurofilaments during neuronal differentiation." Cell Motil Cytoskeleton **56**(3): 193-205.

Yamakawa, N., J. Vanbeselaere, L. Y. Chang, S. Y. Yu, L. Ducrocq, A. Harduin-Lepers, J. Kurata, K. F. Aoki-Kinoshita, C. Sato, K. H. Khoo, K. Kitajima and Y. Guerardel (2018). "Systems glycomics of adult zebrafish identifies organ-specific sialylation and glycosylation patterns." Nat Commun **9**(1): 4647.

Ye, J., G. Coulouris, I. Zaretskaya, I. Cutcutache, S. Rozen and T. L. Madden (2012). "Primer-BLAST: a tool to design target-specific primers for polymerase chain reaction." BMC Bioinformatics **13**: 134.

Ye, Z. and J. D. Marth (2004). "N-glycan branching requirement in neuronal and postnatal viability." Glycobiology **14**(6): 547-558.

Yoo, J. Y., K. S. Ko, H. K. Seo, S. Park, W. I. Fanata, R. Harmoko, N. K. Ramasamy, T. Thulasinathan, T. Mengiste, J. M. Lim, S. Y. Lee and K. O. Lee (2015). "Limited Addition of the 6-Arm beta1,2-linked N-Acetylglucosamine (GlcNAc) Residue Facilitates the Formation of the Largest N-Glycan in Plants." J Biol Chem **290**(27): 16560-16572.

Yuan, A., M. V. Rao, Veeranna and R. A. Nixon (2017). "Neurofilaments and Neurofilament Proteins in Health and Disease." Cold Spring Harb Perspect Biol **9**(4).

Yue, M. S., R. E. Peterson and W. Heideman (2015). "Dioxin inhibition of swim bladder development in zebrafish: is it secondary to heart failure?" Aquat Toxicol **162**: 10-17.

Zalik, S. E., E. Lewandowski, Z. Kam and B. Geiger (1999). "Cell adhesion and the actin cytoskeleton of the enveloping layer in the zebrafish embryo during epiboly." Biochem Cell Biol **77**(6): 527-542.

Zelenchuk, T. A. and J. L. Bruses (2011). "In vivo labeling of zebrafish motor neurons using an mnx1 enhancer and Gal4/UAS." Genesis **49**(7): 546-554.

Zhang, Y., L. Varela, K. Szigeti-Buck, A. Williams, M. Stoiljkovic, M. Sestan-Pesa, J. Henao-Mejia, P. D'Acunzo, E. Levy, R. A. Flavell, T. L. Horvath and L. K. Kaczmarek (2021). "Cerebellar Kv3.3 potassium channels activate TANK-binding kinase 1 to regulate trafficking of the cell survival protein Hax-1." Nat Commun **12**(1): 1731.

Animal Care and Use Committee
003 Ed Warren Life Sciences Building | East Carolina University | Greenville NC 27834 - 4354
252-744-2436 office | 252-744-2355 fax

August 26, 2024

Ruth Schwalbe, Ph.D.
Department of Biochemistry and Molecular Biology, ECU

Subject: Protocol C065a, original approval date 01/28/2022

Dear Dr. Schwalbe:

The amendment#6 to your Animal Use Protocol entitled, "Role of N-glycans and potassium channels in Zebrafish" (AUP#C065a) was reviewed by this institution's Animal Care and Use Committee on 08/26/2024. The following action was taken by the Committee:

"Approved as submitted"

****Prior to EACH hazard use, please contact Aaron Hinkle at least a week before planned hazard use****

A copy of the protocols is enclosed for your laboratory files. Please be reminded that all animal procedures must be conducted as described in the approved Animal Use Protocol. Modifications of these procedures cannot be performed without prior approval of the ACUC. The Animal Welfare Act and Public Health Service Guidelines require the ACUC to suspend activities not in accordance with approved procedures and report such activities to the responsible University Official (Vice Chancellor for Health Sciences or Vice Chancellor for Academic Affairs) and appropriate federal Agencies. Please ensure that all personnel associated with this protocol have access to this approved copy of the AUP/Amendment and are familiar with its contents.

Sincerely yours,

Susan McRae, Ph.D.
Chair, Animal Care and Use Committee

SM/GD

enclosure